(2)

TECHNICAL REPORT BRL-TR-3169

BRL

THE BEHAVIOR OF SHAPED CHARGES WITH OPEN-POLED HEMISPHERICAL LINERS

R.L. SUMMERS
W.P. WALTERS
R.D. DICK

NOVEMBER 1990

U.S. ARMY LABORATORY COMMAND

BALLISTIC RESEARCH LABORATORY
ABERDEEN PROVING GROUND, MARYLAND

NOTICES

Destroy this report when it is no longer needed. DO NOT return it to the originator.

Additional copies of this report may be obtained from the National Technical Information Service, U.S. Department of Commerce, 5285 Port Royal Road, Springfield, VA 22161.

The findings of this report are not to be construed as an official Department of the Army position, unless so designated by other authorized documents.

The use of trade names or manufacturers' names in this report does not constitute indorsement of any commercial product.

REPORT DOCUMENTATION PAGE

Form Approved
OMB No. 0704-0188

1. AGENCY USE ONLY (Leave blank)	2. REPORT DATE	3. REPORT TYPE AND DATES COVERED
	November 1990	Final, January 1989 - June 1990

4. TITLE AND SUBTITLE

The Behavior of Shaped Charges With Open-Poled Hemispherical Liners

5. FUNDING NUMBERS

1L162618AH80

6. AUTHOR(S)

R. L. Summers, W. P. Walters, R. D. Dick*

7. PERFORMING ORGANIZATION NAME(S) AND ADDRESS(ES)

8. PERFORMING ORGANIZATION REPORT NUMBER

9. SPONSORING/MONITORING AGENCY NAME(S) AND ADDRESS(ES)

US Army Ballistic Research Laboratory
ATTN: SLCBR-DD-T
Aberdeen Proving Ground, MD 21005-5066

10. SPONSORING/MONITORING AGENCY REPORT NUMBER

BRL-TR-3169

11. SUPPLEMENTARY NOTES

*Dr. Dick works for the University of Maryland, College Park, MD 20742.

12a. DISTRIBUTION/AVAILABILITY STATEMENT

Approved for public release; distribution unlimited

12b. DISTRIBUTION CODE

13. ABSTRACT (Maximum 200 words)

This paper discusses the effect of an opening at the pole of a hemispherical shaped-charge liner. An experimental study was performed in which various diameter holes were made in otherwise similar shaped-charge liners. Flash radiographs were taken to observe changes in the liner collapse and the jet characteristics.

The collapse process and jet characteristics of a hemispherical liner are significantly altered for a hole diameter which is 10% or more of the outer liner diameter. The jet tip velocity is increased by 26% for a hole diameter-to-liner diameter ratio of 0.25. Two explanations are presented for the behavior of the tip region of the shaped-charge jet. Both of the explanations assume that the pole of the liner impedes the motion of the subsequent liner material.

14. SUBJECT TERMS

shaped charges; hemispherical liner; open apex; open pole; jet formation; liner collapse; flash radiography; jet characteristics; conical liner

15. NUMBER OF PAGES

136

16. PRICE CODE

17. SECURITY CLASSIFICATION OF REPORT	18. SECURITY CLASSIFICATION OF THIS PAGE	19. SECURITY CLASSIFICATION OF ABSTRACT	20. LIMITATION OF ABSTRACT
UNCLASSIFIED	UNCLASSIFIED	UNCLASSIFIED	SAR

INTENTIONALLY LEFT BLANK

TABLE OF CONTENTS

INTENTIONALLY LEFT BLANK

LIST OF FIGURES

LIST OF TABLES

INTENTIONALLY LEFT BLANK

ACKNOWLEDGMENTS

The authors are grateful to Carl Paxton and Joseph Gardiner for their assistance in many aspects of this report; Ed Mullins for his work in modifying the shaped-charge liners; and the BRL Explosive Modeling Facility staff for loading the shaped charges.

INTENTIONALLY LEFT BLANK

1. INTRODUCTION

The purpose of this study is to determine the effect of an opening at the pole of a hemispherical shaped-charge liner. Preliminary experiments performed at the U.S. Army Ballistic Research Laboratory (BRL) indicated that an increase in jet velocity could be achieved by cutting an opening at the pole (Walters 1985). Other research has also indicated the possibility of increased performance by shaped charges with open-poled hemispherical liners compared to shaped charges with full hemispherical liners (Walters and Zukas 1989; AFPAC 1946; Carnegie Institute 1946a). An experimental study was performed in which various sized holes, centered about the pole of the liners, were cut in otherwise similar shaped-charge liners. Figure 1 shows the baseline shaped charge design used in this study. The effect of the hole is observed by measuring the changes in the jet characteristics and the liner collapse process. Flash radiography is used to provide images of the liner collapse and early jet formation and to measure the jet characteristics.

A shaped charge consists of a cylinder of explosive with a lined hollow cavity which is symmetric about the axis of the cylinder. The cavity may take on a variety of shapes, the most common being either conical or hemispherical. In most cases, the cavity is lined with a thin layer of metal. The explosive is, most commonly, point initiated on the axis of symmetry at the end of the cylinder opposite the hollow cavity. When the explosive cylinder (known as the explosive charge, or charge) is detonated, the metal liner collapses to the axis of symmetry and undergoes a jetting process which forms the liner material into a rod (known as a shaped-charge jet). The shaped-charge jet is capable of creating deep cavities in materials such as hardened steel, rock, and fortified concrete. The penetration capability of the jet increases to a maximum and then decreases as the distance from the shaped charge to the target, known as the standoff distance, increases. The most common metal used as a shaped-charge liner is copper. Copper is used because it is highly ductile under dynamic loading conditions, inexpensive, and easily shaped.

The collapse and jet formation of the shaped-charge liner has been the subject of extensive research. Figure 2 shows a typical shaped charge with a conical liner, hereafter referred to as a conical shaped charge. When the detonator is initiated, a detonation wave propagates through the explosive. As the detonation wave reaches the liner, a shock wave is induced, causing the liner to collapse to the axis of symmetry. Figure 3 is a series of flash radiographs, obtained at BRL (Walters and Zukas 1989), which show the collapse and jet formation process of a conical liner. As the liner material collides at the axis of symmetry, a portion of the material is extruded forward at an extremely high velocity (in some cases exceeding 10 km/sec). This portion of the liner

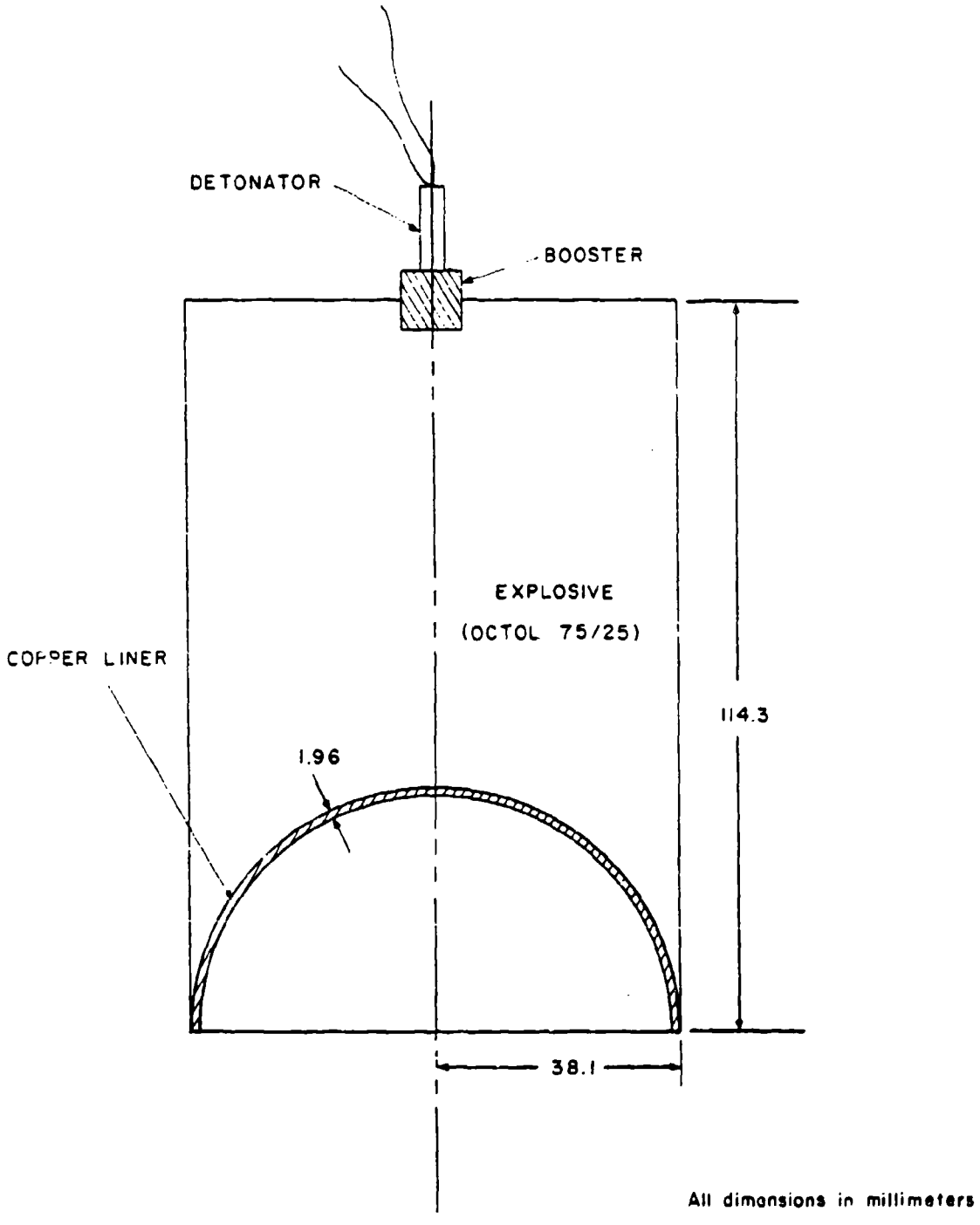

Figure 1. Baseline Hemispherical Shaped Charge.

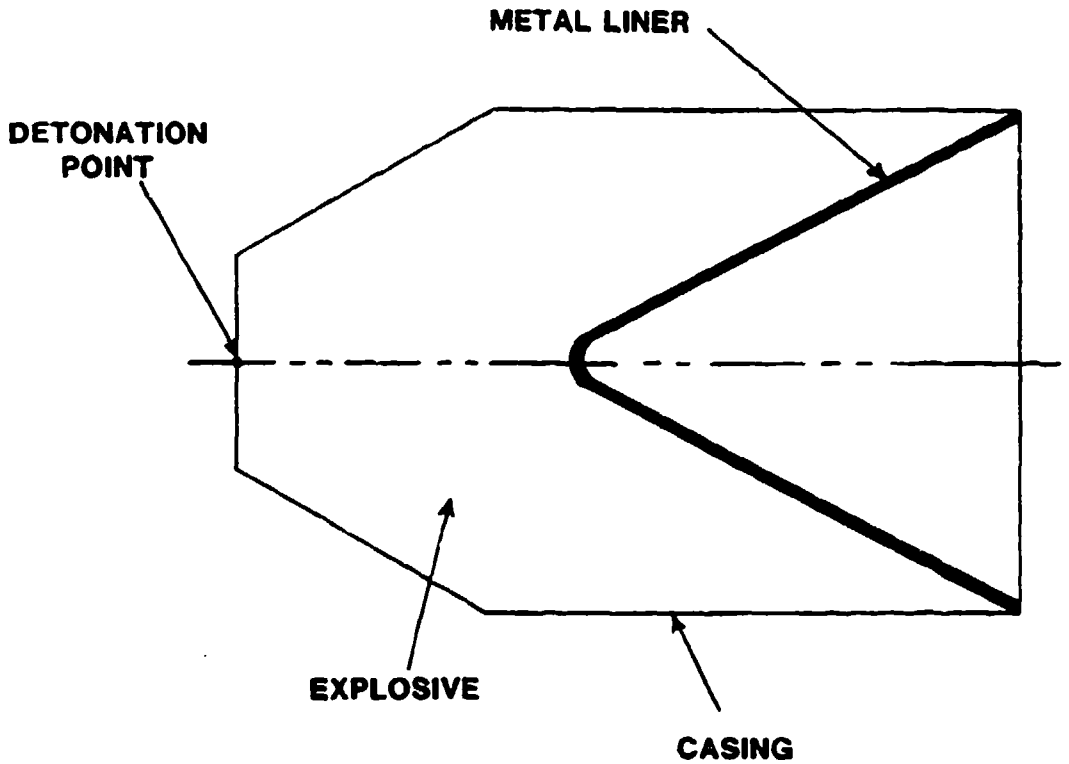

Figure 2. Typical Conical Shaped Charge.

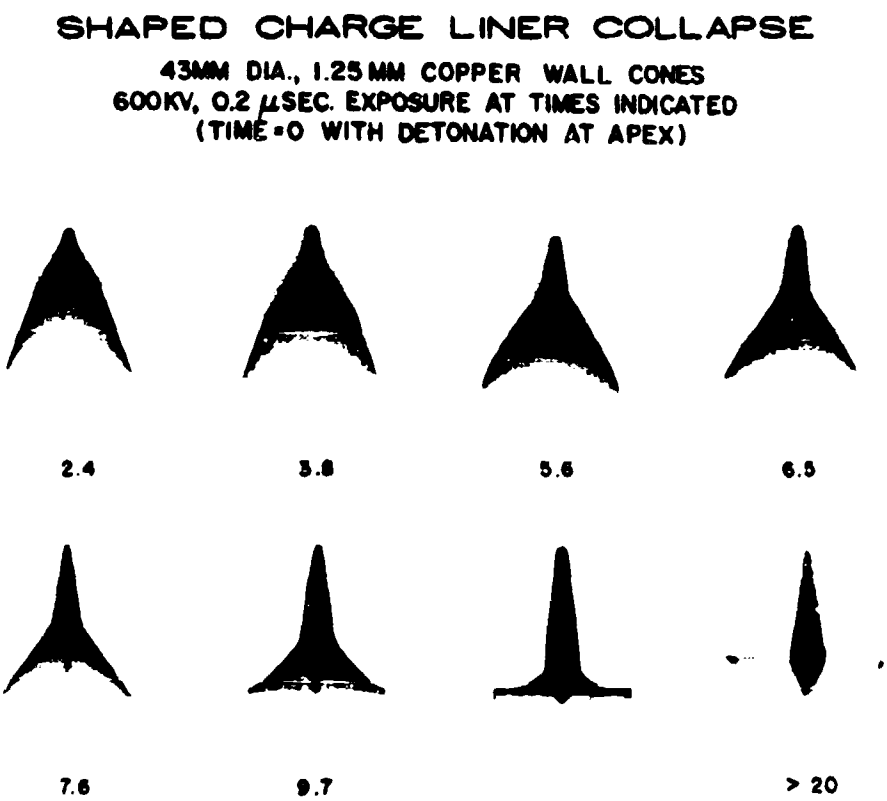

Figure 3. Collapse Sequence of a Conical Liner (Walters and Zukas 1989).

material is known as the jet. The majority of the liner material flows into a massive, slow-moving region at the rear of the jet, known as the slug. The velocity of the shaped-charge jet decreases approximately linearly from the tip of the jet to the slug. The slug velocity is usually on the order of 0.5 km/sec to 1.5 km/sec.

Figure 4 is a series of flash radiographs which illustrate the collapse and jet formation process of a hemispherical liner (Walters and Zukas 1989). The hemispherical liner does not collide at the axis of symmetry in the same manner as the conical liner. The observed jet tip velocities are usually between 3 km/sec and 5 km/sec and, unlike a conical liner, the hemispherical liner does not form a massive slug, although a small portion of the liner may have a negative velocity. As with shaped-charge jets from conical liners, there is a nearly linear decrease in velocity from the tip of the jet to the rear.

The velocity gradient which is observed in shaped-charge jets causes the jet to stretch and eventually break into discrete particles. The jet does not actually break into a series of particles simultaneously, instead, there exists a distribution of breakup times as the jet breaks. In most cases the jet breakup occurs near the jet tip first and proceeds to the tail of the jet. This distribution of breakup times is averaged into one value, called the jet breakup time (Walters and Zukas 1989), for the purpose of evaluation and analysis. Determination of the jet breakup time is discussed in detail later.

The choice of liner geometry is not straightforward but depends on the desired application. Confining our discussion to conical versus hemispherical shapes, conical liners typically produce deeper penetration at optimum standoff distance. However, shaped charges with hemispherical liners are usually effective over a wider range of standoff distances, because jets from hemispherical liners generally have longer breakup times than jets from conical liners (Walters and Zukas 1989). In addition, shaped charges with hemispherical liners require less overall length than conical shaped charges of similar diameters.

1.1 Background. The behavior of a conical liner upon reaching the axis of symmetry has been described by Pugh, Eichelberger, and Rostoker (1952). The theory presented by Pugh, et al., hereafter referred to as the PER theory, treats the liner as an inviscid, incompressible fluid, and uses the conservation of mass, and conservation of momentum to describe the motion of the liner upon collision at the axis. These assumptions are valid, at least to the first order, since the pressures generated during the liner collapse (and target penetration) far exceed the yield strength of

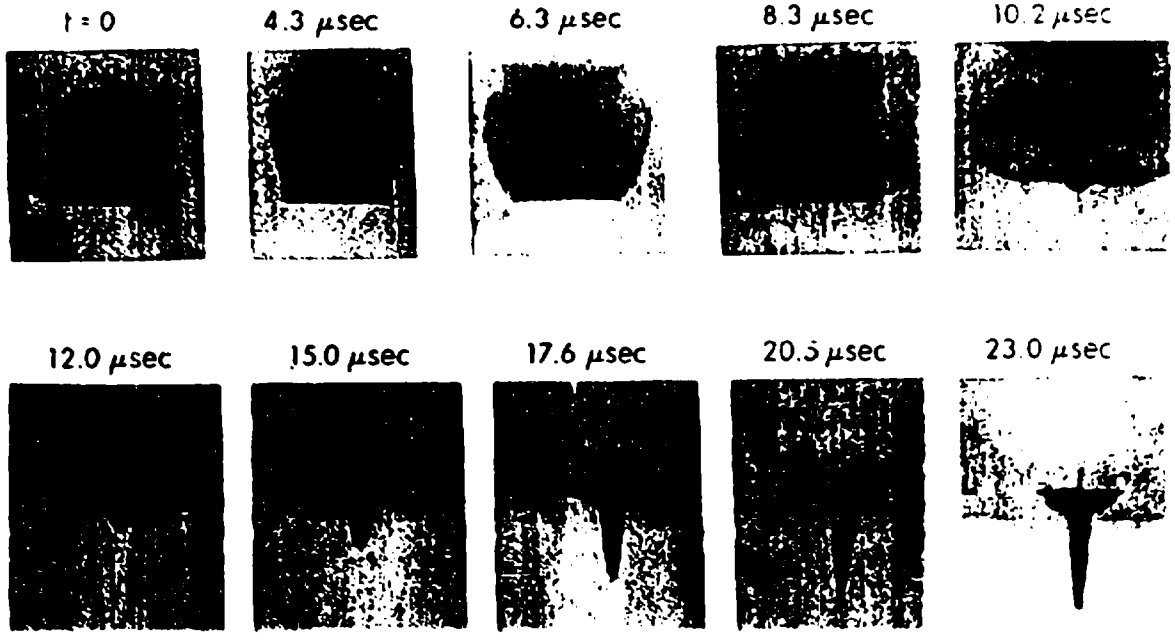

Figure 4. Collapse Sequence of a Hemispherical Liner (Walters and Zukas 1989).

most materials. The PER theory predicts the distribution of the jet velocity and the liner mass, given the velocity with which the liner collapses. One-dimensional models have been developed which divide the liner into many elements and predict the acceleration and final collapse velocity of each liner element. Each liner element is assumed to act independently of neighboring elements, consistent with the hydrodynamic flow assumption. The speed and direction of each liner element as it arrives at the axis combined with the PER theory provides an accurate prediction of the distribution of jet velocity and liner mass. One-dimensional models based on the PER theory of conical liner collapse have been used to successfully predict jet velocities, mass distributions, and other jet characteristics for conical shaped charges with an apex angle of less than 120 degrees and greater than 25 degrees (Walters and Zukas 1989).

The collapse and jet formation process of wide-angle, conical liners and hemispherical liners differs a great deal from that of a conical shaped-charge liner (Kolsky 1949; Singh 1955; Kiwan and Arbuckle 1977). A hemispherical liner appears to turn inside out from the pole (Kolsky 1949; Singh 1955), as shown in Figure 4. Many experimental, analytical, and hydrocode studies have been performed concerning the collapse and jet formation process of shaped charges with hemispherical liners (Kolsky 1949; Singh 1955; Kiwan and Arbuckle 1977; Chou et al. 1983, 1985; Shepherd 1956; Asellne et al. 1978; Arbuckle et al. 1980; Grace et al. 1984; Lee 1985; Walters et al. 1985; Walters and Golaski 1987). However, a closed-form solution, such as the PER model, has not yet been developed for hemispherical liners (Walters and Zukas 1989; Walters 1986). Research performed by Chou, et. al., (1985) and Walters and Golaski (1987) utilized the Eulerian hydrocode, HELP, and the Lagrangian hydrocode, EPIC-2, to simulate jet formation. The hydrocodes predicted that the material near the pole of a hemispherical liner, upon collapsing, forms a rod along the axis of symmetry. As subsequent liner material reaches the axis of symmetry, it forms concentric tubes of increasing average radius which stretch from the tip of the jet to the tail (Walters and Golaski 1987). In contrast, the PER theory of jet formation for conical liners predicts that the material from a radial cross-section of a conical liner splits into two distinct regions, either the jet or the slug, rather than being distributed continuously between the front and the rear of the jet, as suggested for a hemispherical liner.

1.2 Objectives. If a hole is placed at the pole of a hemispherical liner, the jet formation process and the resulting jet characteristics are significantly altered. Since the hemispherical liner forms a jet by turning inside out from the pole, no collision at the axis of symmetry is allowed to take place. Removal of the pole region will allow subsequent liner material to reach the axis and collide in much the same manner as a conical liner. Thus, removal of the pole will provide a

"collapse-transition" between the collapse and formation mechanisms of a hemispherical and a conical shaped-charge liner. The purpose of this study is to experimentally determine the extent to which the collapse process and jet characteristics are changed as the size of the opening at the pole is varied. The data obtained as a result of this study will be helpful in the development of analytical models of the hemispherical liner jet formation process and may also be used to verify the accuracy of hydrocode predictions. In addition, the jet characteristics obtained in this study are used to explain observations of increased penetration performance by open-poled hemispherical liners which have been observed by previous researchers (Walters and Zukas 1989; AFPAC 1946; Carnegie Institute 1946a; Thomanek and Schlesiger 1969).

An analogous study was performed by Carleone, et al. (1977) with a 42 degree, conical shaped-charge liner. The jet tip particle of a conical shaped charge is, usually, more massive than the jet particles immediately following it. The experiments performed by Carleone, et al. were designed to determine those portions of the liner which contribute to the tip particle of a shaped-charge jet. The apex portion of the 81.3-mm BRL Standard shaped charge was filled to different heights with Wood's metal. The purpose of the Wood's metal was to prevent the filled portion of the liner from collapsing and then contributing to the shaped-charge jet. The one-dimensional model, based on the PER theory, predicted that as the filled portion of the cone is increased, the tip velocity will increase slowly to a maximum and then rapidly decrease. In addition, the model predicted a decrease in jet tip mass as the tip velocity is increased. The increase in jet tip velocity and decrease in jet tip mass is predicted because a finite distance is required to accelerate the liner to its terminal velocity. That is, material near the liner apex cannot reach its final velocity before colliding at the axis of symmetry and, therefore, material which is further from the apex reaches a higher collapse velocity and has a larger resultant jet velocity, this phenomena is known as the inverse velocity gradient. As the distance from the apex is further increased, the ratio of explosive mass-to-liner mass is decreased, which results in a lower collapse velocity and a lower resultant jet velocity. When the apex portion is allowed to contribute to the jet the subsequent liner material overtakes and inelastically collides with the material from the apex. The result of this collision is to increase the velocity of the material from the apex of the liner, decrease the velocity of the subsequent liner material, and to form a massive jet tip particle. Theoretically, removing the apex allows the subsequent liner material to travel at a higher velocity and reduces the tip mass because no inelastic collision takes place after jetting has occurred. The experiments performed by Carleone, et al. did not show an increase in tip velocity, however only a small decrease in tip velocity was observed until 38 percent of the liner height was made ineffective. The discrepancy between theory and experiment was attributed to the possibility of

interaction between the Wood's metal plug and the liner collapse. The experiments verified a reduction of tip mass as the filled portion of the liner was increased.

The influence of a hole at the top, or pole, of a hemispherical liner was investigated as early as World War II (Walters and Zukas 1989). A Japanese study (AFPAC 1946) performed during World War II "concluded that a hole at the apex of the conical liner or at the top of the hemispherical liner was desirable and that the size of the hole was critical." A large number of tests were conducted by the Japanese using hemispherical liners with open poles. The hole sizes which were tested ranged from 1/32 to 1/2 of the liner diameter. The Japanese determined that the ratio of liner diameter-to-explosive charge diameter should be approximately 0.80, and the ratio of hole diameter-to-charge diameter should be approximately 0.10. This gives a ratio of hole diameter-to-liner diameter of 0.125. However, in the data which is reported, very little comparison is made between the actual penetration performance of a liner with a hole versus a liner without a hole. One series of tests was reported in which a 96-mm diameter hemispherical charge with a concentric 46-mm diameter, hemispherical, steel liner was fired into armor plate at various standoff distances and the penetration measured. The tests were repeated with a hemispherical liner which had an 8-mm diameter opening at the pole. The collapse of a hemispherical liner driven by a hemispherical explosive configuration, such as the one utilized in this portion of the Japanese study, will differ from that of a liner driven by a cylindrical explosive charge, but this portion of the study indicates that some performance comparisons were made between full and open-poled hemispherical liners. The resulting penetration-standoff curve is shown in Figure 5. The liner with the 8-mm hole penetrated deeper than the liner with no hole. However, the increase in penetration is probably within the expected round-to-round variation, especially when it is considered that liner fabrication techniques, the need for precision fabrication and assembly, and the necessity of a homogenous explosive fill was not well understood in the 1940s.

Another series of experiments, performed by the Carnegie Institute of Technology in 1946, compared the penetration of hemispherical shaped charges with 13-mm outer diameter, spit-back tubes to plain hemispherical shaped charges (Carnegie Institute 1946a). A spit-back tube is a metal tube which is fastened axially to the liner and runs back through the explosive. Spit-back tubes were used in early shaped charges to allow for point initiation by a spit-back fuze. The liners with the spit-back tube contained a central hole of the same inner diameter as the tube. The average depth of penetration versus the standoff distance is plotted in Figure 6. The raw data is given in Table 1. The author indicated that the presence of the spit-back tube produced "a remarkable improvement in the depth of penetration" and "efforts to understand such phenomena may well lead to improvements in the

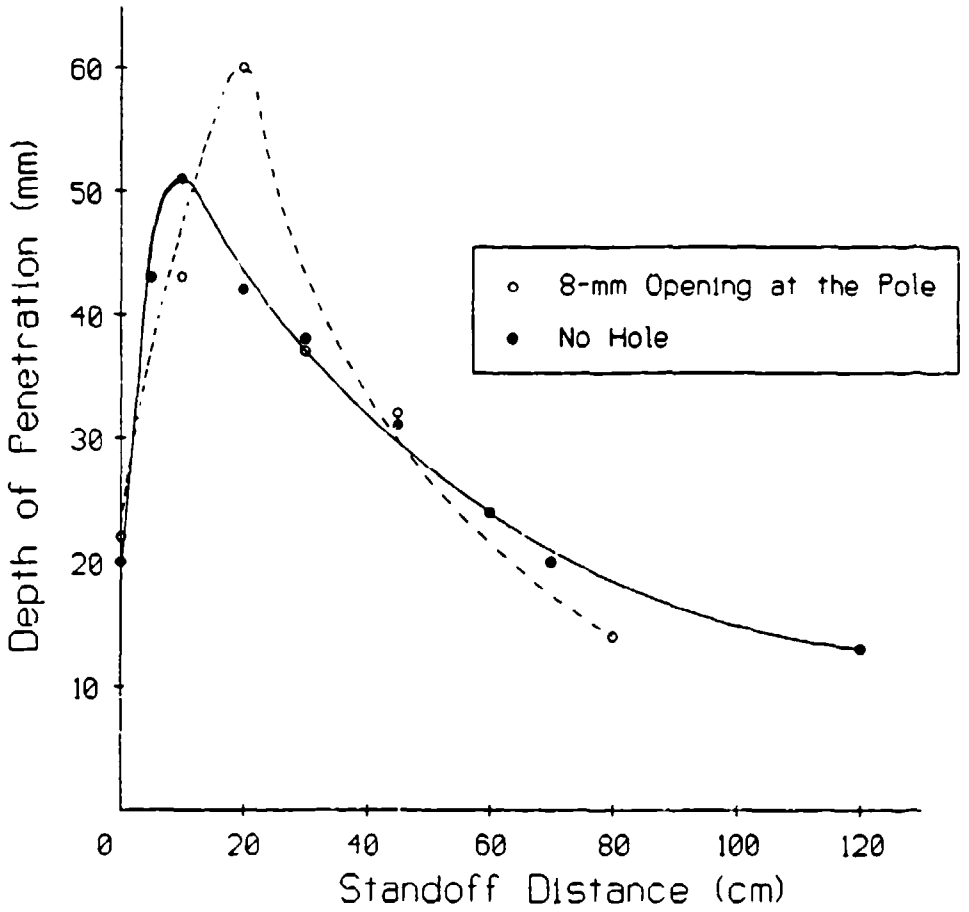

Figure 5. Japanese Hemispherical Liner Performance (AFPAC 1946).

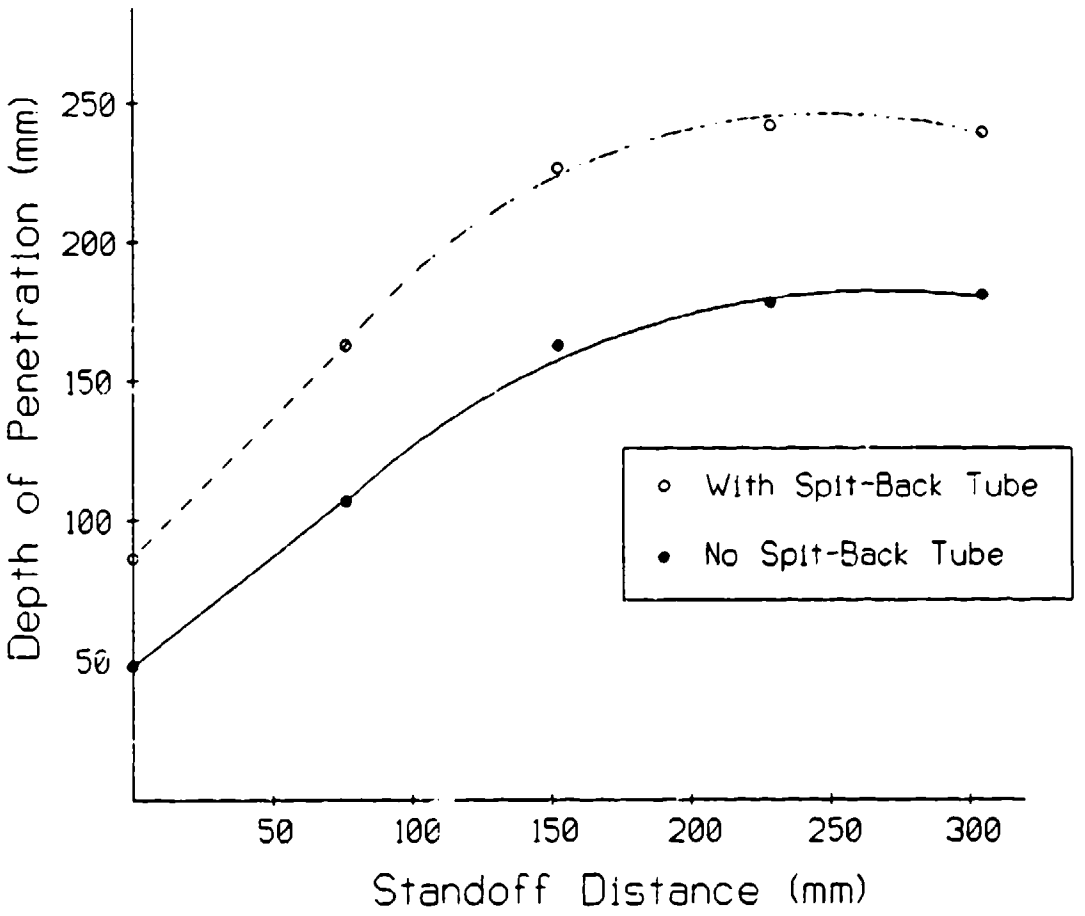

Figure 6. Spit-back Tube Effect on Penetration (Carnegie Institute 1946a).

Table 1. Spit-back Tube Effect (Carnegie Institute 1946a)

Standoff (mm)	Spit-Back Tube (y/n)	Depth of Penetration (mm)	
0	n	53	
0	n	46	Avg. = 48
0	n	46	
0	y	97	
0	y	86	Avg. = 87
0	y	79	
76	n	107	
76	n	107	Avg. = 107
76	n	107	
76	y	157	
76	y	155	Avg. = 163
76	y	175	
152	n	165	
152	n	160	
152	n	152	Avg. = 163
152	n	168	
152	n	168	
152	n	157	
152	y	221	
152	y	226	Avg. = 226
152	y	229	
229	n	180	
229	n	180	Avg. = 178
229	n	170	
229	y	211	
229	y	262	Avg. = 241
229	y	249	
305	n	165	
305	n	163	Avg. = 180
305	n	216	
305	y	246	
305	y	244	Avg. = 239
305	y	226	

theory of jet formation." The presence of the spit-back tube, rather than just an opening, and its potential effects on the shaped-charge performance is discussed later.

Other studies concerning open-poled hemispherical liners have also been performed. For example, the German Racketenpanzerbuchse (Carnegie Institute 1946b), shown in Figure 7, demonstrates that the Germans were aware of the possibility of increased performance from open-poled hemispherical liners as early as World War II. There is also evidence that the Japanese studies using open-poled liners were prompted by the Germans (AFPAC 1946), the Japanese Sakura warhead, shown in Figure 8, was adopted from German designs (Walters and Zukas 1989). In addition, Thomanek and Schlesiger (1969) patented a wide-angle, 120 to 160 degree, conical shaped charge with a small, 90 to 110 degree cone inserted at the apex. The small cone at the apex forms a single pellet which travels with a higher velocity than the jet from the wide-angle cone. The patent disclosure recommended that the base diameter of the inner cone be one-third the outside cone base diameter, which roughly corresponds with the ratio used in the Racketenpanzerbuchse.

2. EXPERIMENTAL SETUP

Liner performance and jet characteristics were determined at BRL's Experimental Research Facility 16 (ERF-16). ERF-16 hosts a shaped charge test facility which utilizes four Hewlett-Packard one MeV x-ray pulsers. The test site has been described by Paxton and Summers (1989). A schematic of the test site is shown in Figure 9.

Two different test setups were used in this study. The first setup utilized all four 1-MeV pulsers. The warhead was placed between the first pulser and a single film cassette, as shown in Figure 10. The single film cassette is allowed to move without constraint when confronted with the explosive blast because constraining the film cassette tends to increase the pressure on the x-ray film and intensifying screen combination causing pressure marks on the film. Pulser 1 was flashed between 20 and 45 μsec after initiation of the round to provide a radiograph of the liner collapse and early jet formation. Pulsers 2, 3, and 4 were flashed at later times to obtain jet characteristics. This setup provides the advantages of a detailed liner collapse image, a redundant measurement of particle velocities, and greater accuracy in the velocity measurement.

The second test setup involved only pulsers 2, 3, and 4. The warhead was placed between pulser 2 and the long film holder, as shown in Figure 11. Pulser 2 was flashed at an early time to view the liner collapse and early jet formation. Pulsers 3 and 4 were used to measure jet

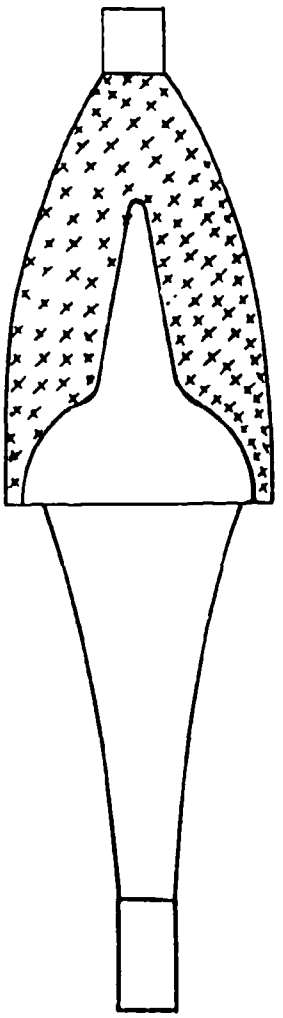

Figure 7. The German Racketenpanzerbuchse (Carnegie Institute 1946b).

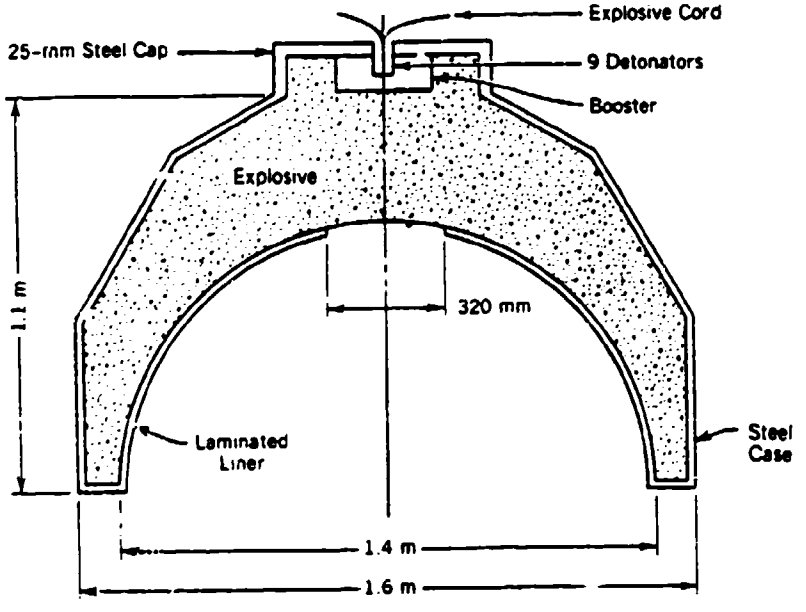

	Type I	Type II
Diameter of bomb	1.6 m	1.12 m
Length of bomb	1.1 m	1.0 m
Diameter of hemispherical liner	1.4 m	1.0 m
Size of hole at top of liner	260 mm 320 mm	200 mm
Liner, laminated steel plates	4 pc 8 mm thick (poor) 8 pc 4 mm thick (good)	4 pc 4 mm thick
Explosive (RDX)	1700 kg	500 kg
Booster (Picric Acid)	2 kg	2 kg
Case of bomb (steel)	7 mm thick	4 mm thick
Total weight	2908 kg	1300 kg

Figure 8. The Japanese SAKURA Bomb (Walters and Zukas 1989).

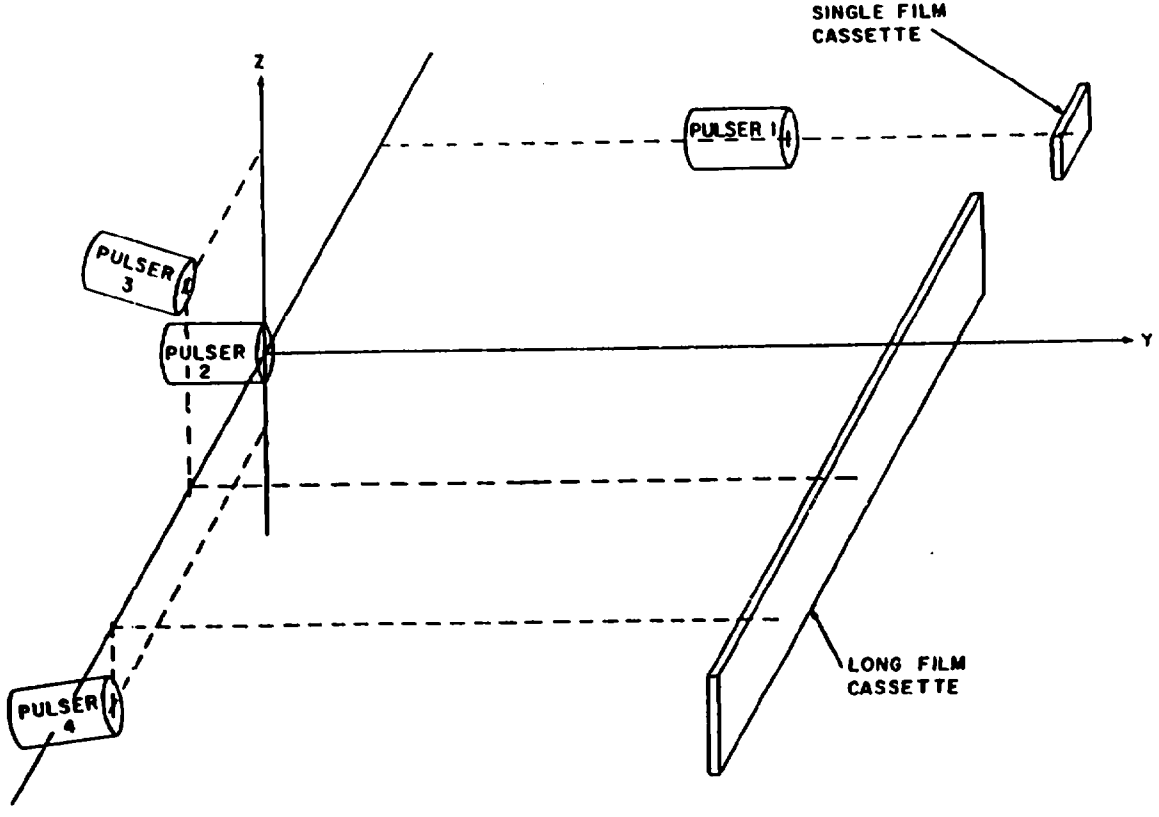

Figure 9. ERF-16's 1-MeV Test Site (Paxton and Summers 1989).

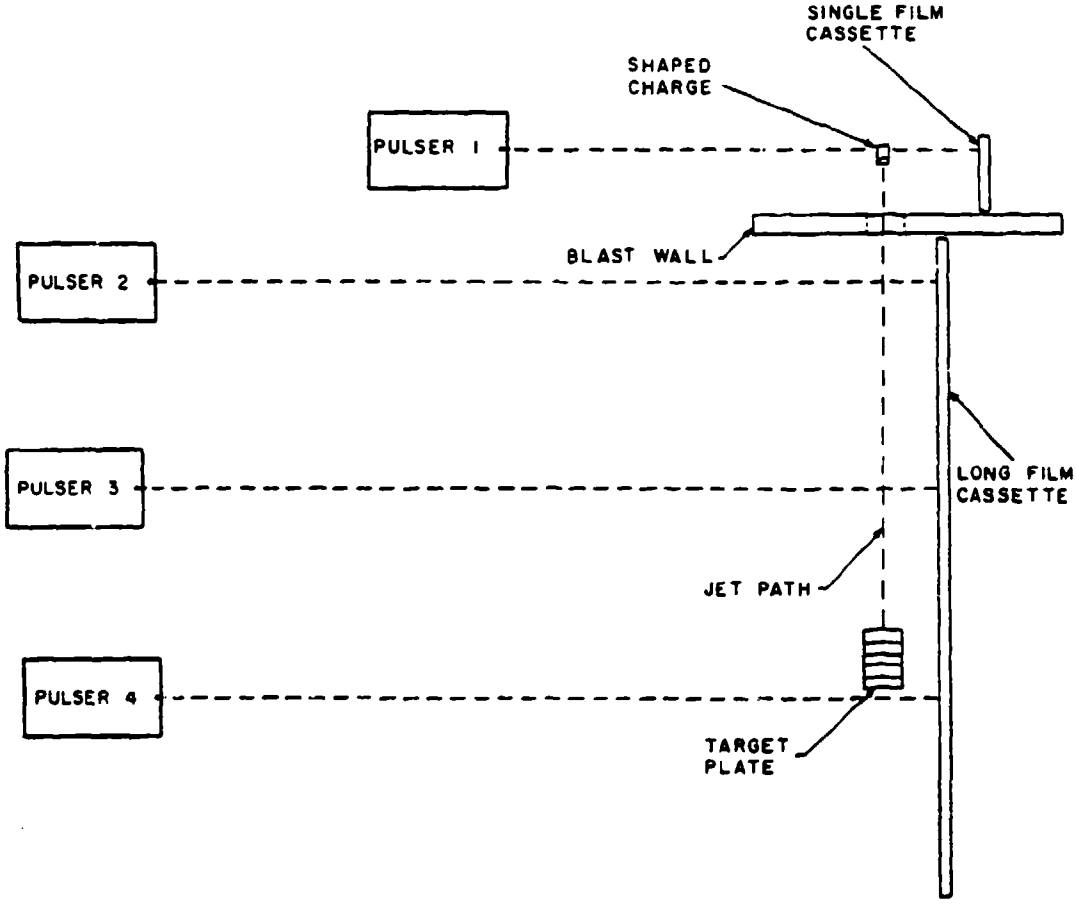

Figure 10. Test Setup Which Utilized All Available 1-MeV Pulsers.

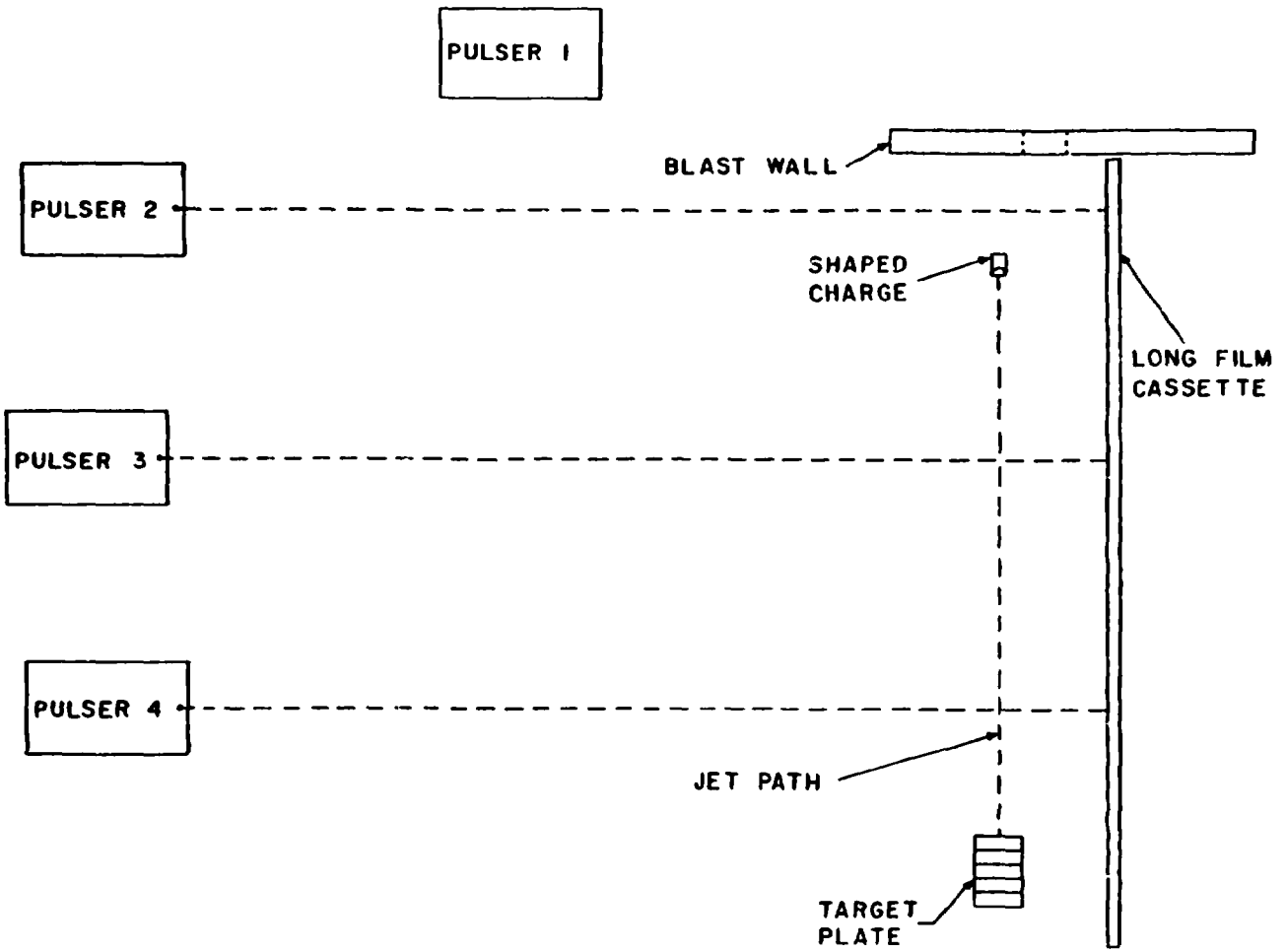

Figure 11. Test Setup Used to View Entire Jet.

characteristics. This setup offers the advantage of viewing the entire jet after it has formed and stretched. Thus, more particles were characterized providing a comparison of the total measured mass with the original liner mass.

Several reference points were established during the test setup in order to analyze the radiographs obtained. One of the most important was the location of the focal level for each x-ray tube. The focal point of a tube is defined as the point of intersection of the film plane and the line which is perpendicular to the film plane and passes through the x-ray source. The focal level of a tube is defined as the line on the film plane which passes through the focal point and is perpendicular to the direction of jet travel. The location of the focal level of each tube is needed to calculate the axial position of each jet particle. An image on the film of a thin steel rod, which was placed on the film protection package, marks the levels for pulsers 1 and 2. The focal levels of pulsers 3 and 4 are not marked on the film during the test setup. Instead, they are determined from the location of the tubes relative to pulser 2. A detailed description of this process is given by Paxton and Summers (1989).

Several measurements are recorded for each test. The distance from the x-ray source to the jet and the distance from the x-ray source to the film are measured for each pulser to calculate the magnification factor associated with each flash. The distances from the base of the liner to the focal levels of pulsers 1 and 2 are measured to establish a common reference point for each set of films. The long film cassette is capable of holding up to twenty 356-mm by 432-mm x-ray films. Fiducial markers are placed at regular intervals along the film cassette to ensure that the location of each film is known. If the films are overlapped or if a gap exists between the films, then the position of each film can be reconstructed using the known fiducial spacings. Finally, the distance from the base of the liner to the target plate, known as the standoff distance, is recorded to correlate penetration measurements among the tests.

Figure 12 shows the wiring schematic used at the 1-MeV site. The round is initiated by manually pressing the trigger which sends a 90-volt pulse to the firing unit. The firing unit sends a high-voltage pulse to the detonator and a Reynolds voltage monitor. The voltage monitor triggers the Hewlett-Packard digital delay generators and pulsed event timers, which are all connected in parallel. The delay generators, in turn, send a pulse to the trigger amplifiers which trigger the x-ray pulsers. The x-ray pulsers are equipped to give a signal at the time the x-rays are emitted which provides the stop pulse for the event timers. The flash time recorded for each tube is read

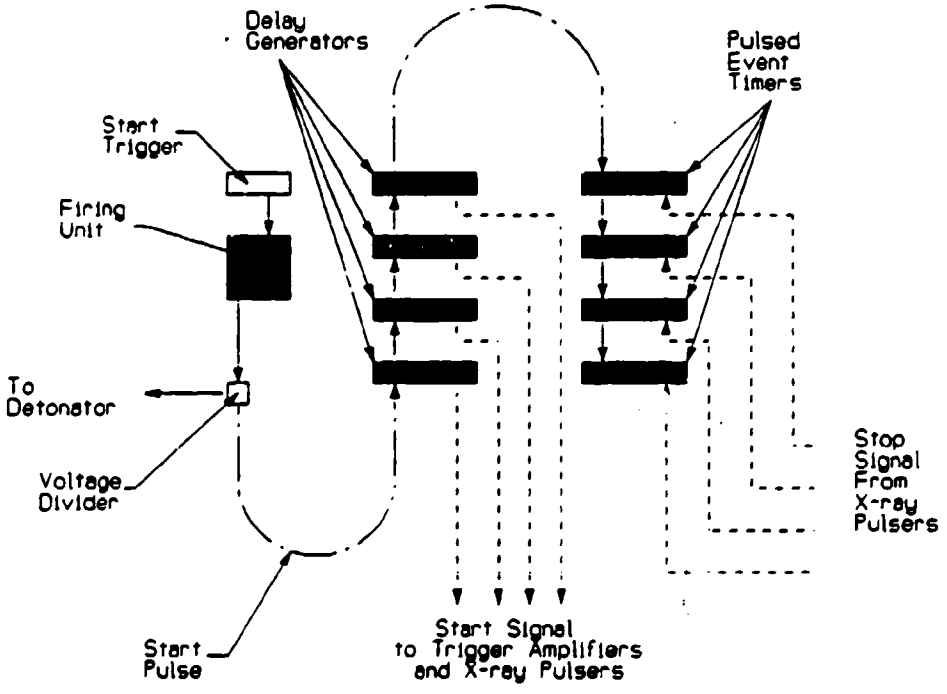

Figure 12. Timing Circuit Wiring Schematic.

from the pulsed event timers. The pulsed event timers usually record a flash time which is 0.5 to 1.0 μsec longer than the delay selected with the digital delay generators.

3. DATA ANALYSIS

The jet characteristics are determined from the radiographs produced after the jet has stretched and broken. The velocity, mass, maximum diameter, and length of each individual jet particle are measured. In addition, the jet breakup time and virtual origin are calculated. The jet breakup time, t_b, is an approximation of the time at which the jet breaks from a continuous jet into numerous particles (Simon 1974). The breakup time is calculated as:

$$t_b = \frac{((\sum_{i=1}^{n} L_i) - (L_1 + L_n)/2)}{(V_1 - V_n)}$$

where,

L_i = the length of the ith particle,

V_i = the velocity of the ith particle.

While the jet does not actually break simultaneously from tip to tail, the breakup time gives an average time which is useful for one-dimensional (1-D) penetration models. The virtual origin is defined as the point from which all of the jet particles are assumed to originate. The virtual origin is determined by plotting the position of each jet particle versus its velocity and, using a linear least squares fit of the data, determining the x-intercept (Blische and Simmons 1981). Since the virtual origin is normally located between the base of a conical liner and its apex, the virtual origin is defined as positive in the direction opposite the motion of the shaped-charge jet. In addition, the virtual origin is assumed to be on the axis of symmetry. Again, the virtual origin is an idealization of the actual case and is used as an input parameter for 1-D penetration models.

The radiographs are digitized with a microcomputer and a digitizer table. The films from a test firing are analyzed using a BASIC program which drives the digitizer and performs initial calculations based on the digitizer input and the test setup. The BASIC program is the result of

programming efforts by Blische and Simmons (1981) and Segletes (1983) with later modifications and additions by Weaver and Summers. Four parameters are obtained as output from the digitizer program: (1) particle position, (2) particle length, (3) particle diameter, and (4) particle mass. The program is structured to read data obtained using up to four flash times. The input required to execute the digitizer program includes the range of particles to be analyzed for each flash time, the number of films which are used, the magnification factor, the fiducial locations on each film, the jet density, and the test setup parameters. Each particle that appears on the film is numbered starting at the tip of the jet. The images from an individual test which are produced at each flash time are compared with the images from other flash times to insure that the same particle is designated with the same particle number in each flash. In some cases, the particles near the tip of the jet are very small and numerous and, for such cases, only the particles which are identifiable at each flash time are numbered.

The magnification factor is determined based on the test setup. As shown in Figure 13, the image of the jet particles on the film will be larger than actual size. Therefore, the values obtained for particle dimensions are multiplied by a magnification factor which is less than one. By similar triangles, this magnification factor, K, is determined as:

$$K = \frac{\text{Distance from x-ray source to jet path}}{\text{Distance from x-ray source to film}} \quad . \tag{1}$$

The location of the fiducials as they are projected onto the shotline are found as follows. The distance from the base of the liner to the focal level of pulser 2 is measured at the test site. The distances between the fiducials are measured at the test site along the film protection and, later, on the films using the digitizer. If the films are properly aligned at the time of the shot the two fiducial separation measurements will correspond with one another. If the two measurements do not register, it may indicate that the films were overlapped or a gap existed between the films.

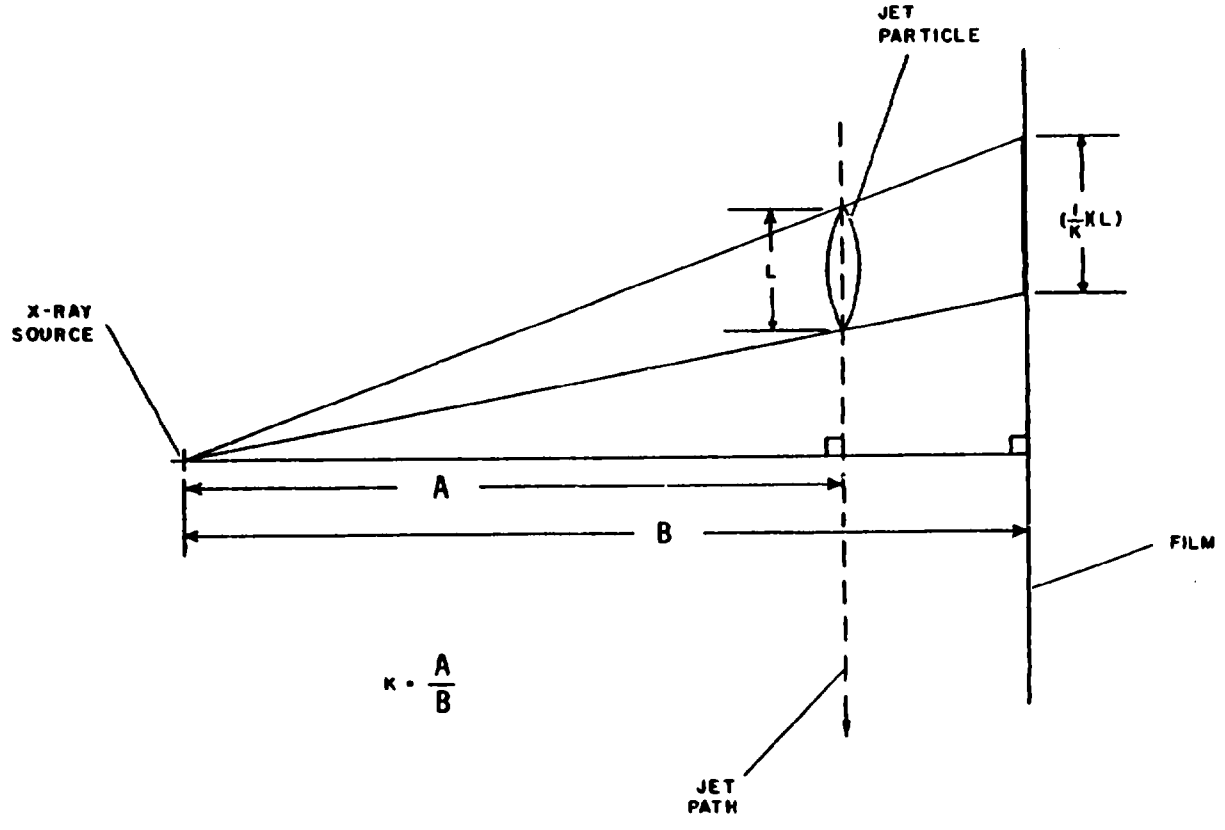

Figure 13. Determination of the Magnification Factor.

Once the distances between the fiducials have been measured, the projected location of the fiducial along the jet path may be determined. First, the distance between the fiducials along the jet path is calculated using:

$$ {}_iD_j = (K)({}_iS_j) \tag{2} $$

where,

${}_iD_j$ = distance between the i^{th} and j^{th} fiducials on the jet path and

${}_iS_j$ = distance between the i^{th} and j^{th} fiducials on the film.

Next, the location of the fiducial with respect to a reference location is found. Since, for example, the distance from the focal level to the base of the liner, X_B, is known, the distance from fiducial on film number 2 to the base of the liner, X_{base}, as projected on the jet path is calculated using:

$$ X_{base} = X_B + {}_fD_2. \tag{3} $$

where,

${}_fD_2$ = distance between the focal level and the second fiducial on the jet path.

The first calculation performed by the program is to obtain individual particle positions. The particle position, X_p, is the center of the particle which is an approximation of the particle's center of mass. Thus, if the particle is tumbling in flight an accurate velocity is still calculated. The particle position is determined by first calculating the distance, along the film, from the center of the particle to the fiducial (see Figure 14). This distance is then multiplied by the magnification factor and added to the actual fiducial location. This gives:

$$ X_p = (X'_2 + (X'_1 - X'_2)/2 - X'_0)(K) + X_{fid} \tag{4} $$

where,

X'_0 = the fiducial location on the film,

X_{fid} = the actual fiducial location,

X'_1, and X'_2 are shown in Figure 14.

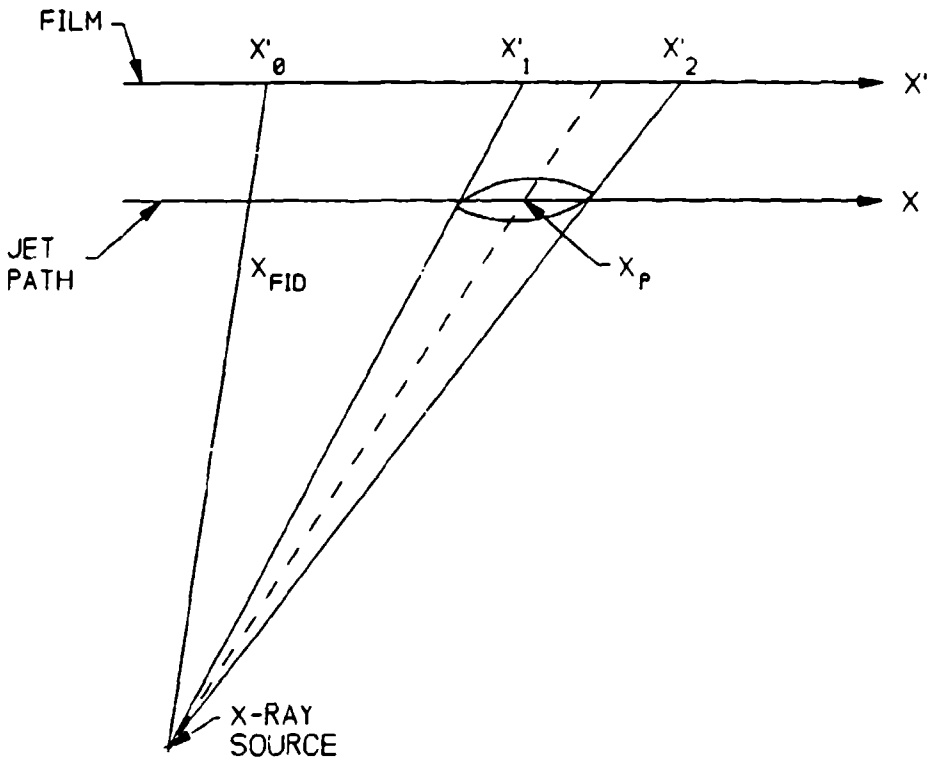

Figure 14. Determination of a Jet Particle's Position on the Shotline.

Equation 4 may be simplified to yield:

$$X_p = [(X'_2 + X'_1)/2 - X'_0](K) + X_{ref}. \quad (5)$$

The next measurements obtained by the digitizer program are the length and the diameter of the individual particles. The length, L, is obtained using the formula for the distance between two points.

$$L = (K)\ [(X'_1 - X'_2)^2 + (Y'_1 - Y'_2)^2]^{(1/2)} \quad (6)$$

where,

X'_1, X'_2, Y'_1, and Y'_2 are shown in Figure 14.

The diameter is obtained using an equation which gives the distance between a point and a line. First, the equation of the centerline of the jet particle (shown in Figure 15) is determined in the form:

$$aX' + bY' + c = 0. \quad (7)$$

Next, the distance between the top of the particle and the centerline, R_1, is determined, as is the distance between the bottom of the particle and the centerline, R_2. These two distances are then summed and multiplied by the magnification factor. This process gives:

$$R_1 = (aX'_3 + bY'_3 + c)/(a^2 + b^2) \quad (8)$$

$$R_2 = (aX'_4 + bY'_4 + c)/(a^2 + b^2) \quad (9)$$

$$Diam = (R_1 + R_2)\ (K) \quad (10)$$

Finally, the mass of each individual particle is calculated. Up to 50 consecutive points are digitized on both the top half and the bottom half of each particle. The volume is calculated assuming that each section between two digitized points is a truncated cone. Figure 16 shows how a section is defined. The points previously digitized as the front and back of the particle are used in this calculation automatically, and need not be digitized again. The first step in calculating the mass is to translate the origin to the rear of the jet particle and rotate the coordinate system such

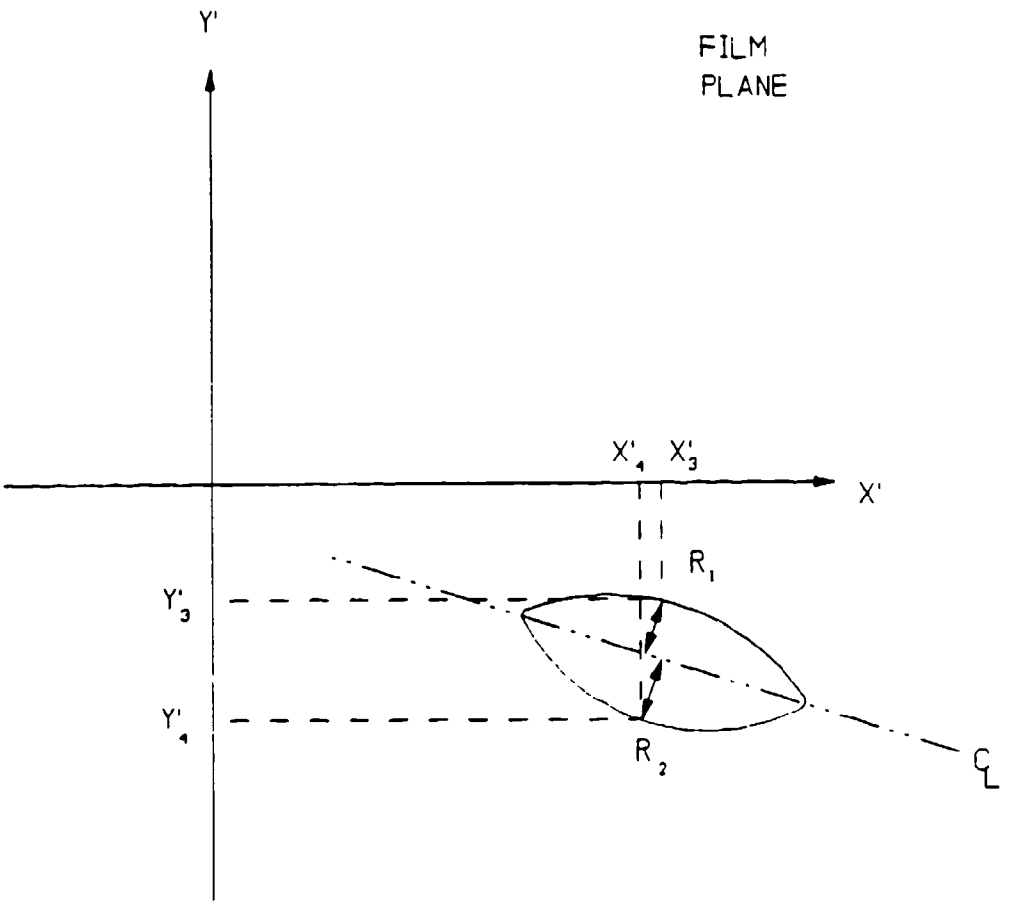

Figure 15. Determination of a Jet Particle's Diameter.

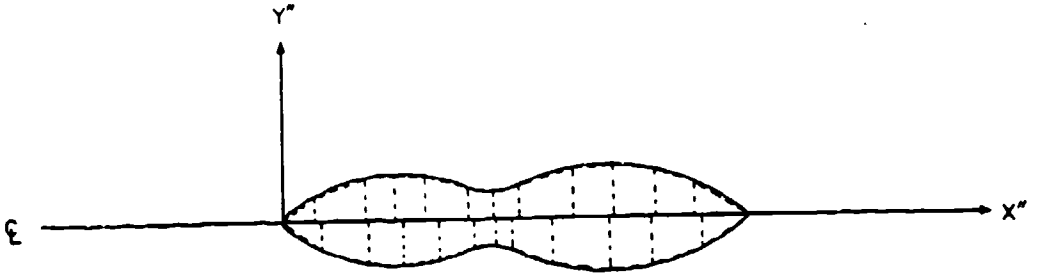

Volume = $(\pi/6)(H)(r_1^2 + r_1 r_2 + r_2^2)$

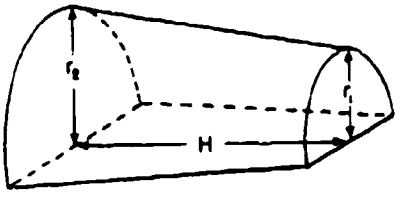

Figure 16. Jet Particle Volume Calculation.

that the X''-axis falls on the centerline of the particle. Next, the height of the truncated cone, H, and the two radii, r_1 and r_2, are determined. The volume of each section is then calculated. The total volume is obtained by summing the volumes of each section and multiplying the sum by the magnification factor cubed. The mass is given by the total volume multiplied by the virgin jet density.

After all the jet particles have been digitized, the data file generated by the BASIC digitizer program is transferred to a FORTRAN program. The FORTRAN program prepares tables of the raw data, determines the particle velocities, the jet breakup time, the virtual origin, average values of particle length, diameter, and mass, and cumulative properties such as total length, mass, energy, and momentum. If three flash times are used, the particle velocities are calculated between the first and second flash times, the first and third flash times, and the second and third flash times. An average value is then calculated. This repetitive measurement of jet particle velocity provides an indication of errors in the test setup or in the digitization process. In each experiment, the three velocity measurements for a single particle differed by no more than +/- 0.13 km/sec from the average of the three measurements.

The error involved in the data analysis process stems from three primary sources. The testing procedures and the experimental setup introduce one set of errors. Another source of error arises from the electronic equipment used to both produce and measure the elapsed time between the warhead detonation and the x-ray pulses. The final primary source of error occurs in the film digitization process.

The reported length, maximum diameter, and mass of each jet particle are the least accurate of the data produced. Although the digitizer table used to analyze the radiographs is accurate to 0.025 mm, the errors involved in the measurement of the particle dimensions stem primarily from the digitization process. One source of error is the x-ray source is treated as a point source, actually the x-ray source has a finite diameter which will have a small effect on the size of the particle image projected onto the film. Operator error in choosing the maximum diameter and the axis of symmetry of a jet particle will also effect the reported mass and diameter. In addition, the particle mass is calculated assuming the particle is circular in cross-section, however, some of the particles have elliptical cross-sections and/or exhibit asymmetries. Finally, the projected length, diameter, and mass of each particle may vary significantly between flashes due to tumbling and rotation of the particle. The result of these sources of error is to

reduce the accuracy and consistency of the length, diameter, and mass measurements. Thus, such values are used only to show trends rather than as absolute values.

The error associated with the measured jet particle velocity will vary with each test and with the actual velocity of the jet particle. The velocity is calculated based on the digitized particle locations and the recorded flash times. The measurements required to calculate the velocity of a jet particle using flash radiographs from ERF-16's 1-MeV site are listed below.

XS_3 = Horizontal distance from the x-ray source of tube 2 to the source of tube 3 measured parallel to the shotline,

XS_4 = Horizontal distance from the x-ray source of tube 2 to the source of tube 4 measured parallel to the shotline,

YS_3 = Horizontal distance from the source of tube 2 to the source of tube 3 measured perpendicular to the shotline. Positive in the direction of the film.

YS_4 = Horizontal distance from the source of tube 2 to the source of tube 4 measured perpendicular to the shotline. Positive in the direction of the film.

A = Horizontal distance from the source of tube 2 to the shotline.

B = Horizontal distance from the source of tube 2 to the film.

F_j = Distance from the fiducial on the ith film to the fiducial on the jth film.

XP_i = Distance, on the film, from the center of a jet particle to the fiducial. The subscript refers to the tube number.

t_i = Flash time of tube i.

In order to obtain an estimate of the magnitude of the error in the measurement of the tip velocity, three experiments are examined. Error estimates are provided for Rounds 4129, 4134, and 4131. Rounds 4129 and 4134 were both fired using the test setup shown in Figure 10, and represent the highest and lowest tip velocities, respectively, measured using this setup. Round 4131 was fired using the test setup shown in Figure 11 and gave the highest tip velocity.

Tables 2 - 4 list the values required to calculate the velocity and a worst case estimate of their accuracy for each of the three experiments. The x- and y-coordinates of tubes 3 and 4 relative to tube 1 are estimated to be within 50 mm (worst case) of their actual location. The uncertainty involved in determining the location of the x-ray source stems from errors which may arise in establishing a line parallel to the film plane, and errors in measuring angles with the transit. The accuracy of the measurement from tube 2 to the jet path is also estimated to be +/- 50 mm (worst case). While the measurement error to the desired jet path is less than +/- 6 mm (worst case), the actual jet path may vary due to misalignment of the shaped charge or bowing in the shaped-charge jet. Errors in determining fiducial separation may occur if the films become overlapped or separated when placed in the film holder. The fiducial separation is estimated to be within +/- 6 mm (worst case). The particle location on the film may be determined within +/- 3 mm (worst case), which reflects errors due to particle tumbling and operator errors.

The flash times are estimated to be within +/- 1.0 μsec of the recorded value. The error in determining the actual initiation of the warhead is larger. The digital delay generators and the pulsed event timers start counting when the high-voltage pulse from the firing unit is sent to the exploding bridgewire detonator. The detonator is actually initiated after some finite delay time which stems from the time for the pulse to travel through the wire to the detonator and for the bridgewire to break and initiate the primary explosive in the detonator. This delay time does not affect velocity measurements because it is independent of the time between flash x-ray pulses. The accuracy of the digital delay generators, and the pulsed event timers will affect both velocity and breakup time measurements. The HP digital delay generators are accurate to within +/- 0.1 μsec as are the pulsed event timers. However, if the trigger level required to start the delay generators and event timers is not identical on each unit, the time at which each delay generator and event timer starts counting may differ. The uncertainty which arises due to the trigger level adjustment is on the order of +/- 1 μsec.

Table 5 gives the measured values of jet tip velocity for Rounds 4129, 4134, and 4131. The range of tip velocities which may be calculated using the values in Tables 2 - 4 are also reported

Table 2. Round 4129 Measurement Accuracy

Quantity		Measured Value (mm)	Accuracy (mm)
XS_3		1353.	+/- 50
XS_4		2715.	+/- 50
YS_3		-141.	+/- 50
YS_4		31.	+/- 50
A		4826.	+/- 50
B		5217.	+/- 6
$_1F_2$		415.	+/- 6
$_2F_3$		439.	+/- 6
$_3F_4$		439.	+/- 6
$_4F_5$		439.	+/- 6
XP_2		-56.	+/- 3
XP_3		-68.	+/- 3
XP_4		-131.	+/- 3
t_2	(μsec)	270.2	+/- 1
t_3	(μsec)	450.3	+/- 1
t_4	(μsec)	540.2	+/- 1

Table 3. Round 4134 Measurement Accuracy

Quantity		Measured Value (mm)	Accuracy (mm)
XS_3		1354.	+/- 50
XS_4		2713.	+/- 50
YS_3		-146.	+/- 50
YS_4		30.	+/- 50
A		4817.	+/- 50
B		5210.	+/- 6
$_1F_2$		319.	+/- 6
$_2F_3$		441.	+/- 6
$_3F_4$		440.	+/- 6
XP_2		81.	+/- 3
XP_3		42.	+/- 3
XP_4		-115.	+/- 3
t_2	(μsec)	254.5	+/- 1
t_3	(μsec)	434.6	+/- 1
t_4	(μsec)	524.5	+/- 1

Table 4. Round 4131 Measurement Accuracy

Quantity	Measured Value (mm)	Accuracy (mm)
XS_3	1353.	+/- 50
XS_4	2715.	+/- 50
YS_3	-141.	+/- 50
YS_4	31.	+/- 50
A	4359.	+/- 50
B	5201.	+/- 25
XP_3	-304.	+/- 3
XP_4	-98.	+/- 3
t_3	175.1	+/- 1
t_4	250.0	+/- 1

Table 5. Measured Jet Tip Velocities

Round Number	Calculation	Measured Value (km/sec)	Range (km/sec)
4129	${}_1V_3$	5.01	+/- 0.20
4129	${}_1V_2$	5.01	+/- 0.20
4129	${}_2V_3$	5.01	+/- 0.44
4129	V_{avg}	5.01	+/- 0.24
4134	${}_1V_3$	4.20	+/- 0.20
4134	${}_1V_2$	4.26	+/- 0.20
4134	${}_2V_3$	4.08	+/- 0.44
4134	V_{avg}	4.18	+/- 0.24
4131	${}_2V_3$	5.29	+/- 0.67

in Table 5. The apparent inaccuracy of the second test setup is due primarily to the shorter change in time between flashes. As the time between x-ray flashes increases the significance of the measurement inaccuracies decreases. For example, the flash time of a single pulser can be measured to +/-1.0 μsec regardless of the time at which the next pulser flashes. The velocities reported using the test setup shown in Figure 10 are accurate to approximately +/-0.2 km/sec (worst case). The velocities measured using the test setup shown in Figure 11 are accurate to +/-0.7 km/sec. While the measurement of absolute jet tip velocity may, in the worst case, be accurate only to +/-0.7 km/sec, it is important to note that tip velocity measurements performed for liners with similar hole dimensions were extremely reproducible. For example, in the two experiments performed using liners with a 3.8-mm opening at the pole, the tip velocity was measured to be 4.2 km/sec in both experiments. Thus, relative increases or decreases in tip velocity between experiments can be measured with a large degree of confidence.

4. SHAPED CHARGE DESIGN

No effort was made to design a shaped charge which would yield optimum penetration performance. Instead, the shaped charge design chosen was based on standards which have been developed through previous parametric studies. The shaped-charge liners used were surplus from an earlier study performed at the BRL. Each of the liners used in testing were 76.2 mm in diameter with a constant wall thickness of 1.96 mm. Figure 1 is a schematic of the shaped charge design used. This charge, previously tested, was used as the baseline.

The type of explosive and the shape of the explosive fill, or charge, was also chosen based on established standards. The explosive chosen to drive the liner is 75/25 Octol (75% HMX, 25% TNT). 75/25 Octol was chosen because it is highly energetic, readily available at BRL, and commonly used in shaped charge warheads. The explosive was loaded in a casting process by the BRL Explosive Modeling Facility. The distance from the pole of the liner to the rear of the explosive cylinder, known as the head height, was chosen to be 76.2 mm, or one charge diameter (CD). Parametric studies have shown that decreasing the explosive head height below one CD can adversely affect the liner performance, while increasing the head height above one CD has little effect on the jet performance (Walters and Zukas 1989). This can be explained, in part, by considering the shape of the detonation wavefront. The detonation wave travels at an approximately constant velocity in all directions causing the wave shape to be an arc of a sphere centered about the detonation point. Thus, as head height is increased the radius of curvature of the wavefront, as it impacts the liner, will also increase. As the radius of curvature is increased, the detonation wavefront approaches a plane wave at a very large radius of curvature. A head

height of one CD is large enough that increasing the head height further does not significantly change the wave shape. The amount of explosive head height required may be significantly reduced by using devices which artificially shape the detonation wavefront. The wave shape may be changed by using different initiation techniques, such as peripheral initiators and plane wave generators, or by introducing a barrier in the explosive fill. The latter technique causes the detonation wavefront to alter its path around the barrier. In the study performed by the Carnegie Institute (1946a), discussed earlier, the spit-back tube which is attached to the liner will act as a waveshaper and may alter the liner behavior.

Once the design of the baseline shaped charge was determined, the most suitable method for covering the hole in the liner was investigated. The hole must be covered in some manner for two reasons. First, the explosive is cast about the liner and must be kept from entering the liner cavity during the casting process. Second, if the hole is left unplugged, the explosive products would blow through the hole upon detonation and disrupt the collapse process. The criterion used in the selection of the plug is non-interference in the liner collapse and jet formation process. That is, the plug can not interfere with the motion of the liner nor can it allow the explosive products to interfere.

Table 6 shows the different plug materials and designs which were tested and the measured tip velocity for each test. In several cases the tip region was incoherent. An incoherent region in the jet is one in which the collapse process does not produce a jet of material on the axis of symmetry, rather upon reaching the axis the liner material fragments resulting in a cluster of numerous small particles. If the leading portion of the jet is incoherent, the tip particle of the jet is difficult to determine. In such cases, the tip particle is defined as the first particle which is clearly identifiable at each flash time. Figure 17 shows a case in which the particle identified as the tip particle is not actually the leading particle of the jet. The faster particles are extremely small and in a cloud of many particles, rendering it impossible to identify the same particle in each flash. The affect of this difficulty is to lower the measured tip velocity and introduce more round-to-round variation in the jet characteristics.

An incoherent jet tip may be caused by several factors. First, the explosive fill must be uniform, if the HMX crystals in the explosive are inhomogeneous and concentrated either near the pole or asymmetrically, then incoherency in the tip region may result. Second, any asymmetries introduced by either improper alignment of the hole or plug, or by liner defects, such as wall thickness variations, may also cause incoherence in the tip region. Also, the construction of the

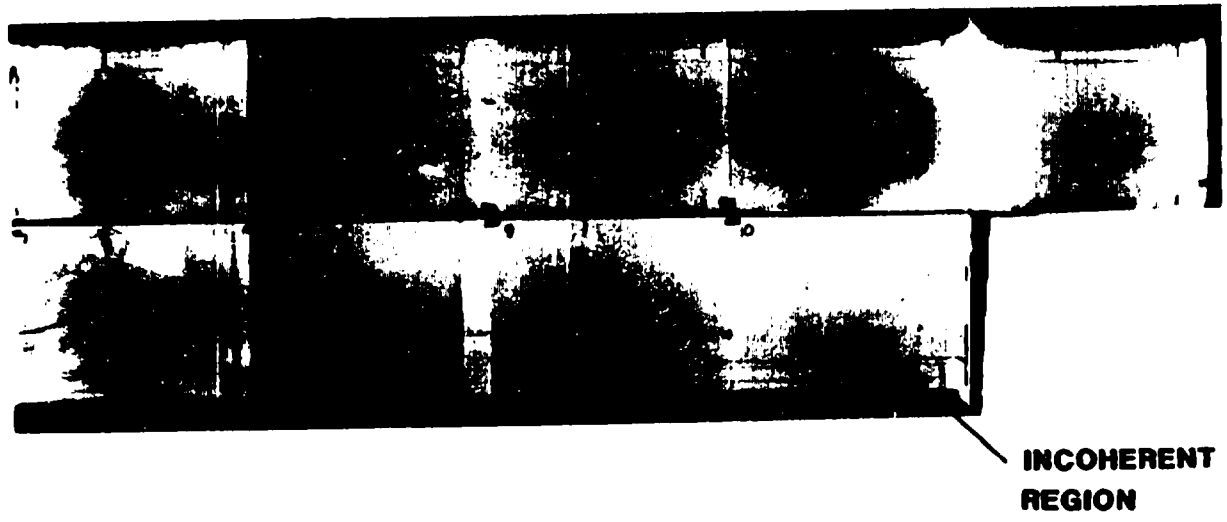

Figure 17. Flash Radiograph of Round 4104.

Table 6. Plug Selection Experiments

Round Number	Outer Hole Diameter (mm)	Inner Hole Diameter (mm)	Description	Tip Velocity (km/sec)
4064	27.9	25.4	0.76 mm Al	4.9 +/-0.2
4065	27.9	25.4	0.76 mm Al	4.7 +/-0.2
4078	22.7	20.3	1.78 mm W alloy	4.8 +/-0.2
4102	22.7	20.3	1.78 mm Polycarb	4.3 +/-0.2
4104	22.7	20.3	1.96 mm Copper	3.6 +/-0.7
4105	22.7	20.3	1.27 mm Al	4.7 +/-0.7
4106	22.7	20.3	Hemi. W alloy	4.5 +/-0.7
4110	22.7	20.3	1.27 mm W alloy	4.8 +/-0.7

seat machined in the hole to hold the plug in place may influence the tip formation. The design selected here is based on previous experimentation (Walters 1985) and is believed to minimize the effect of the geometric discontinuity on the tip formation. The factors listed above are observed, to some degree, in every test performed with the open-poled, hemispherical liners. In addition, if the plug interferes in the jet formation process, as in Round 4104 (Figure 17), the jet tip will be incoherent. Interference in the collapse process by the explosive products can also result in an incoherent tip region, this is demonstrated by Round 4102 (Figure 18).

Both the copper plug and the polycarbonate plug were rejected as final plug designs. The copper plug was rejected because it interfered in the motion of the liner, as shown in Figure 17. The polycarbonate plug was rejected because it allowed the explosive products to interfere in the collapse process, as shown in Figure 18.

Two groups of plug materials and designs provided satisfactory results. These were the aluminum disks and each of the tungsten alloy designs. The aluminum disks have less mass than the copper wall of the liner and, therefore, move out of the collapse region before any interference takes place between the copper and the aluminum. The disadvantage of the aluminum disks is that explosive products precede the disk and interfere in the collapse process. This interference is evidenced by hollowness in the jet, shown in Figure 19. The tungsten designs, on the other hand, move much slower than the neighboring copper and allow the walls of the liner to collapse in front of the plug. The disadvantage of the tungsten designs is that they caused a tube of copper to be formed, stretching from the rear of the liner to the front of the plug (Figure 20), which, would have otherwise entered the jet. Thus, both sets of plug materials have some deleterious effect on the jet formation process.

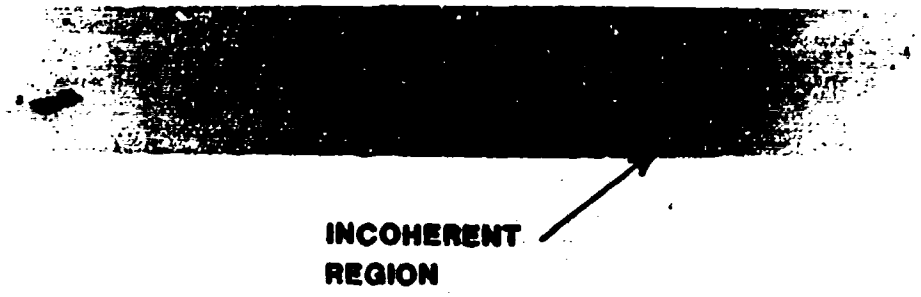

Figure 18. Flash Radiograph of the Tip Region of Round 4102.

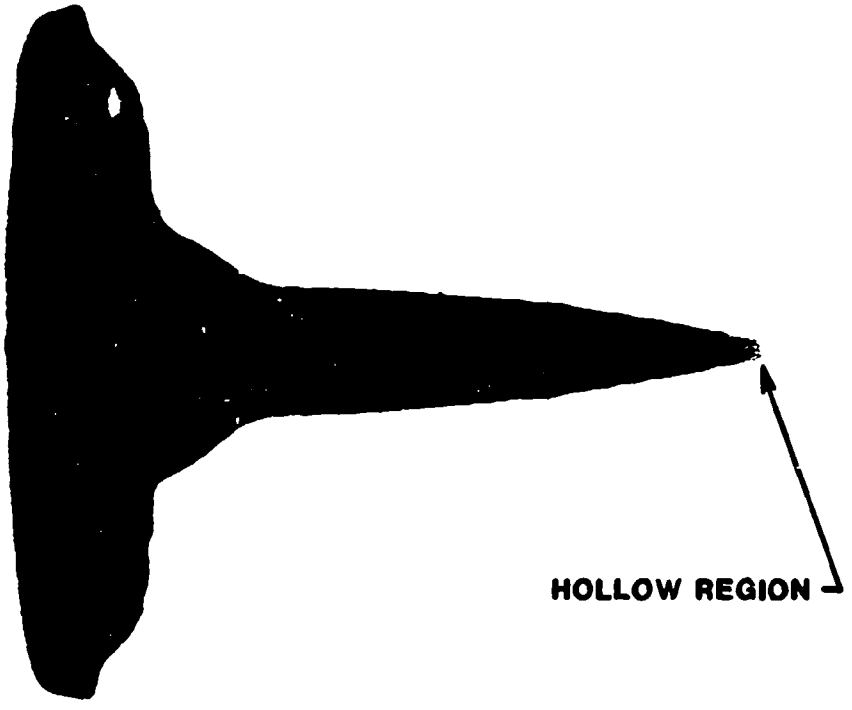

Figure 19. Flash Radiograph Produced 45 μsec After Initiation of Round 4065.

Figure 20. Flash Radiograph Produced 27.0 μsec After Initiation of Round 4078.

The 1.27-mm-thick aluminum disk was chosen as the final plug design. A disk shape was chosen for ease of fabrication and to minimize waveshaping effects. Aluminum is also cheaper, easier to machine, and more readily available than the tungsten alloy. The thickness of 1.27 mm was chosen because it moves slower than the 0.76-mm design, thus minimizing the amount of explosive products entering the jet formation region, and it still moves out of the collapse region ahead of the copper liner, as shown in Figure 21, hence avoiding any interference between the plug and the liner. Figure 22 shows the final plug design and the method used to hold the plug in place.

5. EXPERIMENTAL RESULTS

A series of tests were performed in which the outer diameter of the hole in the liner was varied from 2.5 mm to 30.5 mm. The liner and plug design used for each hole diameter is shown in Appendix A. Appendix B contains a complete listing of the data obtained from each experiment. The results of this series of experiments indicate that the collapse process and the jet characteristics of a hemispherical liner are significantly altered by removing material from the pole of the liner.

The penetration performance of a shaped-charge jet has been linked to several of the jet characteristics. Included among these are the total jet length, mass, momentum, kinetic energy, the breakup time, and the tip velocity. The penetration of a shaped-charge jet into steel increases as the jet length, jet breakup time, and tip velocity are increased. The total jet mass and the distribution of mass in the jet provide a measure of the efficiency of the shaped charge design. As the mass of the jet is increased, the length of the jet increases and/or the diameter of the jet increases. Increasing the jet diameter tends to increase the diameter of the hole in the target. In addition, an increase in the total jet kinetic energy will increase the volume of the hole in the target (Carleone et al. 1977). Plots of the total jet length, mass, momentum, kinetic energy, the breakup time, and the tip velocity versus the ratio of outer hole diameter-to-outer liner diameter are given.

Figure 23 is a plot of the cumulative jet length versus the ratio of outer hole diameter-to-outer liner diameter. The measured cumulative jet length will vary from round-to-round based on how much of the jet is visible on the film at the final flash time. In order to normalize the total jet length, an arbitrary cutoff velocity is used. Jet particles which are travelling with a velocity which is lower than the cutoff velocity are not included in the calculation of the total jet length. This is

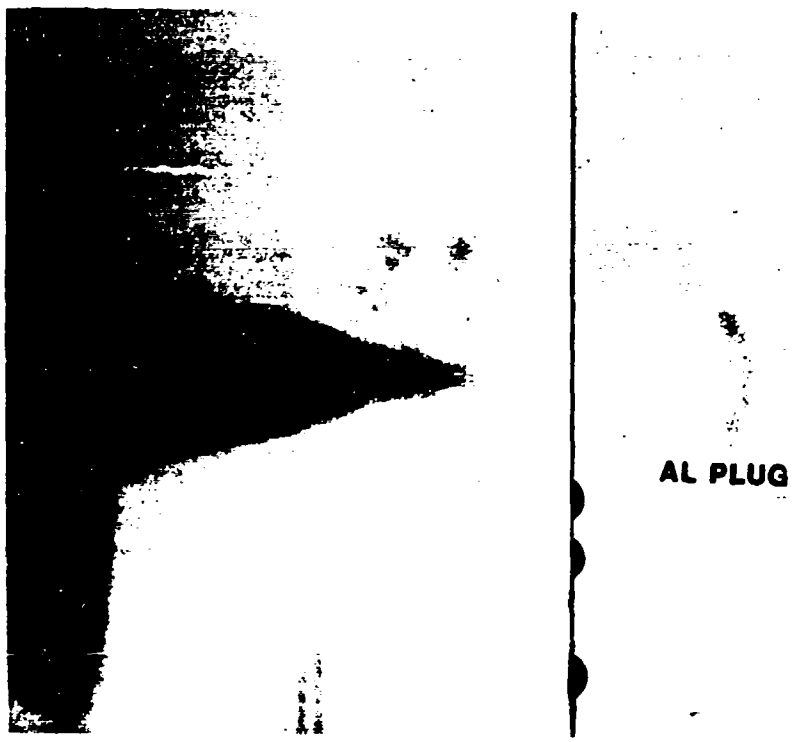

Figure 21. Flash Radiograph Produced 35.5 μsec After Initiation of Round 4105.

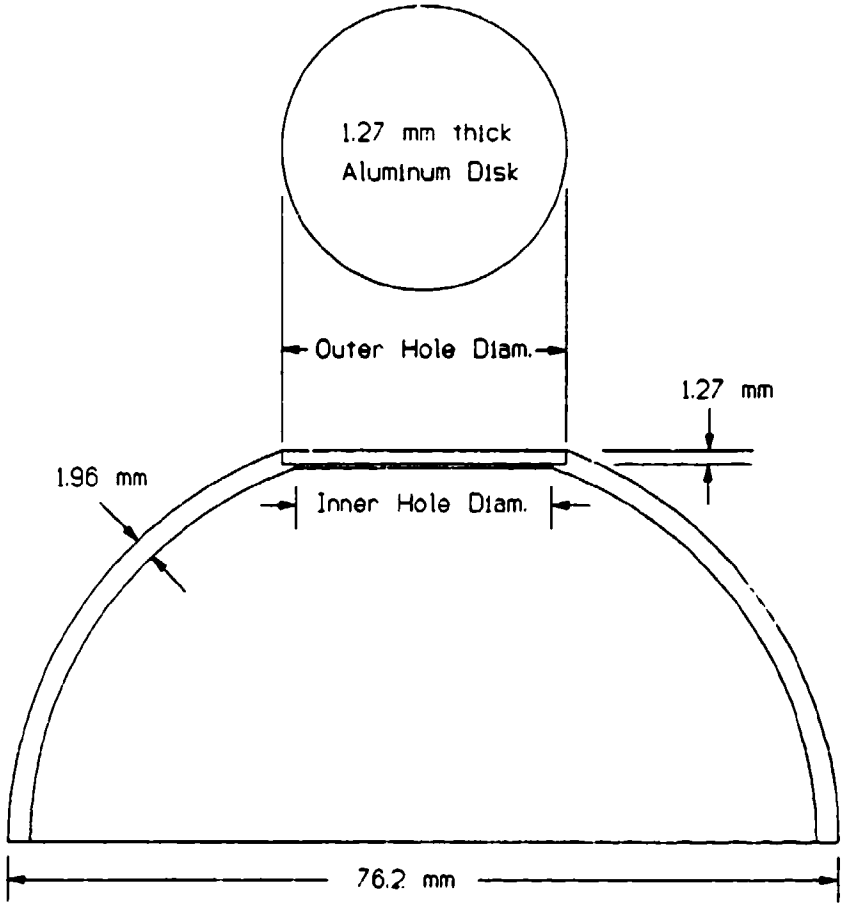

Figure 22. Final Liner Modification and Plug Design.

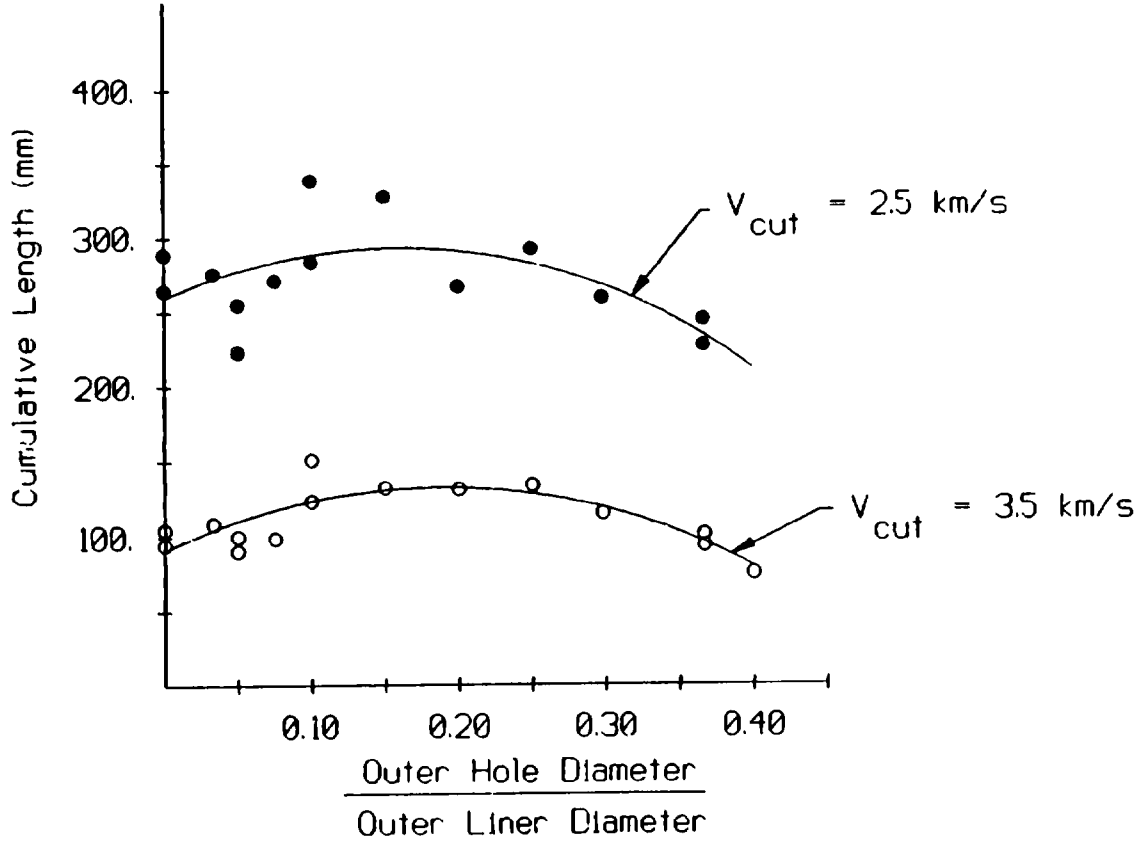

Figure 23. Cumulative Jet Length vs. Hole Size.

necessary since the total film length available does not allow all of the jet particles to appear on the film. The total jet length is plotted for two cutoff velocities, 3.5 km/sec and 2.5 km/sec. The cutoff velocity of 3.5 km/sec was chosen to show the behavior of the leading portion of the jet, which is most affected by removing the pole of the liner. The cutoff velocity of 2.5 km/sec was chosen because it is the lowest velocity for which data exists from every experiment. The line shown through each data set is a second-order least squares fit of the data. As shown in Figure 23, the total jet length increases with the hole diameter to a maximum and then slowly decreases.

Figure 24 is a plot of the total jet mass versus the ratio of outer hole diameter-to-outer liner diameter. The cutoff velocities are the same as in Figure 23, and, again, a second order least squares fit of the data is shown. In addition, the dashed line represents the theoretical reduction in jet mass assuming that all of the mass removed from the liner would have entered the jet and travelled faster than the cutoff velocity. The initial mass chosen for the theoretical curve is the average of the total measured jet mass from the experiments involving liners with no hole at the pole. The shape of the theoretical curve matches the data quite well, although the theoretical curve for the 2.5 km/sec cutoff velocity is offset from the majority of the data.

Figures 25 and 26 are plots of the cumulative jet momentum and energy versus the hole diameter-to-liner diameter ratio. Again, cutoff velocities of 2.5 km/sec and 3.5 km/sec were used, and a second order least squares fit of the data was performed. The shape of these curves closely resemble that of the cumulative jet mass. In fact, the cumulative jet momentum divided by the cumulative jet mass for each hole diameter yields a nearly constant value. The cumulative jet energy divided by the cumulative jet mass also yields a nearly constant value for each experiment. Tables 7 and 8 give the cumulative values of jet mass, momentum, and kinetic energy, as well as, the ratios of cumulative momentum-to-cumulative mass and cumulative energy-to-cumulative mass.

The breakup time of the shaped-charge jet decreases rapidly as the ratio of outer hole diameter-to-outer liner diameter is increased, as shown in Figure 27. The breakup time is dependent upon several factors. First, as the tip velocity is increased the velocity gradient in the jet is also increased causing the jet to stretch and break at a faster rate. Second, as the hole size is increased symmetry in the collision of the liner walls at the axis is more difficult to maintain. The breakup time will decrease if any asymmetries or misalignments are present during the jet formation process. Third, since the holes were machined in the pole of a full hemispherical liner, residual

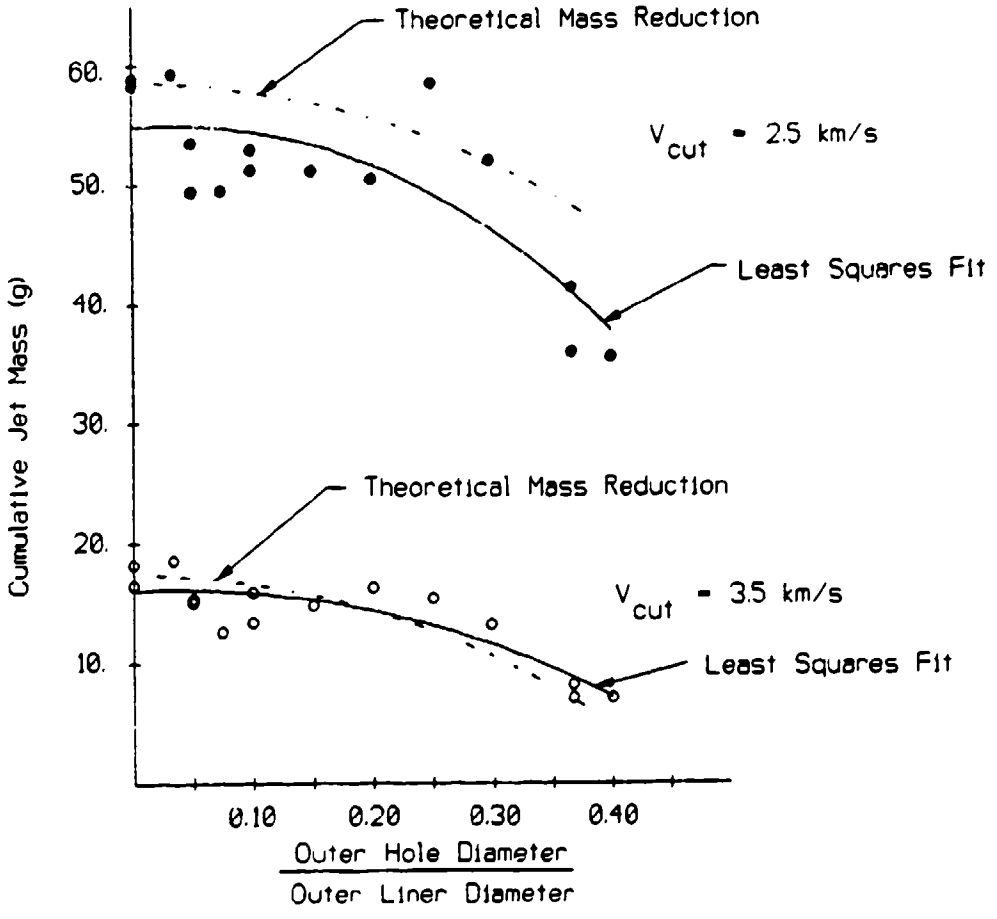

Figure 24. Cumulative Jet Mass vs. Hole Size.

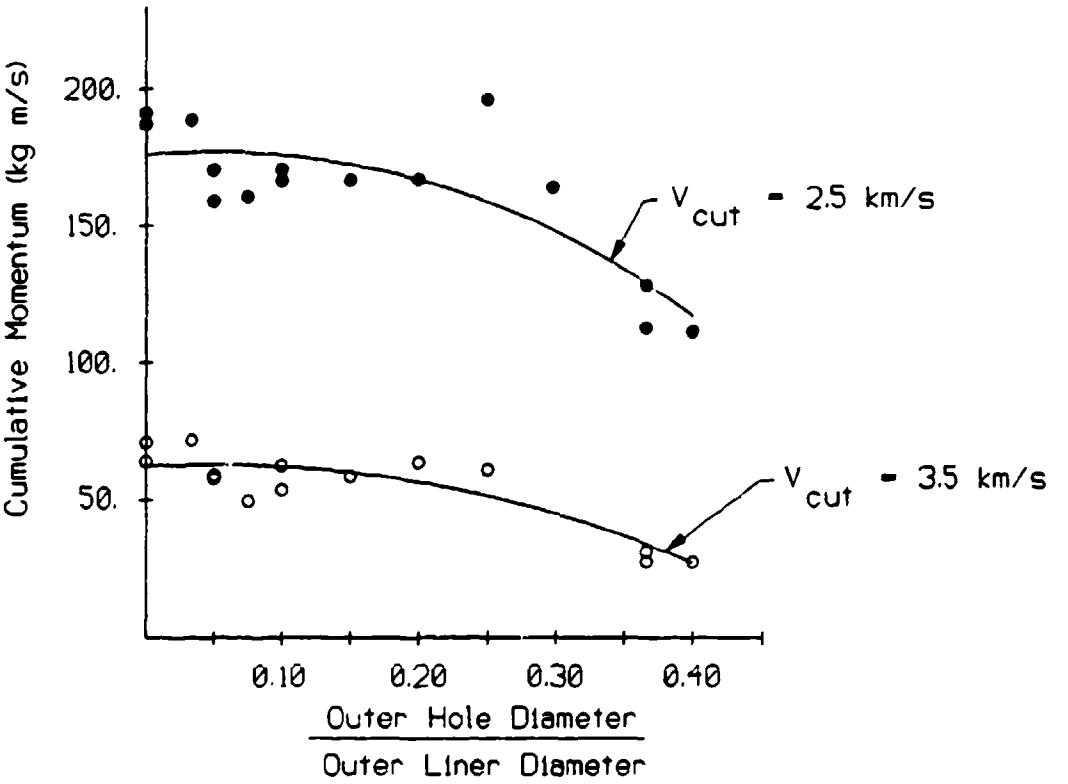

Figure 25. Cumulative Jet Momentum vs. Hole Size.

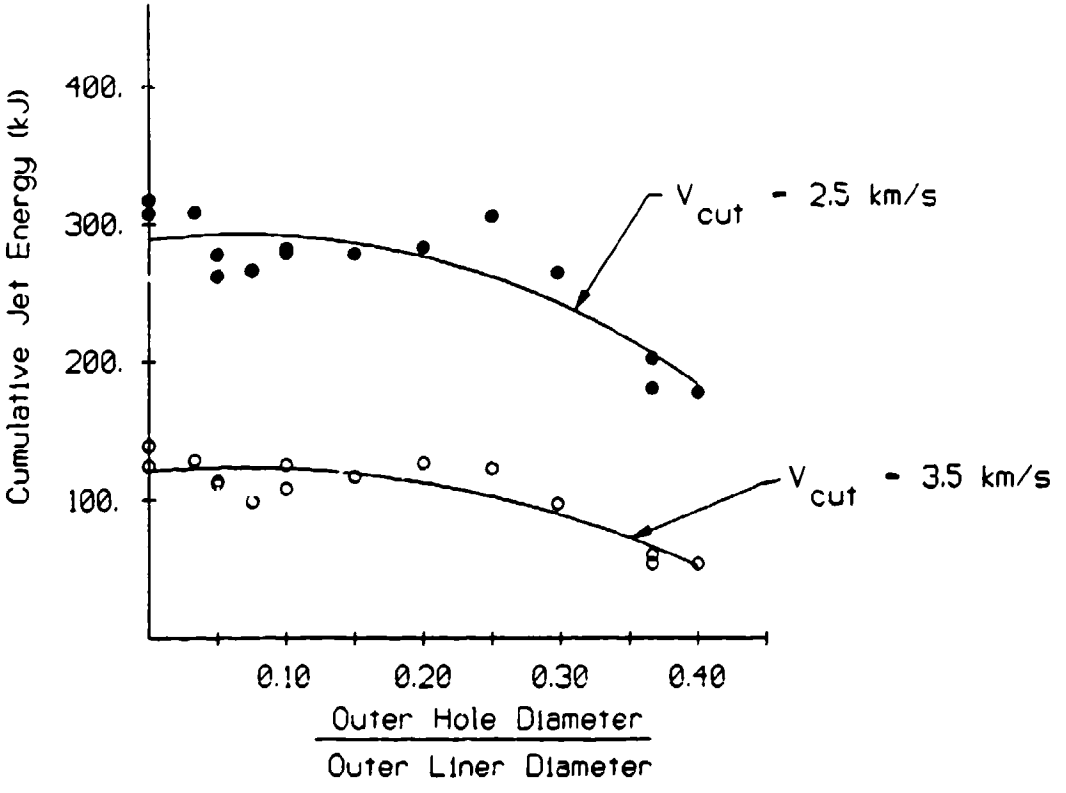

Figure 26. Cumulative Jet Energy vs. Hole Size.

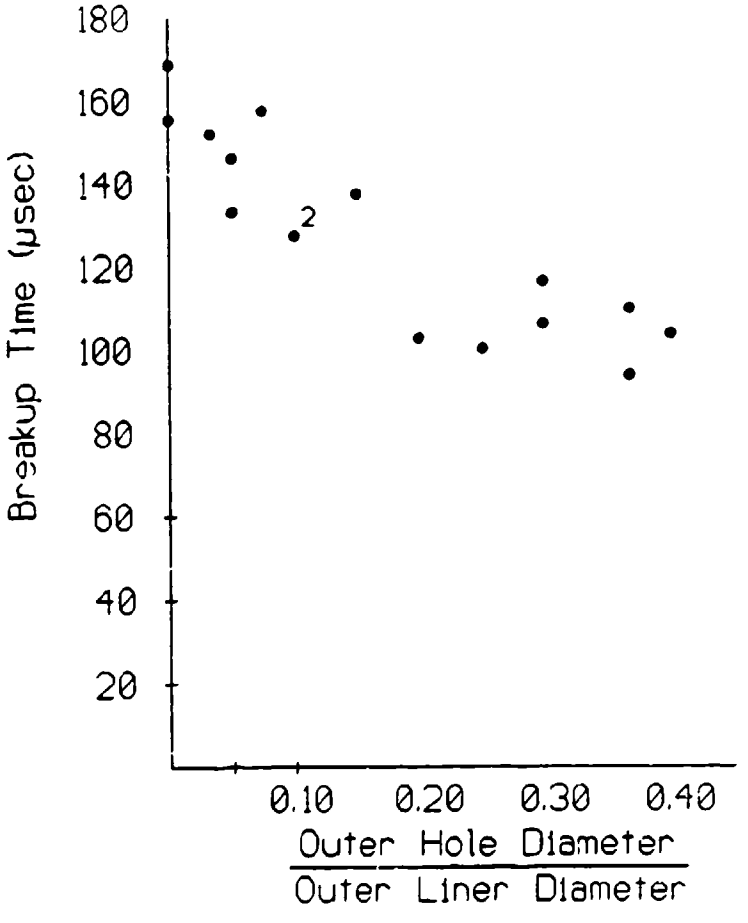

Figure 27. Jet Breakup Time vs. Hole Size.

Table 7. Cumulative Momentum and Energy (Cutoff Velocity = 2.5 km/sec)

Round Number	Outer Hole Diameter (mm)	Total Mass (gm)	Total Momentum (kg m/sec)	Total Energy (kJ)	Momentum / Mass	Energy / Mass
4066	0.0	58.3	187.1	307.6	3.21	5.28
4135	0.0	58.9	191.2	317.6	3.25	5.39
4141	2.5	59.3	188.7	308.4	3.18	5.20
4134	3.8	49.4	159.0	262.0	3.22	5.30
4146	3.8	53.5	170.4	277.8	3.19	5.19
4145	5.7	49.5	160.5	266.1	3.24	5.38
4129	7.6	52.9	170.5	282.3	3.22	5.34
4140	7.6	51.2	166.4	278.8	3.25	5.45
4127	11.4	51.1	166.4	278.2	3.26	5.44
4130	15.2	50.4	166.8	282.8	3.31	5.61
4131	19.1	58.4	185.7	305.1	3.18	5.22
4105	22.7	51.9	163.6	264.1	3.15	5.09
4064	27.9	35.9	112.6	180.5	3.14	5.03
4065	27.9	41.3	127.9	202.1	3.10	4.89
4128	30.5	35.5	111.1	177.5	3.13	5.00

Table 8. Cumulative Momentum and Energy (Cutoff Velocity = 3.5 km/sec)

Round Number	Outer Hole Diameter (mm)	Total Mass (gm)	Total Momentum (kg m/sec)	Total Energy (kJ)	Momentum / Mass	Energy / Mass
4066	0.0	16.5	64.2	124.8	3.89	7.56
4135	0.0	18.2	71.0	139.0	3.90	7.64
4141	2.5	18.6	71.8	138.9	3.86	7.47
4134	3.8	15.1	58.0	112.0	3.84	7.42
4146	3.8	15.4	59.1	113.7	3.84	7.38
4145	5.7	12.6	49.9	98.6	3.96	7.83
4129	7.6	13.4	53.8	108.4	4.01	8.09
4140	7.6	15.9	62.8	125.5	3.95	7.89
4127	11.4	14.8	58.7	116.8	3.97	7.89
4130	15.2	16.3	64.0	127.0	3.93	7.79
4131	19.1	15.4	61.2	122.8	3.97	7.97
4105	22.7	13.2	50.4	97.3	3.82	7.37
4064	27.9	8.2	31.3	60.5	3.82	7.38
4065	27.9	7.1	27.7	54.1	3.90	7.62
4128	30.5	7.1	27.6	54.2	3.88	7.63

stresses in the liner may have an effect. Finally, the explosive products are more likely to interfere in the liner collapse as the hole diameter is increased, leading to a shortened breakup time.

The most striking result of removing the pole of a hemispherical liner is observed in the behavior of the tip region. The tip velocity achieved by the baseline hemispherical liner, with no hole, was measured to be 4.2 km/sec. The tip velocity was increased to 5.3 km/sec by creating a hole 19.1 mm in diameter at the pole, for an increase of 26%. Figure 28 shows the tip velocity vs. the hole diameter-to-liner diameter ratio. A significant increase in tip velocity occurs between the 3.8-mm diameter hole and the 7.6-mm diameter hole. The average tip velocity measured from a liner with a 3.8-mm hole is 4.2 km/sec. The measured tip velocity increases slightly to 4.3 km/sec for a hole diameter of 5.7-mm. A further increase in hole diameter to 7.6 mm results in an average tip velocity of 4.9 km/sec. Two liners were tested with a hole diameter of 7.6 mm. The measured tip velocity of the first liner, Round 4129, was 5.0 km/sec. The measured tip velocity of the second liner, Round 4140, was 4.8 km/sec. The variation in the measured tip velocity is due to a small incoherent region at the tip of Round 4140. The particle, defined as the tip particle for Round 4140, is not the particle with the highest velocity, rather it is the first identifiable particle in each flash. Thus, the velocity of the fastest moving particle (which would usually be termed the tip particle) in the jet of Round 4140 is higher than the tip velocity which is reported. The tip region of Round 4129 is more coherent and, therefore, the velocity of nearly every jet particle is reported. The tip region from every liner with a hole diameter which is less than 7.6 mm was coherent. The tip velocity which was measured in each of the hole diameter experiments is given in Table 9.

The measured increase in tip velocity corresponds with a dramatic decrease in the mass of the tip particle. Figures 29 - 33 are radiographs of the first several jet particles from liners with no opening, a 2.5-mm opening, a 3.8-mm opening, a 5.7-mm opening, and a 7.6-mm opening at the pole, respectively. The first particle which is identifiable in each flash is marked as the tip particle in each of the four figures. In Figures 29 and 30 the tip particle is actually the leading jet particle. The tip particle from the liner with the 5.7-mm opening is preceded by a single, small particle visible in Figure 31. This particle is decelerating more rapidly than the succeeding particles and is eventually overtaken by the tip particle. The rapid deceleration of this particle, combined with its size and shape, indicate that it is the aluminum plug. The particles identified as the tip particle in Figure 32 and 33 are preceded by several small particles which could not be accurately identified in later flashes. Particles such as these account for much of the round-to-round variation observed

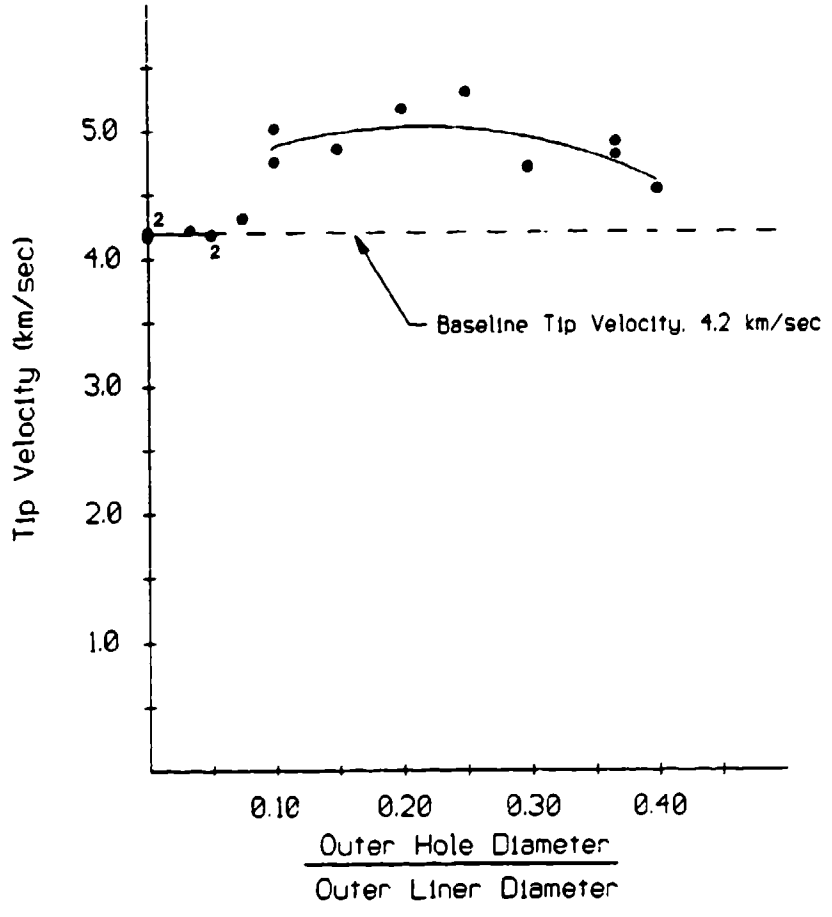

Figure 28. Jet Tip Velocity vs. Hole Size.

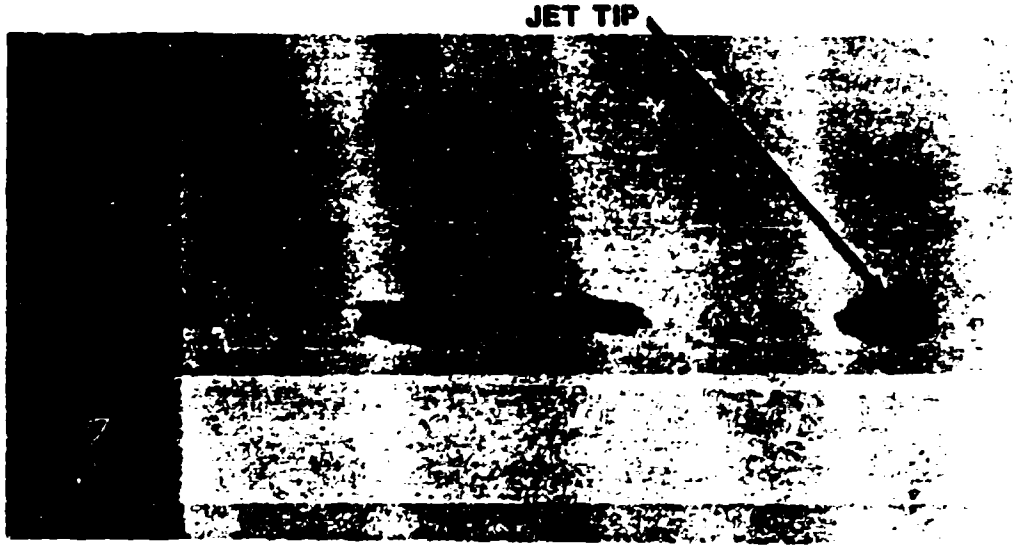

Figure 29. Flash Radiograph of the Tip Region of Round 4066.

Figure 30. Flash Radiograph of the Tip Region of Round 4141.

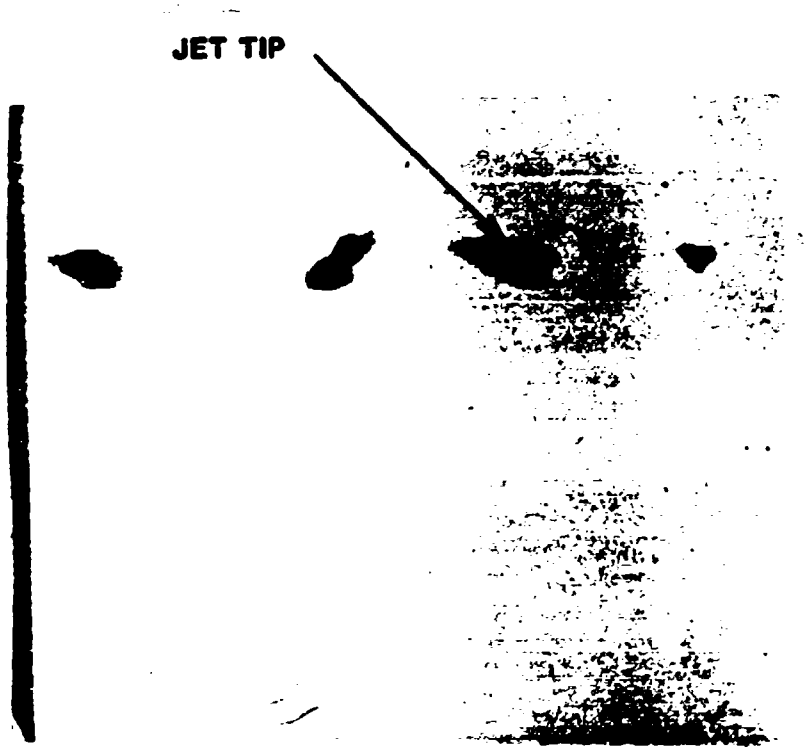

Figure 31. Flash Radiograph of the Tip Region of Round 4146.

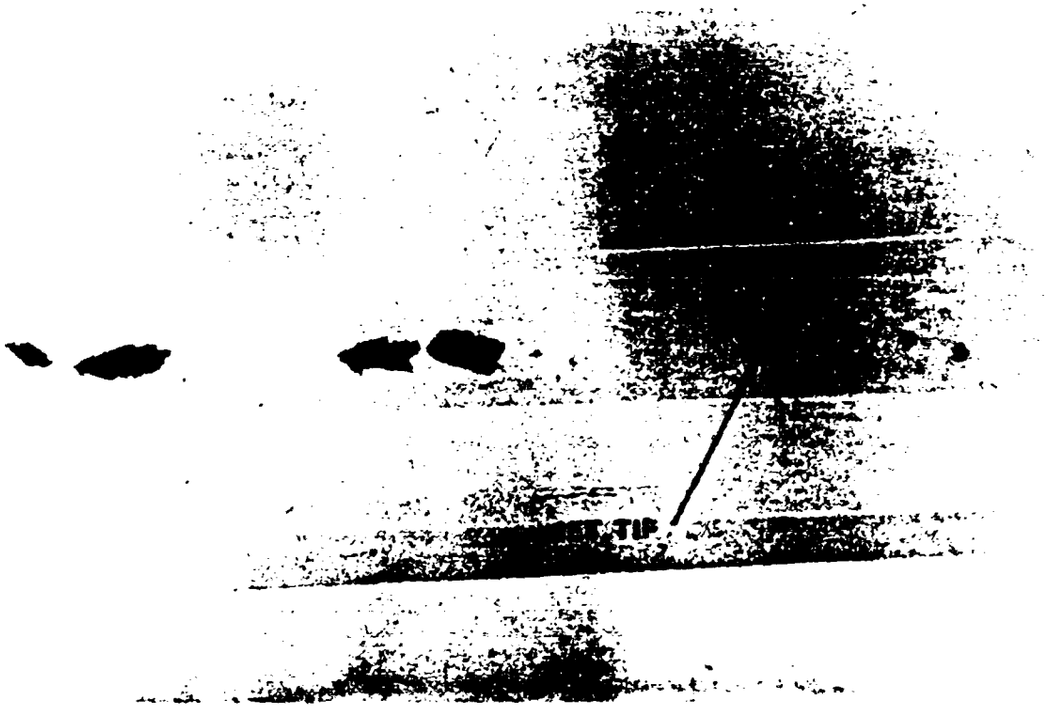

Figure 32. Flash Radiograph of the Tip Region of Round 4145.

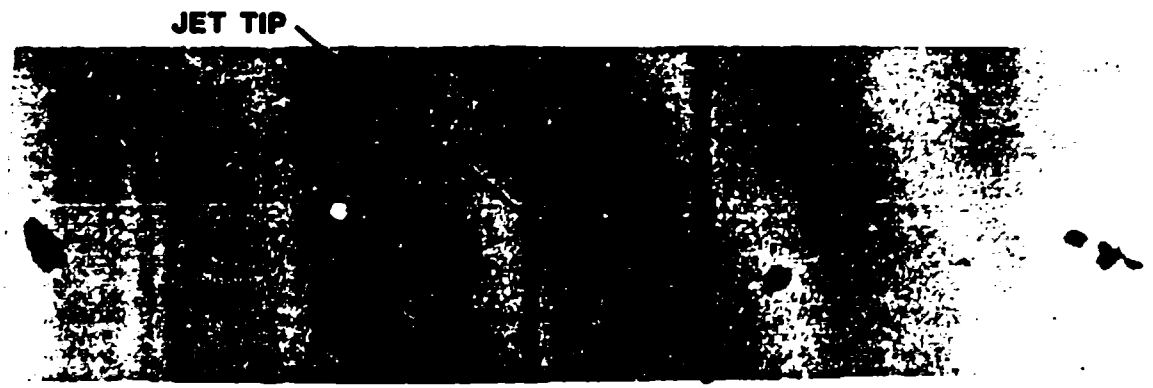

Figure 33. Flash Radiograph of the Tip Region of Round 4140.

Table 9. Measured Tip Mass and Velocity

Round Number	Outer Hole Diameter (mm)	Calculated Mass (mm)	Measured Velocity (km/sec)
4066	0.0	3.98	4.2 +/-0.2
4135	0.0	4.34	4.2 +/-0.2
4141	2.5	2.77	4.2 +/-0.2
4134	3.8	1.53	4.2 +/-0.2
4146	3.8	2.48	4.2 +/-0.2
4145	5.7	0.62	4.3 +/-0.2
4129	7.6	0.17	5.0 +/-0.2
4140	7.6	0.03	4.8 +/-0.2
4127	11.4	0.08	4.9 +/-0.2
4130	15.2	0.12	5.2 +/-0.7
4131	19.1	0.10	5.3 +/-0.7
4105	22.7	0.35	4.7 +/-0.7
4064	27.9	0.09	4.9 +/-0.2
4065	27.9	0.22	4.7 +/-0.2
4128	30.5	0.15	4.5 +/-0.2

from liners with hole diameters of 7.6 mm or greater. As shown in Figures 32 and 33, the size of the jet particles in the tip region decreases markedly for holes with diameters of 5.7 mm and 7.6 mm. This phenomena was only observed in the tip region, slower moving jet particles were of the same approximate size regardless of the hole diameter. Table 9 lists the measured tip particle mass for each of the hole diameter experiments performed. The tip mass is plotted versus the normalized hole diameter in Figure 34. The rapid decrease in tip particle size directly corresponds with the rapid increase in the observed tip velocity.

Flash radiographs of the collapse and jet formation process also show significant changes between the open-poled liners with a hole diameter greater than or equal to 7.6 mm and the liner with no hole. Figures 35 - 37 show the liner profile approximately 27 μsec after the charge was initiated for liners with no opening, a 3.8-mm opening, and a 7.6-mm opening, respectively. The liner with a 3.8-mm opening (see Figure 36) appears to collapse in much the same manner as the full hemispherical liner. However, a small protrusion is visible on the axis of symmetry. As the hole diameter is increased to 7.6 mm (see Figure 37) the protrusion becomes more pronounced and the leading edge of the liner, near the axis of symmetry, becomes more wedge-shaped. Figure 38 shows the liner profile 30 μsec after initiation for a 19.1-mm opening at the pole. At this instant the liner profile is entirely wedge-shaped and no longer displays any roundness in the tip region.

The decrease in jet diameter near the jet tip is also observed in radiographs taken at later times during the collapse process. Figure 39 shows the full hemispherical liner 45 μsec after initiation of the detonator. The liner forms into a rod which increases only slightly in diameter from the tip to the rear of the jet. Figures 40 and 41 are radiographs, taken 40 μsec after initiation, of a liner with a 3.8-mm and a 5.7-mm opening, respectively. The shape of the liners shown in Figures 40 and 41 closely resemble that of the baseline liner, although some disturbance is evident in the tip region of Figure 40. The disturbance may be caused by the aluminum plug interfering with the collapse. A significant decrease in the jet diameter near the tip is clearly evident for the liner with a 27.9-mm opening as shown in Figure 19. The radiograph shown in Figure 19 was taken 45 μsec after initiation. Note, that while the tip region is noticeably changed between Figures 38 and 19, the rear of the jets appear to be the same. Radiographs produced after the jet has stretched and broken also indicate that only particles in the tip region of the jet appear to be affected by the presence of an opening in the liner.

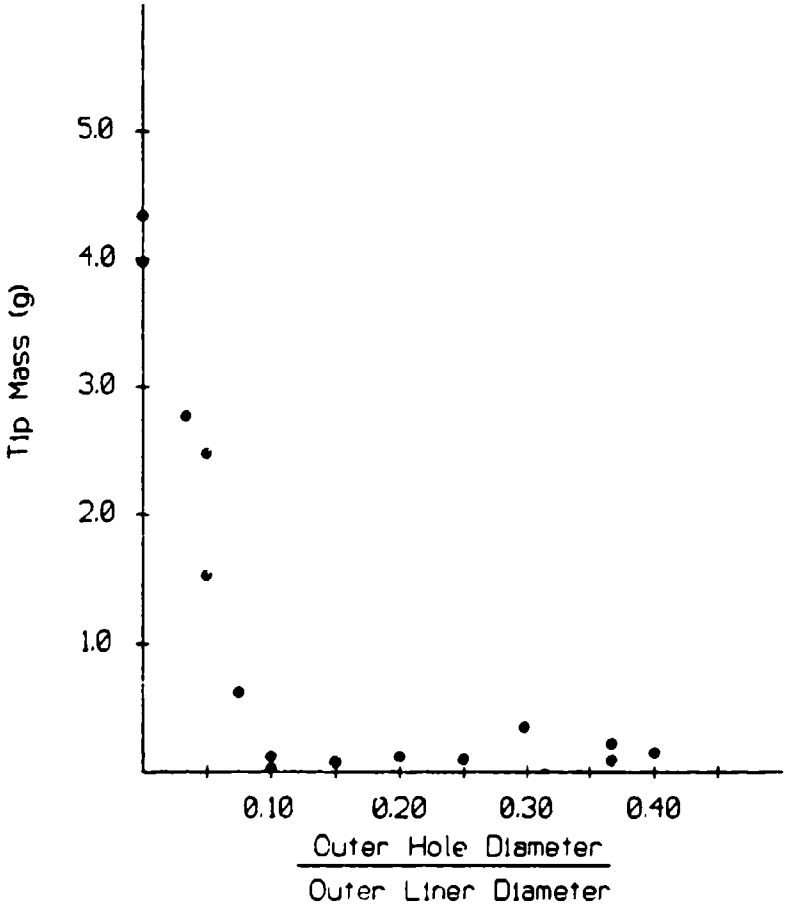

Figure 34. Tip Particle Mass vs. Hole Size.

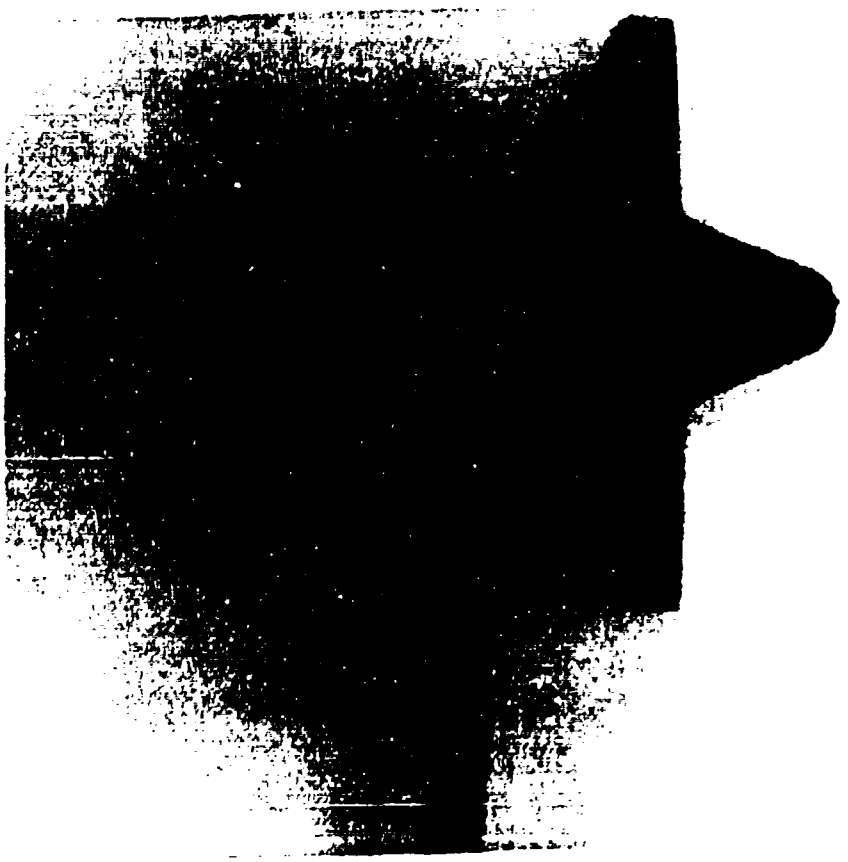

Figure 35. Flash Radiograph Produced 26.5 μsec After Initiation of Round 4135

Figure 36. Flash Radiograph Produced 26.5 μsec After Initiation of Round 4146.

Figure 37. Flash Radiograph Produced 27.0 μsec After Initiation of Round 4129.

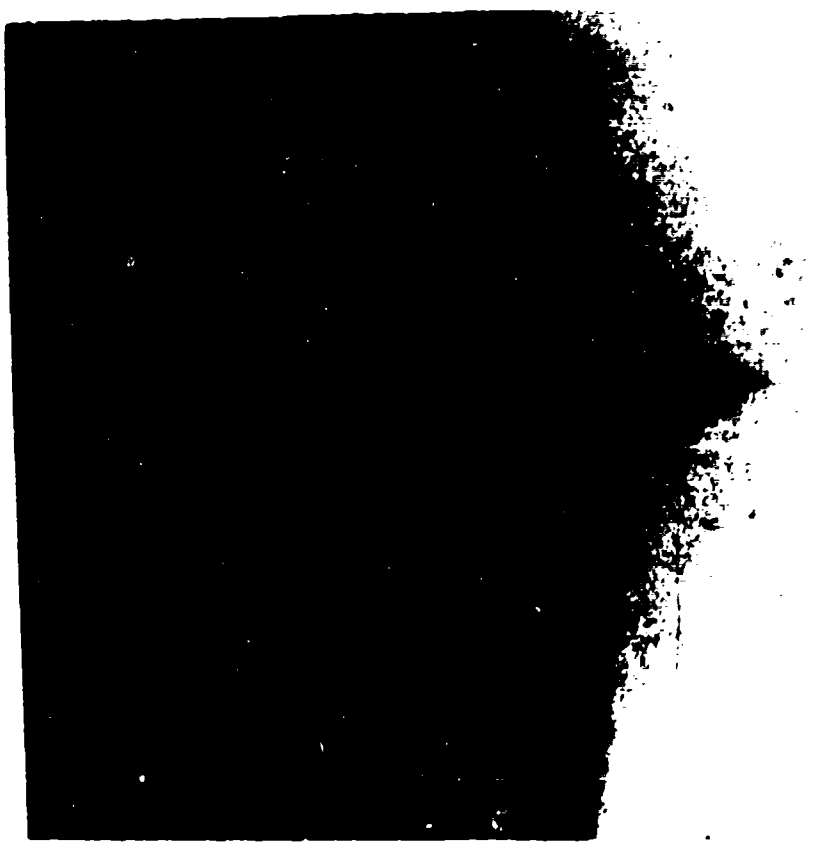

Figure 38. Flash Radiograph Produced 30.0 μsec After Initiation of Round 4131.

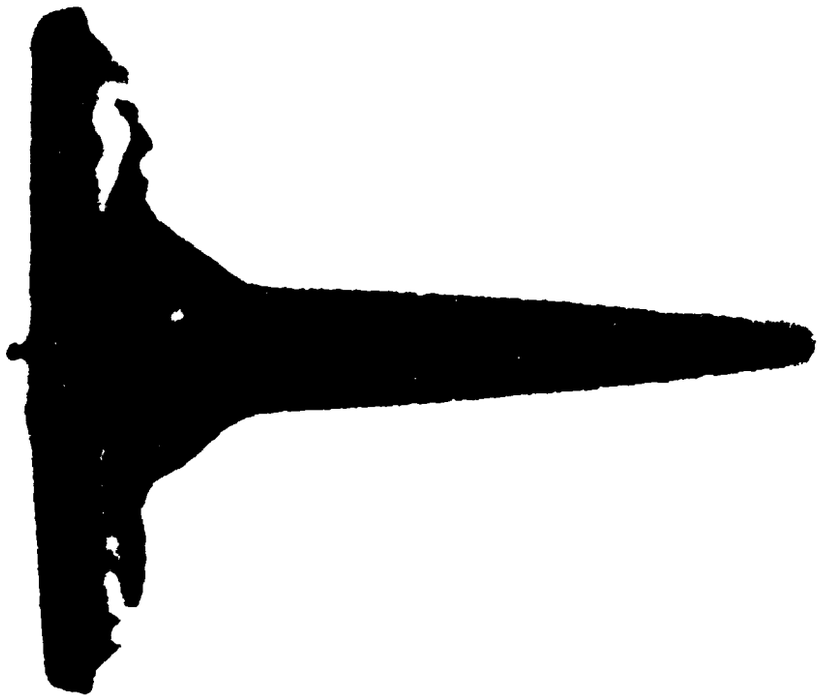

Figure 39. Flash Radiograph Produced 45.0 μsec After Initiation of Round 4066.

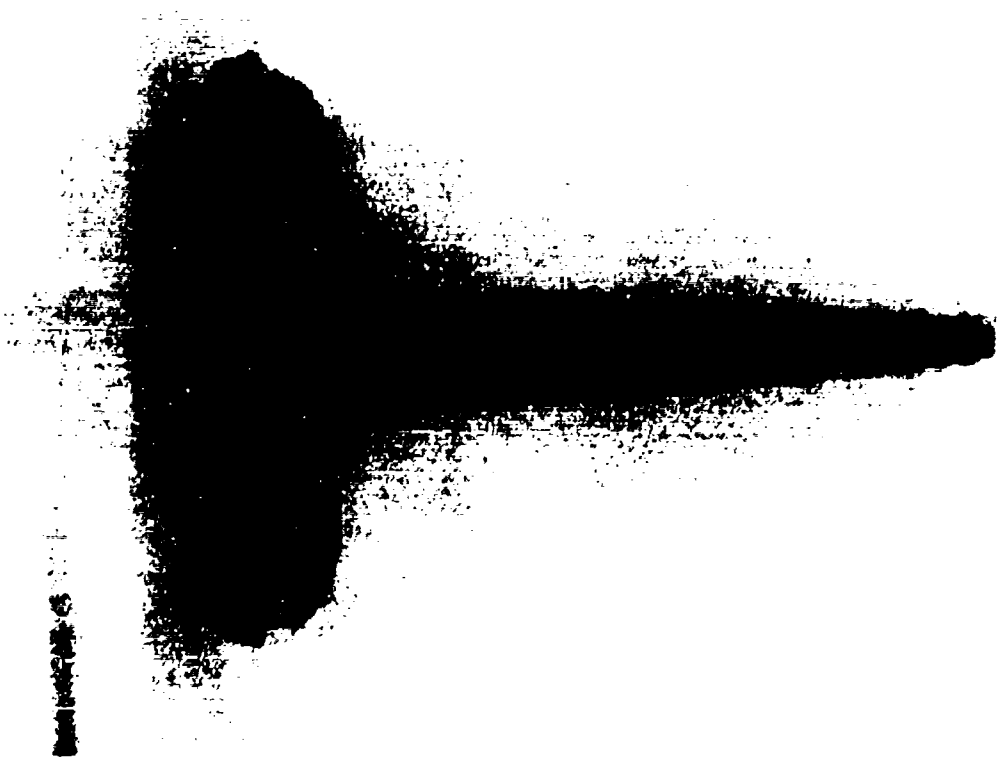

Figure 40. Flash Radiograph Produced 39.5 μsec After Initiation of Round 4134.

Note: The lines obscuring this image were caused by a static electric discharge

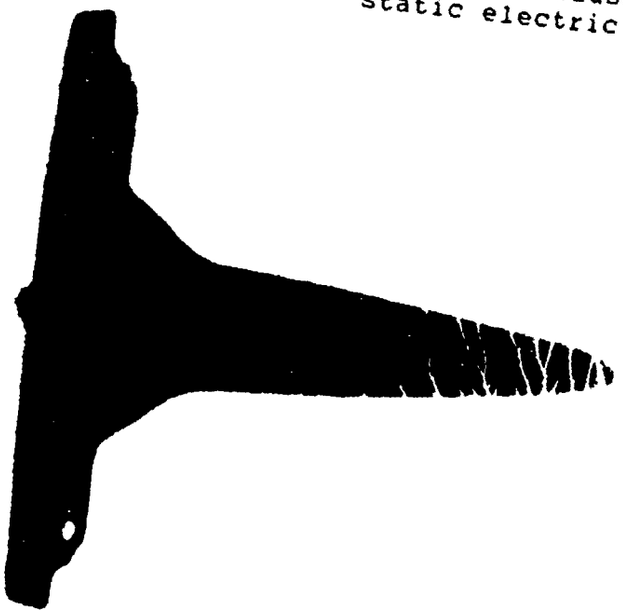

Figure 41. Flash Radiograph Produced 39.5 μsec After Initiation of Round 4145.

6. DISCUSSION

The results of this study help to explain the findings of earlier researchers (Walters and Zukas 1989; AFPAC 1946; Carnegie Institute 1946a, 1946b; Thomanek and Schlesiger 1969). Figure 42 is a plot of the tip velocity versus the ratio of outer hole diameter-to-outer liner diameter. The vertical dashed lines indicate values of relative hole size which were previously studied and/or recommended as optimal. Japanese researchers studied open-poled hemispherical liners extensively during World War II and determined that the ratio of hole diameter-to-liner diameter should be approximately 0.125. In the study performed by the Carnegie Institute of Technology (1946a), the ratio of the outer diameter of the spit-back tube-to-the outer liner diameter was 0.31. The Carnegie Institute did not study the effect of the hole size on the liner performance and, therefore, did not recommend an optimum size. However, the design used by the Carnegie Institute did provide increased target penetration and is very close to the ratio of inner cone diameter-to-outer liner diameter recommended by Thomanek, et al. (1969), and the value used in the German Racketenpanzerbuchse (Carnegie Institute 1946b).

The ratio which was chosen to be optimal by the Japanese is in agreement with the results of the present study. The penetration of a shaped-charge jet into hardened steel is most dependent on the jet tip velocity, cumulative jet length, and jet breakup time. Both the jet tip velocity and jet length are maximized when the relative hole size is in the range of 0.15 to 0.25. However, the breakup time decreases steadily as the hole diameter is increased. Thus, there exists a tradeoff between increased tip velocity and jet length and decreased jet breakup time. In order to take advantage of the increased tip velocity, the normalized hole size must be at least 0.10. For ratios greater than 0.10, both the jet length and the tip velocity increase slowly with increased hole diameter, while the jet breakup time continues to rapidly decrease. Thus, the optimal ratio of outer hole diameter-to-outer liner diameter, as determined by the jet characteristics, is between 0.10 and 0.20. In order to verify this a series of penetration-standoff curves need to be developed for several hole sizes. However, an experimentally derived penetration standoff curve requires numerous experiments, as evidenced by Table 1, and was not within the scope of this study.

The values recommended by Thomanek and Schlesiger (1969) and utilized in the German Racketenpanzerbuchse (Carnegie 1946b) and in the spit-back tube study (Carnegie 1946a) are based on liner designs in which the pole or apex is removed and replaced with a cone or tube which can contribute to the shaped-charge jet. The tip velocity achieved by an open-poled liner changes only slightly over a ratio range of 0.10 to 0.37. Thus, the values used by the Carnegie Institute,

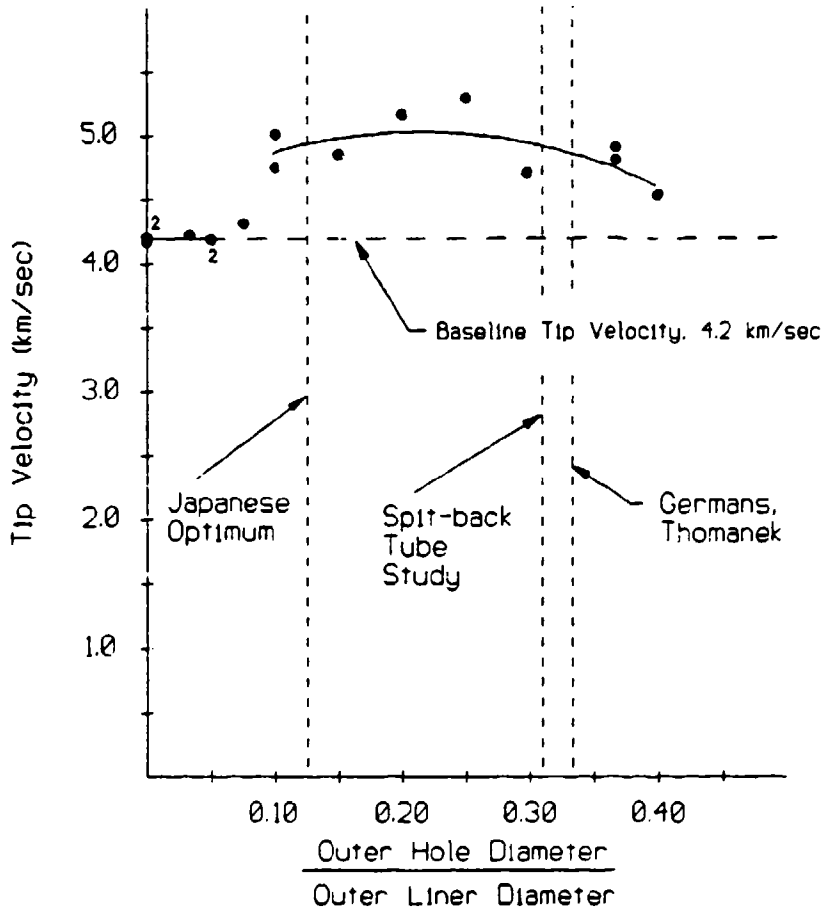

Figure 42. Comparison of Tip Velocity Behavior and Earlier Research.

Thomanek, and the German warhead design still take advantage of the increase in tip velocity which was observed in the present study. In addition, a ratio of 0.3 or greater allows a larger diameter cone to be placed at the pole and, therefore, allows the inner cone to contribute more mass to the shaped-charge jet.

The reason for the observed liner behavior is not well understood, but two theories, the "collapse-transition" theory and the "mass build-up" theory, are offered. The first explanation for the observed increase in tip velocity for an open-poled hemispherical shaped charge is that the pole of the liner impedes the collapse of subsequent liner material. Hydrocode calculations (Walters and Golaski 1987) predict that the material from the pole of the liner forms into a cylinder along the axis of symmetry. This cylinder of liner material does not allow the collapsing walls of the hemisphere to collide at the axis. When the pole is removed, the material in the liner nearest the axis of symmetry is allowed to reach the axis, as shown in Figure 37. The resulting collision and mass-splitting process resembles that described in Pugh et al. 1952, and allows the jet tip to attain a higher final velocity. Although the jet formation process of an open-poled hemispherical liner is similar to that of a conical liner, the collapse angle (the angle at which the liner walls collide at the axis) is greater than that typically observed with a conical shaped charge, thus, the open-poled hemispherical liner provides a "collapse-transition" between a hemispherical shaped charge and a conical shaped charge. This explanation is supported by the change in the jet characteristics. That is, the observed jet characteristics showed a higher tip velocity and a lower jet mass, diameter, and jet breakup time, all of which indicate a transition between the characteristics of a hemispherical shaped-charge jet and a conical shaped-charge jet (Walters and Zukas 1989).

The "mass build-up" theory for the observed increase in tip velocity is similar to the theory of the origin of the tip particle of a conical shaped-charge jet (Carleone et al. 1977). The tip particle of a conical shaped-charge jet originates from a mass build-up which occurs because the material near the apex of the liner can not reach its final collapse velocity before colliding at the axis of symmetry. In the case of a hemispherical liner, the pole of the liner can travel unconstrained to its terminal velocity. However, flash radiographs (Singh 1955; Kiwan and Arbuckle 1977) and high-speed photographs (Walters and Zukas 1989) of collapsing hemispherical liners indicate that the liner turns inside out from the pole, indicating that material near the pole is pushed from the explosive cylinder in the same manner as an explosive flyer plate. Thus, as subsequent liner material forms a jet, it will overtake the material originating from the pole. If the material from the pole and the faster moving material are assumed to undergo a perfectly inelastic collision, the result will

be to increase the tip particle mass and to decrease the velocity of the subsequent material. Thus, when the pole is removed, the tip particle mass is decreased and the tip velocity is increased.

The "mass build-up" theory is supported by the similarity in the behavior of the jet tip reported in this study and in the study by Carleone, et al. (1977), involving a conical liner. In both studies the tip velocity was not shown to begin to decrease significantly until approximately 40% of the liner diameter was rendered ineffective. In addition, both studies observed a steady decrease in tip mass as the hole diameter increased. However, there are several factors which tend to refute the "mass build-up" theory. First, if the tip particle of a hemispherical liner did originate from a mass build-up process, one would expect the tip particle to be much more massive than the particles immediately following it, as in the case of a conical shaped-charge jet. The tip particle of the baseline hemispherical shaped-charge jet used in this study is similar in size to the other jet particles. Second, this theory appears to be in conflict with hydrocode calculations (Walters and Golaski 1987) which predict the material from the pole is distributed in a cylinder along the axis of symmetry. Finally, neither of the two theories presented here seem to explain the rapid increase in tip velocity which was observed between the hole diameter-to-liner diameter ratios of 0.05 and 0.10.

7. CONCLUSIONS

The collapse process and jet characteristics of a shaped charge with a hemispherical liner can be significantly altered by placing an opening in the pole of the liner. The effect of the opening is strongly dependent on its diameter. The changes observed in the liner behavior are most dramatically characterized by the change in jet tip velocity as a function of the hole diameter. The jet tip velocity was nearly constant, 4.2 km/sec, for hole diameter-to-liner diameter ratios of less than 0.075. For a ratio of 0.10, the tip velocity increased to 4.9 km/sec and reached a maximum of 5.3 km/sec for a hole diameter-to-liner diameter ratio of 0.25. Based on the trends of the tip velocity, cumulative jet length, and jet breakup time, an optimum ratio, for which enhanced performance may be expected, was determined to be in the range of 0.10 to 0.20. However, a performance tradeoff exists between the increase in tip velocity and jet length and the decrease in jet breakup time. These results correspond with the findings of Japanese and German research which was performed during the 1940s.

The mechanism by which the tip velocity is increased is still not well understood, but two explanations were presented. Both of the explanations assume that the pole of the liner impedes the motion of the subsequent liner material. The first explanation assumes that the material near the pole of the liner interferes in the collapse process and does not allow a collision at the axis of symmetry. Removing the pole allows the material to reach the axis and undergo a mass-splitting process similar to that of a conical liner. Thus, removal of the pole provides a "collapse-transition" between the collapse and formation mechanisms of a shaped charge with a hemispherical and a shaped charge with a conical liner. The second explanation assumes the pole of the liner does not impede the subsequent material until after the jet has formed and is analogous to the theory of the tip particle origin of a jet from a shaped charge with a conical liner. Neither of the two theories explain the abrupt increase in tip velocity which was observed for a hole diameter-to-liner diameter ratio of 0.10.

Two areas of further research in this topic would be valuable. First, penetration-standoff curves are needed to verify the optimum value of the hole diameter and to determine how the performance of a shaped charge with an open-poled hemispherical liner compares with a full hemispherical liner. Second, computer simulations of the liner collapse and jet formation process of shaped charges with open-poled hemispherical liners would be helpful in determining the mechanism by which the tip velocity is increased.

8. REFERENCES

Arbuckle, A. L., W. P. Walters, and C. L. Aseltine. "Analysis of Uniform Wall and Tapered Hemispherical Liners with Several Explosive Confinement Geometries." BRL-TR-2214, U.S. Army Ballistic Research Laboratory, Aberdeen Proving Ground, MD, 1980.

Aseltine, C. L., W. P. Walters, A. L. Arbuckle, and J. E. Lacetera. "Hemispherical Shaped Charges Utilizing Tapered Liners." Proc. 4th Int. Symp. on Ballistics, Monterey, CA, 17 - 19 October 1978.

Blische, H. J., and B. M. Simmons. "A Method for Reducing Data from Radiographs of Shaped Charge Jets." BRL-TR-02330, U.S. Army Ballistic Research Laboratory, Aberdeen Proving Ground, MD, 1981.

Carleone, J., R. Jameson, and P. C. Chou. "The Tip Origin of a Shaped Charge Jet." Propellants and Explosives 2, 126-130, 1977.

Carnegie Institute of Technology. "Steel Target Penetration in Air by Small-Scale Cavity Charges." OSRD Report No. 5604, National Defense Research Committee, Division 8, 1946a.

Carnegie Institute of Technology. "Protection Against Shaped Charges." OSRD Report No. 6384, National Defense Research Committee, Division 2, 1946b.

Chou, P. C., R. D. Ciccarelli, and W. P. Walters. "The Formation of Jets from Hemispherical Liner Warheads." Proc. 7th Int. Symp. on Ballistics, The Hague, Netherlands, 19 - 21 April 1983.

Chou, P. C., W. P. Walters, R. D. Ciccarelli, and G. W. Weaver. "Jet Formation Mechanics of Hemispherical Warheads." BRL-CR-545, U.S. Army Ballistic Research Laboratory, Aberdeen Proving Ground, MD, 1985.

Grace, F. I., S. K. Golaski, and B. R. Scott. "The Nature of Jets from Hemispherical Lined Explosive Charges." Proc. 8th Int. Symp. on Ballistics, Orlando, FL, October 1984.

Kiwan, A. R. and A. L. Arbuckle. "Study of Liner Collapse, Jet Formation and Characteristics from Implosive Shaped Charge Systems." BRL-R-2028, U.S. Army Ballistic Research Laboratory, Aberdeen Proving Ground, MD, 1977.

Kolsky, H. "A Study of the Mechanism of Munroe Charges, Part II -- Charges with Hemispherical Liners." Res. Supp., 2-2, 1949.

Lee, W. H. "High Explosive Modelling in 2D Euler Code for Shaped Charge Problems." Report LA-UR-85-2954, Los Alamos National Laboratory, Los Alamos, NM, 1985.

Ordnance Technical Intelligence Report Number 11. Office of the Chief Ordnance Officer GHQ, AFPAC, Tokyo, Japan, ca. 1946.

Paxton, C. V., and R. L. Summers. "The BRL 1-MeV Shaped Charge Test Facility." Proc. of the 1989 Flash Radiography Topical, Welches, OR, 14 - 18 August 1989.

Pugh, E., R. Eichelberger, and N. Rostoker. "Theory of Jet Formation by Charges with Lined Conical Cavities." J. Appl. Phys., 23, 532-536, 1952.

Segletes, S. B. "Drift Velocity Computations for Shaped-Charge Jets." BRL-MR-03306, U.S. Army Ballistic Research Laboratory, Aberdeen Proving Ground, MD, 1983.

Shepherd, W. C. F. "Strength of High Explosives and Effects Due to Shape." Science of Explosives, C. E. H. Bawn, G. Rotter (editors). Ministry of Supply, London, 1956.

Simon, J. "The Effect of Explosive Detonation Characteristics on Shaped Charge Performance." BRL-MR-2414, U.S. Army Ballistic Research Laboratory, Aberdeen Proving Ground, MD, 1974.

Singh, S. "On the Jet Formation by Explosives with Lined Hemispherical Cavities." Research Notes. Proc. Phys. Soc., 68B, 785-789, 1955.

Thomanek, F. R., and H. Schlesiger. "Projectile with High Initial Velocity." U.S. Pat. 3,478,685, 1969.

Walters, W. P. Unpublished work regarding Explosive Research Facility Round Number 3684. U.S. Army Ballistic Research Laboratory, Aberdeen Proving Ground, MD, tested October 1985.

Walters, W. P. "Explosive Loading of Metals and Related Topics." BRL-SP-56, U.S. Army Ballistic Research Laboratory, Aberdeen Proving Ground, MD, 1986.

Walters, W. P., G. H. Jonas, and J. A. Zukas. "Explosive Loading of Lead Hemispherical Liners." Comput. Struct., 20, 615-621, 1985.

Walters, W. P., and J. A. Zukas. Fundamentals of Shaped Charges. New York: John Wiley and Sons, 1989.

Walters, W. P., and S. K. Golaski. "Hemispherical and Conical Shaped Charge Liner Collapse and Jet Formation." BRL-TR-2781, U.S. Army Ballistic Research Laboratory, Aberdeen Proving Ground, MD, 1987.

APPENDIX A:

LINER DESIGNS

INTENTIONALLY LEFT BLANK

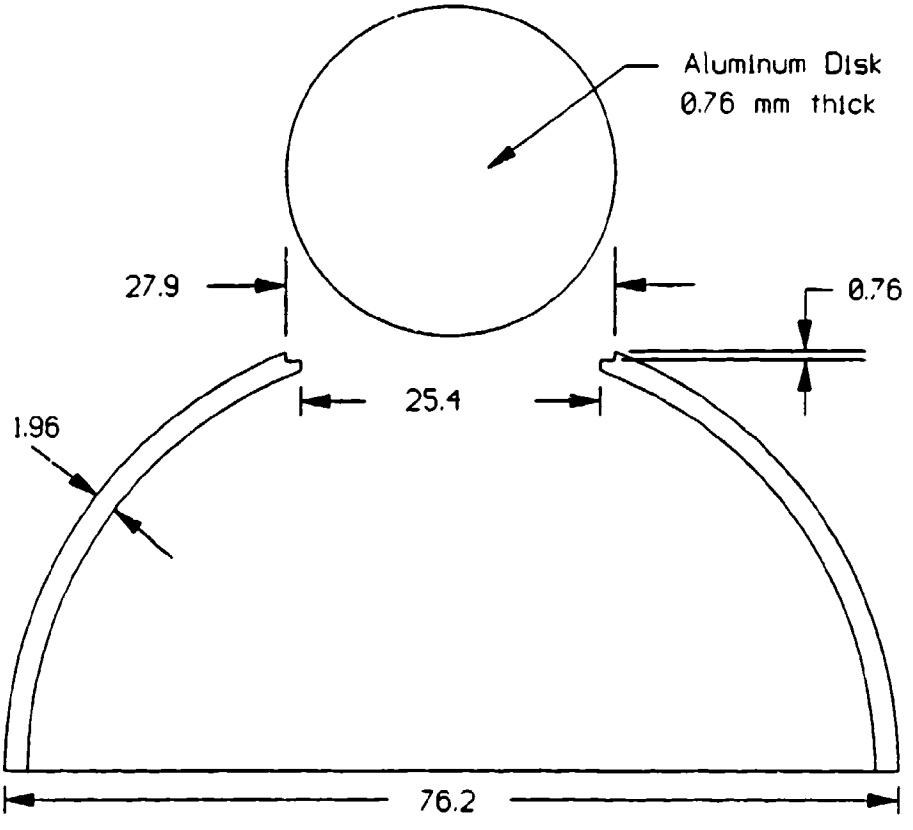

Figure A-1. Liner and Plug Design for Rounds 4064 and 4065.

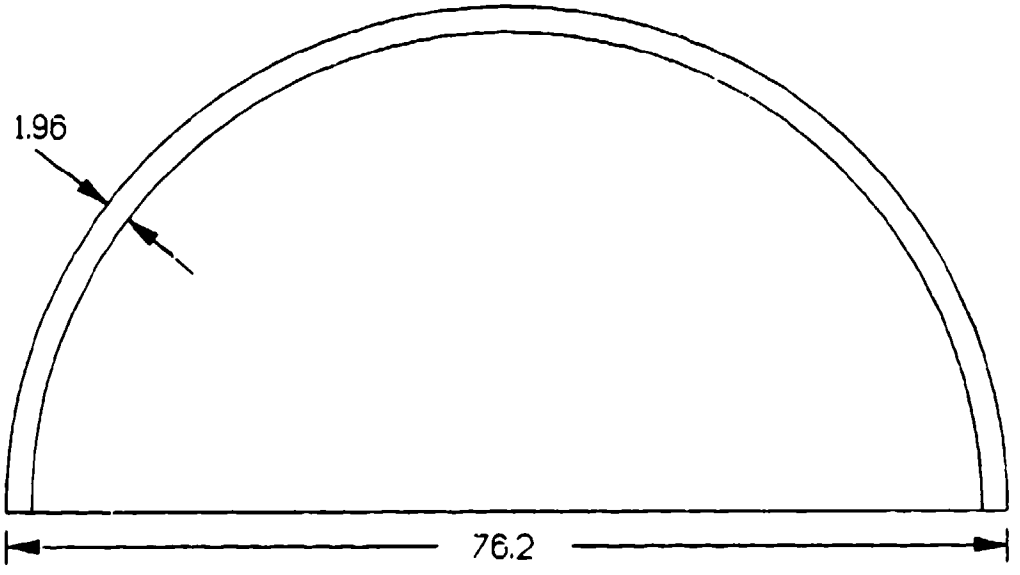

Figure A-2. Baseline Liner Design for Rounds 4066 and 4135.

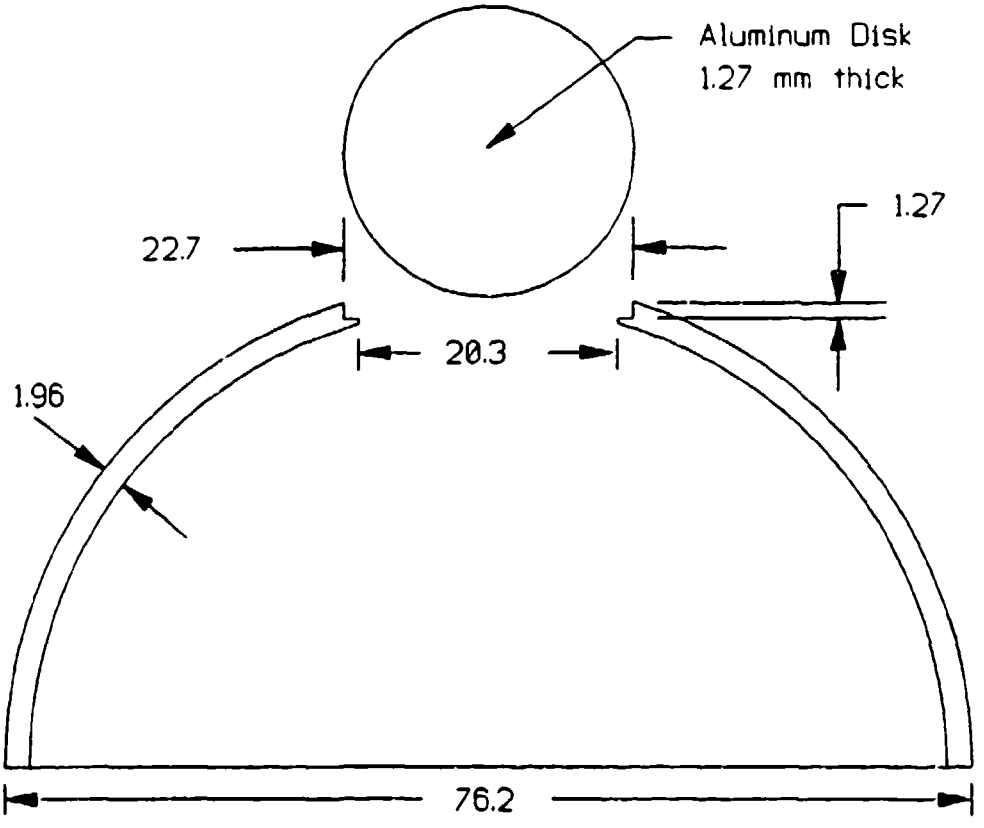

Figure A-3. Liner and Plug Design for Round 4105.

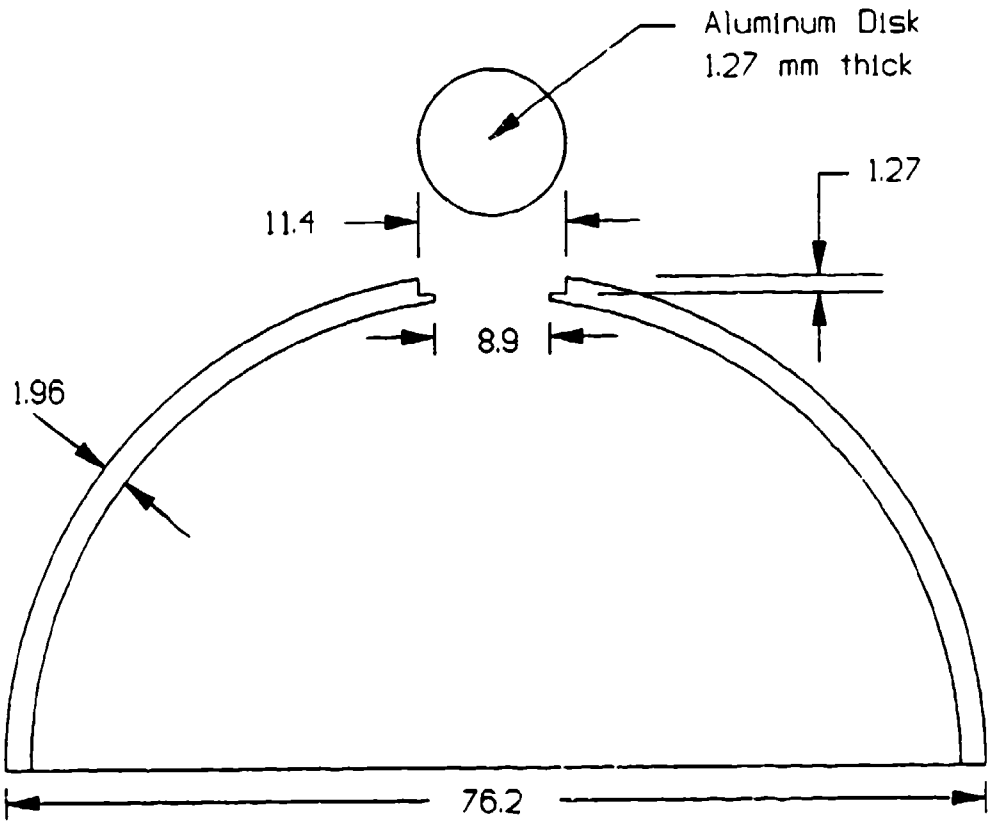

Figure A-4. Liner and Plug Design for Round 4127.

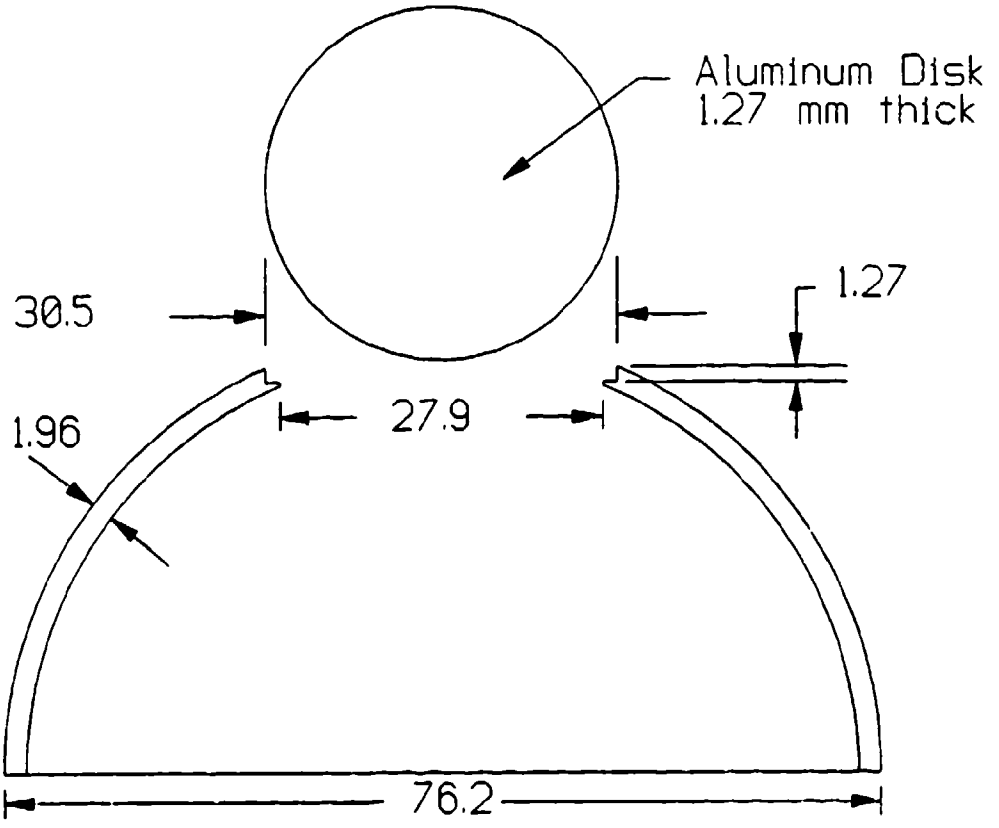

Figure A-5. Liner and Plug Design for Round 4128.

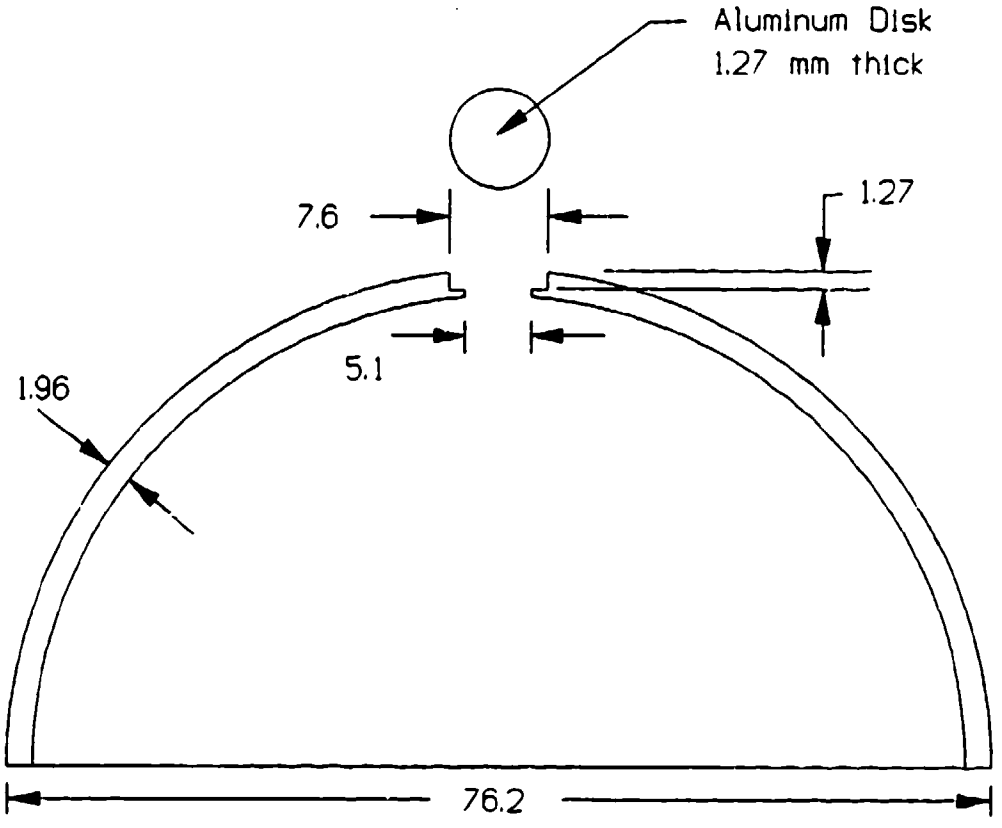

Figure A-6. Liner and Plug Design for Rounds 4129 and 4140.

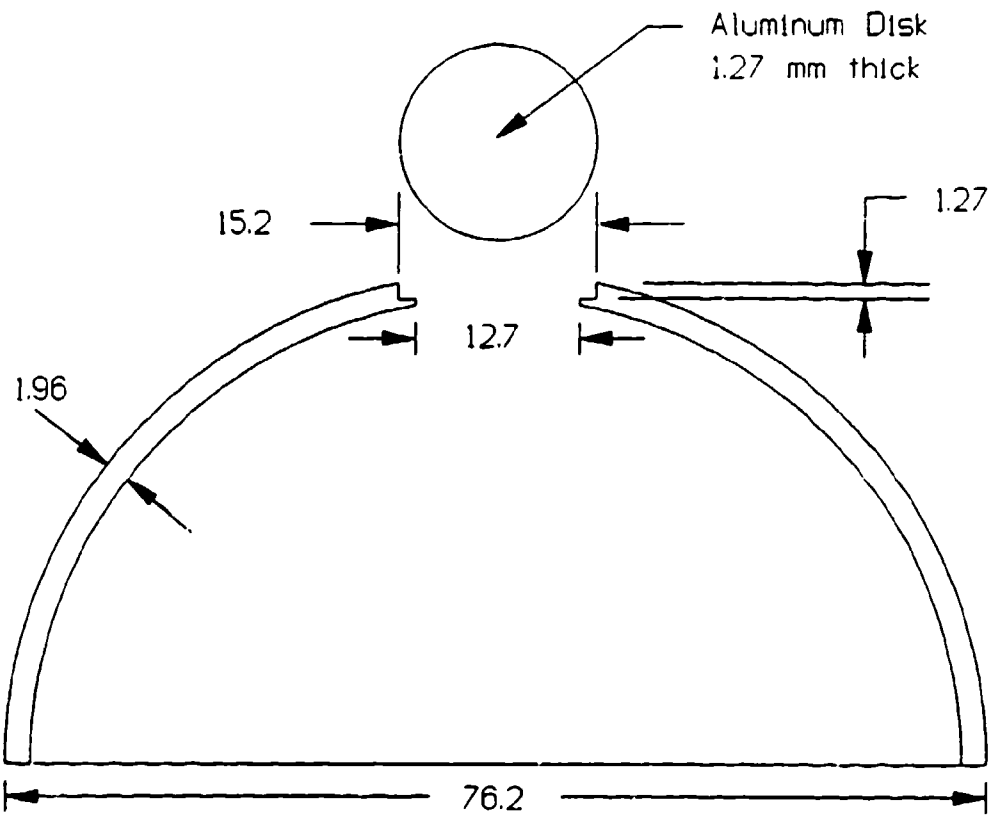

Figure A-7. Liner and Plug Design for Round 4130.

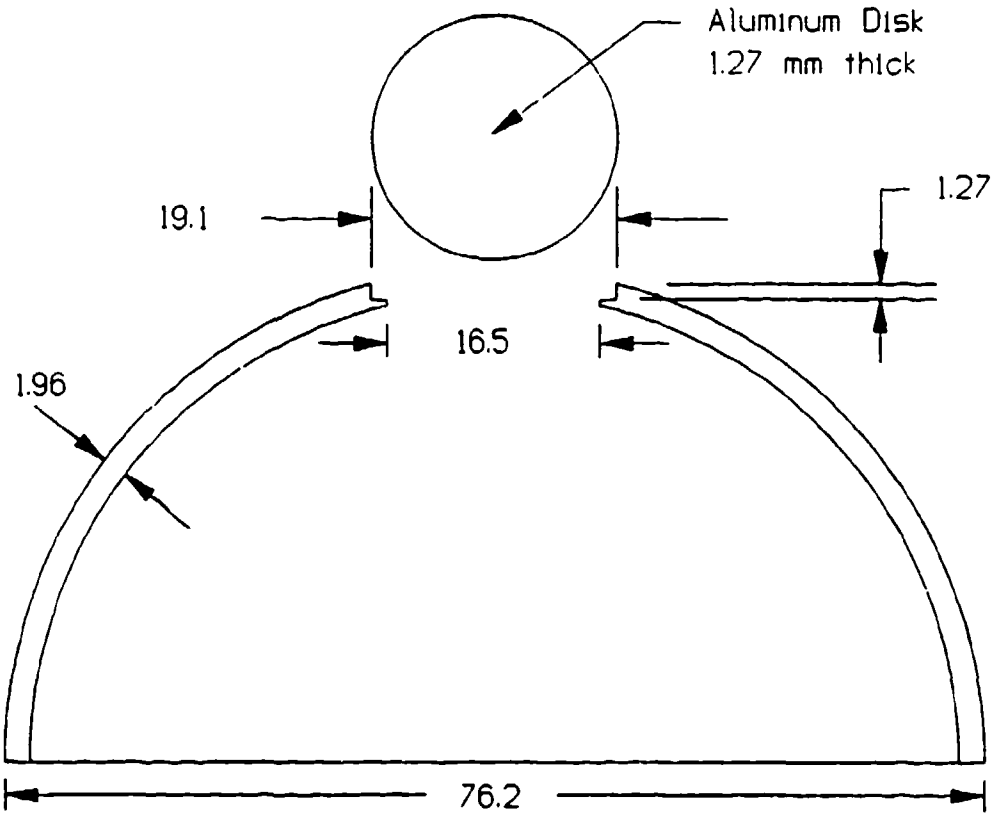

Figure A-8. Liner and Plug Design for Round 4131.

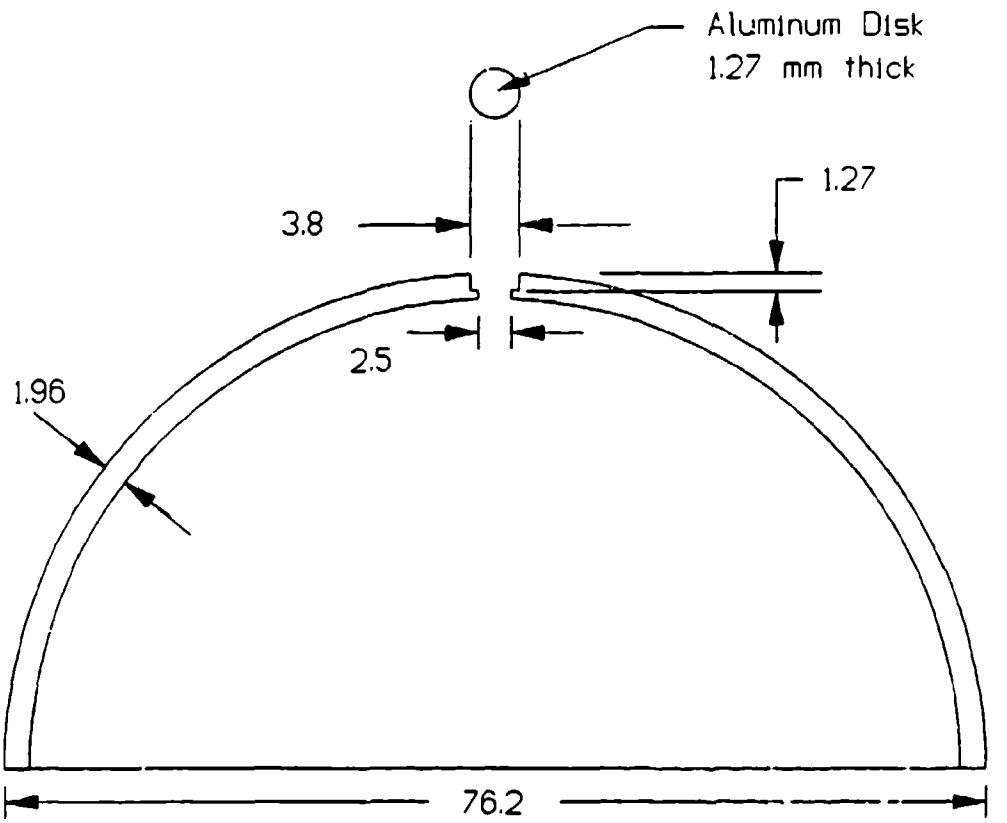

Figure A-9. Liner and Plug Design for Rounds 4134 and 4146.

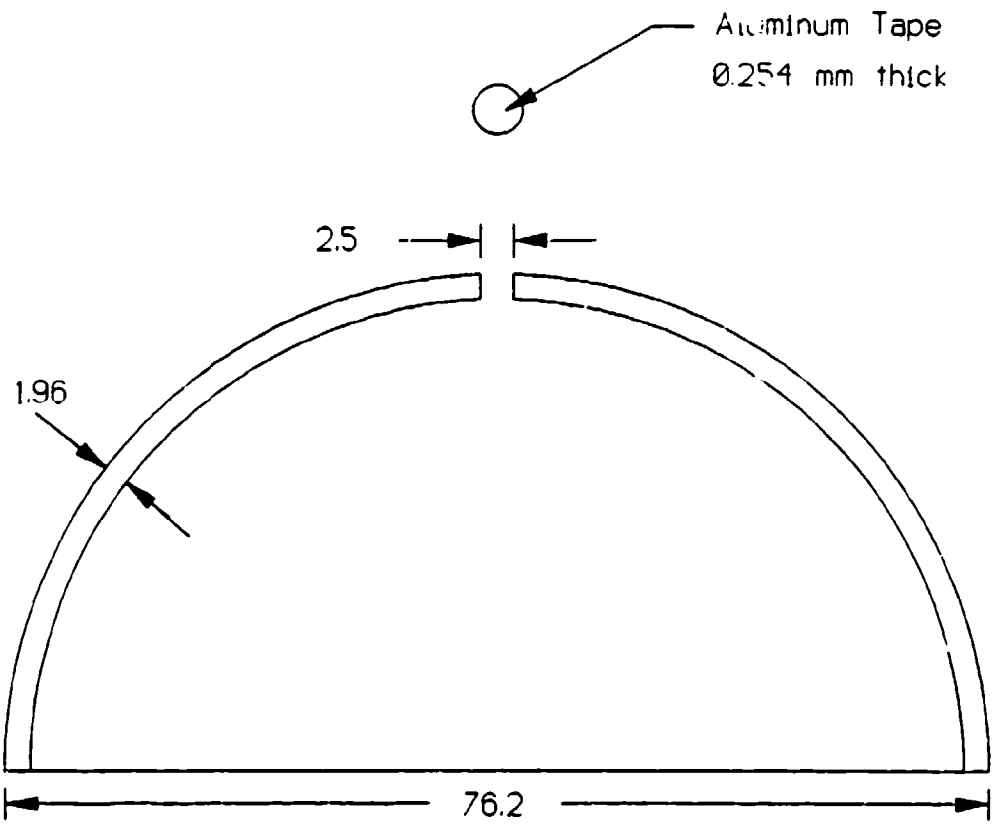

Figure A-10. Liner and Plug Design for Round 4141.

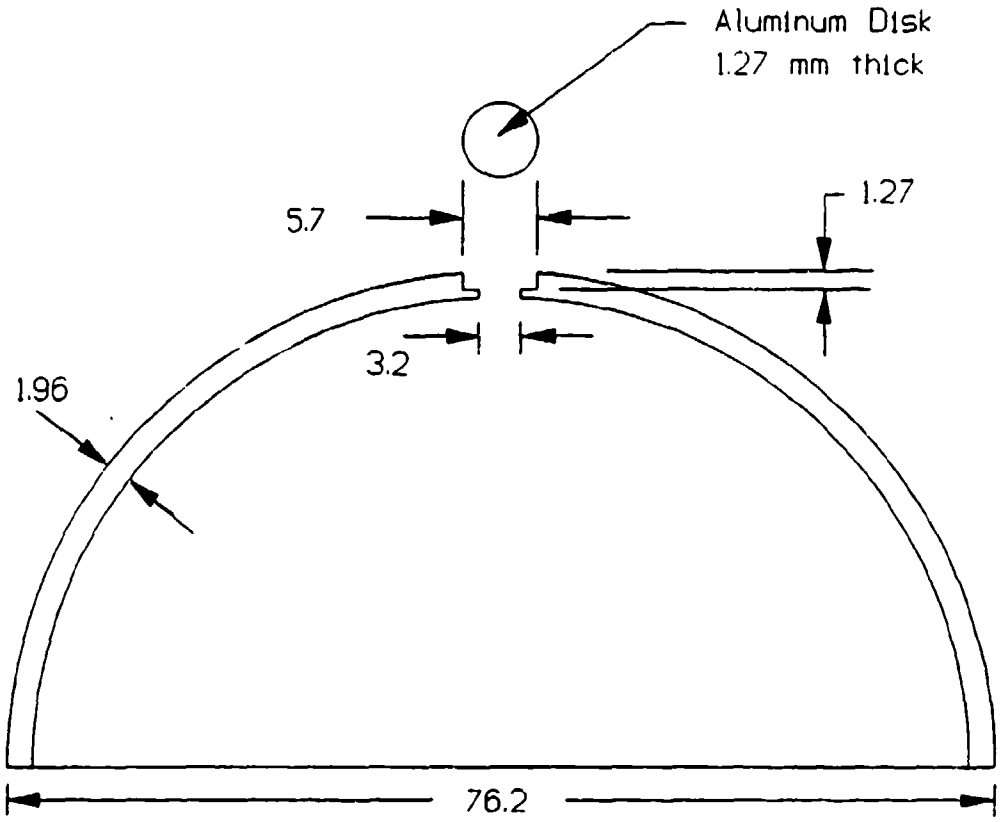

Figure A-11. Liner and Plug Design for Round 4145.

INTENTIONALLY LEFT BLANK

APPENDIX B:

EXPERIMENTAL DATA

INTENTIONALLY LEFT BLANK.

Summary Table For Round 4064

Particle	Length (mm)	Diameter (mm)	L/D	Mass (gm)	Velocity (km/s)
1	4.73	1.91	2.48	0.09	4.90
2	4.07	2.48	1.64	0.10	4.78
3	5.77	2.77	2.08	0.16	4.69
4	6.01	2.48	2.42	0.21	4.63
5	6.08	2.97	2.05	0.27	4.45
6	5.06	3.95	1.28	0.41	4.20
7	6.06	3.57	1.70	0.29	4.07
8	6.16	4.27	1.44	0.36	4.00
9	4.96	1.73	2.87	0.07	3.99
10	3.27	1.99	1.65	0.04	3.99
11	11.96	3.77	3.17	1.15	3.85
12	3.22	2.27	1.42	0.05	3.77
13	17.49	5.10	3.43	3.21	3.69
14	10.23	4.85	2.11	1.50	3.56
15	5.93	3.43	1.73	0.24	3.54
16	6.45	5.29	1.22	0.92	3.40
17	17.69	6.51	2.72	3.93	3.32
18	24.39	7.03	3.47	5.46	3.09
19	10.18	6.15	1.66	1.62	2.96
20	16.76	6.70	2.50	3.98	2.90
21	21.33	7.54	2.83	5.41	2.78
22	7.87	6.74	1.17	1.71	2.67
23	13.64	7.05	1.94	3.55	2.62
24	7.14	6.23	1.15	1.17	2.55
25	24.69	7.60	3.25	6.93	2.46
26	13.42	6.88	1.95	4.06	2.39
27	4.37	2.67	1.64	0.13	2.31
28	15.09	7.52	2.01	3.94	2.24
29	17.30	6.89	2.51	4.43	2.16

Cumulative Quantities for Round 4064

Particle	Cumulative Length (mm)	Cumulative Mass (gm)	Cumulative Momentum (kg m/s)	Cumulative Energy (kJ)	Breakup Time (us)
1	4.7	0.1	0.4	1.0	0.
2	8.8	0.2	0.9	2.2	36.7
3	14.6	0.3	1.7	4.0	43.7
4	20.6	0.6	2.7	6.3	55.2
5	26.7	0.8	3.9	8.9	46.4
6	31.7	1.2	5.6	12.6	38.2
7	37.8	1.5	6.8	15.0	38.6
8	43.9	1.9	8.2	17.9	42.6
9	48.9	2.0	8.5	18.4	48.3
10	52.2	2.0	8.7	18.8	53.0
11	64.1	3.2	13.1	27.3	52.8
12	67.4	3.2	13.3	27.7	55.9
13	84.8	6.4	25.1	49.5	60.6
14	95.1	7.9	30.4	58.9	65.1
15	101.0	8.2	31.3	60.5	69.9
16	107.5	9.1	34.4	65.8	68.0
17	125.1	13.0	47.5	87.5	72.1
18	149.5	18.5	64.4	113.6	74.5
19	159.7	20.1	69.2	120.7	78.2
20	176.5	24.1	80.7	137.5	82.9
21	197.8	29.5	95.8	158.3	87.0
22	205.7	31.2	100.3	164.4	89.4
23	219.3	34.7	109.7	176.7	92.2
24	226.5	35.9	112.6	180.5	93.5
25	251.2	42.8	129.7	201.5	96.9
26	264.6	46.9	139.4	213.1	101.8
27	268.9	47.0	139.7	213.5	102.0
28	284.0	51.0	148.6	223.4	103.0
29	301.3	55.4	158.1	233.7	105.6

Virtual Origin = -14.9748

	With Tip	Without Tip
Average Length	10.39	10.59
Average Diameter	4.77	4.87
Average L/D	2.119	2.107
Average Velocity Change	0.098	0.097

Summary Table For Round 4065

Particle	Length (mm)	Diameter (mm)	L/D	Mass (gm)	Velocity (km/s)
1	6.23	2.80	2.22	0.22	4.70
2	7.04	2.12	3.32	0.17	4.53
3	6.09	4.41	1.38	0.58	4.27
4	11.97	4.78	2.50	0.96	4.11
5	6.99	4.36	1.60	0.66	4.01
6	15.22	5.21	2.92	1.91	3.83
7	4.53	1.82	2.49	0.04	3.82
8	6.58	5.12	1.29	0.64	3.74
9	3.19	1.64	1.95	0.02	3.66
10	4.29	1.89	2.27	0.08	3.67
11	4.22	2.60	1.62	0.11	3.66
12	8.08	3.46	2.33	0.58	3.60
13	8.75	5.51	1.59	1.13	3.55
14	8.41	5.02	1.68	1.01	3.45
15	15.93	5.44	2.93	3.39	3.39
16	10.32	6.65	1.55	2.95	3.26
17	4.55	4.14	1.10	0.38	3.20
18	5.74	3.14	1.83	0.25	3.12
19	16.27	4.91	3.32	3.09	3.06
20	15.66	6.93	2.26	3.22	3.03
21	13.80	7.27	1.90	3.73	2.87
22	23.81	7.05	3.38	7.51	2.76
23	14.92	7.04	2.12	3.36	2.74
24	21.49	5.69	3.78	5.32	2.60
25	9.36	7.37	1.27	2.29	2.43
26	14.97	8.33	1.80	3.97	2.41
27	16.88	7.06	2.39	3.95	2.27
28	18.20	6.92	2.63	5.21	0.
29	27.07	8.43	3.21	10.53	0.
30	9.17	9.13	1.00	3.44	0.

Cumulative Quantities for Round 4065

Particle	Cumulative Length (mm)	Cumulative Mass (gm)	Cumulative Momentum (kg m/s)	Cumulative Energy (kJ)	Breakup Time (us)
1	6.2	0.2	1.0	2.4	0.
2	13.3	0.4	1.8	4.2	39.0
3	19.4	1.0	4.3	9.5	30.8
4	31.3	1.9	8.2	17.6	37.5
5	38.3	2.6	10.9	22.9	45.7
6	53.5	4.5	18.2	36.9	49.0
7	58.1	4.5	18.4	37.2	59.4
8	64.7	5.2	20.7	41.7	60.3
9	67.8	5.2	20.8	41.8	60.6
10	72.1	5.3	21.1	42.4	64.7
11	76.4	5.4	21.5	43.1	68.2
12	84.4	6.0	23.6	46.9	70.3
13	93.2	7.1	27.7	54.1	74.5
14	101.6	8.1	31.1	60.1	75.4
15	117.5	11.5	42.6	79.5	80.8
16	127.8	14.5	52.2	95.1	82.7
17	132.4	14.8	53.4	97.1	84.4
18	138.1	15.1	54.2	98.3	83.7
19	154.4	18.2	63.7	112.8	87.1
20	170.1	21.4	73.4	127.5	95.1
21	183.9	25.1	84.1	142.9	94.8
22	207.7	32.6	104.9	171.5	99.3
23	222.6	36.0	114.1	184.1	107.8
24	244.1	41.3	127.9	202.1	109.5
25	253.4	43.6	133.5	208.9	108.2
26	268.4	47.6	143.0	220.4	112.6
27	285.3	51.5	152.0	230.6	112.4
28	303.5	56.7	152.0	230.6	0.
29	330.6	67.3	152.0	230.6	0.
30	339.7	70.7	152.0	230.6	0.

Virtual Origin = -23.0271

	With Tip	Without Tip
Average Length	11.32	11.50
Average Diameter	5.21	5.29
Average L/D	2.188	2.186
Average Velocity Change	0.094	0.091

Summary Table For Round 4066

Particle	Length (mm)	Diameter (mm)	L/D	Mass (gm)	Velocity (km/s)
1	13.59	8.00	1.70	3.98	4.17
2	5.21	3.71	1.41	0.21	4.11
3	2.89	1.61	1.80	0.02	3.94
4	16.81	4.65	3.62	2.26	3.97
5	20.97	6.36	3.30	4.39	3.90
6	6.09	4.35	1.40	0.53	3.70
7	21.62	6.62	3.27	4.63	3.60
8	7.20	3.93	1.83	0.52	3.58
9	21.73	5.11	4.25	4.02	3.42
10	12.31	6.90	1.78	3.08	3.36
11	11.15	6.59	1.69	2.09	3.25
12	20.08	6.64	3.02	4.31	3.16
13	35.02	6.59	5.32	9.13	2.97
14	3.31	2.49	1.33	0.05	2.97
15	16.90	7.75	2.18	5.57	2.84
16	20.33	6.87	2.96	5.70	2.68
17	24.69	8.04	3.07	7.60	2.57
18	4.19	3.48	1.20	0.22	2.53
19	15.81	7.34	2.15	3.86	2.43
20	16.86	6.23	2.71	5.25	0.
21	28.51	7.35	3.88	8.18	0.
22	14.11	11.13	1.27	3.00	0.
23	20.62	8.71	2.37	6.40	0.

Cumulative Quantities for Round 4066

Particle	Cumulative Length (mm)	Cumulative Mass (gm)	Cumulative Momentum (kg m/s)	Cumulative Energy (kJ)	Breakup Time (us)
1	13.6	4.0	16.6	34.7	0.
2	18.8	4.2	17.5	36.5	138.1
3	21.7	4.2	17.6	36.6	57.8
4	38.5	6.5	26.5	54.5	116.1
5	59.5	10.9	43.7	87.8	153.2
6	65.6	11.4	45.6	91.4	117.4
7	87.2	16.0	62.3	121.5	122.3
8	94.4	16.5	64.2	124.8	141.7
9	116.1	20.6	77.9	148.3	130.2
10	128.4	23.6	88.3	165.7	141.4
11	139.6	25.7	95.0	176.7	137.1
12	159.6	30.0	108.7	198.2	141.3
13	194.7	39.2	135.8	238.5	141.8
14	198.0	39.2	135.9	238.8	157.9
15	214.9	44.8	151.7	261.2	149.4
16	235.2	50.5	167.0	281.7	146.3
17	259.9	58.1	186.6	306.9	150.5
18	264.1	58.3	187.1	307.6	155.3
19	279.9	62.2	196.5	319.0	152.3
20	296.7	67.4	196.5	319.0	0.
21	325.3	75.6	196.5	319.0	0.
22	339.4	78.6	196.5	319.0	0.
23	360.0	85.0	196.5	319.0	0.

Virtual Origin = -48.0710

	With Tip	Without Tip
Average Length	15.65	15.74
Average Diameter	6.11	6.02
Average L/D	2.500	2.536
Average Velocity Change	0.097	0.098

Summary Table For Round 4105

Particle	Length (mm)	Diameter (mm)	L/D	Mass (gm)	Velocity (km/s)
1	7.14	3.56	2.01	0.35	4.71
2	1.73	1.98	0.87	0.02	4.65
3	1.60	1.80	0.89	0.01	4.68
4	5.90	3.77	1.57	0.44	4.59
5	4.52	3.45	1.31	0.26	4.48
6	1.69	1.40	1.21	0.01	4.41
7	8.76	4.52	1.94	0.62	4.36
8	3.72	1.99	1.87	0.05	4.31
9	4.26	3.59	1.18	0.35	4.12
10	10.11	4.05	2.50	0.96	4.06
11	8.46	5.19	1.63	0.95	4.03
12	15.39	5.93	2.59	2.44	3.86
13	3.05	2.40	1.27	0.07	3.82
14	8.27	5.59	1.48	1.32	3.70
15	1.74	1.70	1.03	0.02	3.61
16	9.57	5.31	1.80	1.35	3.55
17	18.92	6.69	2.83	3.95	3.52
18	18.92	6.97	2.71	3.55	3.39
19	7.97	5.37	1.49	1.05	3.29
20	28.92	7.97	3.63	8.74	3.14
21	14.99	7.89	1.90	4.58	2.96
22	19.11	8.15	2.34	5.43	2.87
23	23.35	8.88	2.63	6.99	2.76
24	15.80	8.80	1.79	3.82	2.67
25	14.81	9.58	1.55	4.53	2.58
26	13.69	8.85	1.55	3.95	2.46
27	20.76	8.00	2.60	7.13	2.38
28	5.64	3.53	1.60	0.30	2.35
29	12.09	6.97	1.73	3.26	2.33
30	4.78	2.91	1.64	0.18	2.24
31	21.73	8.09	2.69	7.53	2.18
32	20.31	8.49	2.39	8.26	2.06
33	28.11	9.68	2.90	12.17	2.00
34	5.36	3.79	1.41	0.29	1.92
35	11.85	6.82	1.74	2.27	1.89
36	4.76	4.44	1.07	0.40	1.86
37	23.70	15.86	1.49	17.96	1.73
38	8.37	7.84	1.07	1.59	1.61

Cumulative Quantities for Round 4105

Particle	Cumulative Length (mm)	Cumulative Mass (gm)	Cumulative Momentum (kg m/s)	Cumulative Energy (kJ)	Breakup Time (us)
1	7.1	0.3	1.6	3.8	0.
2	8.9	0.4	1.7	4.1	76.3
3	10.5	0.4	1.8	4.2	186.8
4	16.4	0.8	3.8	8.8	83.8
5	20.9	1.1	5.0	11.5	64.9
6	22.6	1.1	5.0	11.5	60.3
7	31.3	1.7	7.7	17.5	67.1
8	35.1	1.8	8.0	17.9	74.5
9	39.3	2.1	9.4	20.9	56.9
10	49.4	3.1	13.3	28.8	62.7
11	57.9	4.0	17.1	36.5	73.7
12	73.3	6.5	26.5	54.6	73.0
13	76.3	6.5	26.8	55.2	80.0
14	84.6	7.8	31.7	64.2	76.0
15	86.3	7.9	31.7	64.3	74.4
16	95.9	9.2	36.5	72.8	75.5
17	114.8	13.2	50.4	97.3	85.5
18	133.7	16.7	62.4	117.6	91.2
19	141.7	17.8	65.9	123.3	94.5
20	170.6	26.5	93.3	166.4	97.1
21	185.6	31.1	106.9	186.4	99.6
22	204.7	36.5	122.4	208.7	104.1
23	228.1	43.5	141.7	235.3	109.1
24	243.9	47.3	152.0	249.0	114.2
25	258.7	51.9	163.6	264.1	116.1
26	272.4	55.8	173.3	276.0	116.3
27	293.1	62.9	190.3	296.2	119.9
28	298.8	63.2	191.0	297.0	124.0
29	310.9	66.5	198.6	305.9	126.7
30	315.6	66.7	199.0	306.3	125.5
31	337.4	74.2	215.5	324.3	127.9
32	357.7	82.5	232.5	341.9	130.0
33	385.8	94.6	256.9	366.3	136.1
34	391.2	94.9	257.5	366.9	138.1
35	403.0	97.2	261.8	370.9	139.7
36	407.8	97.6	262.5	371.6	141.0
37	431.5	115.5	293.5	398.5	139.5
38	439.8	117.1	296.1	400.5	139.2

Virtual Origin = -60.3245

	With Tip	Without Tip
Average Length	11.57	11.69
Average Diameter	5.84	5.90
Average L/D	1.839	1.835
Average Velocity Change	0.084	0.085

Summary Table For Round 4127

Particle	Length (mm)	Diameter (mm)	L/D	Mass (gm)	Velocity (km/s)
1	4.64	1.77	2.63	0.08	4.85
2	3.99	2.59	1.54	0.10	4.84
3	2.79	1.29	2.16	0.02	4.80
4	4.05	2.64	1.53	0.15	4.70
5	3.43	2.36	1.45	0.06	4.67
6	4.94	3.32	1.49	0.35	4.65
7	3.64	1.79	2.03	0.06	4.48
8	2.76	1.91	1.44	0.03	4.39
9	4.91	3.75	1.31	0.40	4.35
10	11.11	4.62	2.40	1.22	4.31
11	11.88	5.36	2.22	2.44	4.07
12	6.05	4.26	1.42	0.49	4.06
13	11.75	5.73	2.05	1.92	4.07
14	4.05	1.60	2.53	0.04	3.96
15	5.60	3.89	1.44	0.42	3.90
16	24.28	5.83	4.17	3.80	3.78
17	7.02	4.64	1.51	0.75	3.73
18	15.37	5.56	2.77	2.47	3.62
19	16.76	5.85	2.87	2.75	3.47
20	15.28	5.55	2.76	2.22	3.38
21	18.22	5.89	3.10	3.41	3.23
22	5.82	3.88	1.50	0.48	3.24
23	19.59	5.60	3.50	3.28	3.18
24	15.69	6.82	2.30	2.68	3.12
25	19.27	6.77	2.85	3.78	2.96
26	9.12	6.08	1.50	1.41	2.90
27	19.09	6.06	3.15	3.79	2.84
28	22.88	7.34	3.11	6.28	2.72
29	13.55	5.54	2.45	1.64	2.71
30	19.81	7.55	2.62	4.59	2.56
31	21.87	6.94	3.15	5.26	2.47
32	9.33	6.76	1.38	1.75	2.34
33	6.00	4.22	1.42	0.54	2.36
34	21.74	7.17	3.03	7.32	2.28
35	5.52	5.36	1.03	0.82	2.13
36	28.23	7.67	3.68	10.21	2.07
37	25.02	8.63	2.90	9.59	1.99
38	3.02	2.27	1.33	0.05	1.94
39	18.24	6.39	2.86	3.66	1.91
40	8.97	5.54	1.62	1.63	1.89
41	22.13	17.95	1.23	16.06	1.74

Cumulative Quantities for Round 4127

Particle	Cumulative Length (mm)	Cumulative Mass (gm)	Cumulative Momentum (kg m/s)	Cumulative Energy (kJ)	Breakup Time (us)
1	4.6	0.1	0.4	0.9	0.
2	8.6	0.2	0.9	2.1	232.2
3	11.4	0.2	1.0	2.4	135.8
4	15.5	0.4	1.7	4.0	69.9
5	18.9	0.4	2.0	4.7	79.4
6	23.8	0.8	3.6	8.5	93.5
7	27.5	0.8	3.9	9.2	62.2
8	30.2	0.9	4.0	9.4	57.4
9	35.1	1.3	5.8	13.2	60.3
10	46.2	2.5	11.0	24.6	70.9
11	58.1	4.9	21.0	44.8	63.7
12	64.2	5.4	23.0	48.9	74.4
13	75.9	7.3	30.8	64.7	86.0
14	80.0	7.4	31.0	65.1	84.9
15	85.6	7.8	32.6	68.3	84.6
16	109.9	11.6	46.9	95.4	88.5
17	116.9	12.3	49.7	100.6	99.2
18	132.3	14.8	58.7	116.8	99.0
19	149.0	17.6	68.2	133.4	100.0
20	164.3	19.8	75.8	146.1	105.0
21	182.5	23.2	86.8	163.9	105.0
22	188.4	23.7	88.3	166.4	113.3
23	207.9	27.0	98.7	183.0	117.3
24	223.6	29.6	107.1	196.0	123.0
25	242.9	33.4	118.3	212.6	122.1
26	252.0	34.8	122.4	218.5	125.5
27	271.1	38.6	133.2	233.9	129.0
28	294.0	44.9	150.3	257.1	131.4
29	307.5	46.5	154.7	263.1	139.0
30	327.3	51.1	166.4	278.2	137.2
31	349.2	56.4	179.4	294.2	140.8
32	358.5	58.1	183.5	299.0	139.7
33	364.5	58.7	184.8	300.5	144.0
34	386.3	66.0	201.5	319.5	145.2
35	391.8	66.8	203.2	321.4	141.8
36	420.0	77.0	224.4	343.3	144.9
37	445.1	86.6	243.4	362.2	150.1
38	448.1	86.7	243.6	362.3	152.6
39	466.3	90.3	250.5	369.0	154.5
40	475.3	92.0	253.6	371.9	158.0
41	497.4	108.0	281.6	396.3	155.5

Virtual Origin = -36.9443

	With Tip	Without Tip
Average Length	12.13	12.32
Average Diameter	5.24	5.32
Average L/D	2.230	2.220
Average Velocity Change	0.078	0.079

Summary Table For Round 4128

Particle	Length (mm)	Diameter (mm)	L/D	Mass (gm)	Velocity (km/s)
1	4.42	2.73	1.62	0.15	4.53
2	6.83	4.46	1.53	0.63	4.47
3	3.02	1.52	1.99	0.04	4.28
4	4.68	2.68	1.75	0.15	4.26
5	5.82	4.96	1.17	0.90	4.13
6	5.18	4.16	1.24	0.45	3.98
7	7.40	5.59	1.32	1.17	3.98
8	5.07	4.83	1.05	0.55	3.91
9	3.54	1.85	1.92	0.05	3.78
10	3.49	1.68	2.07	0.05	3.74
11	11.48	6.02	1.91	2.41	3.64
12	8.36	3.39	2.47	0.40	3.51
13	5.21	2.40	2.17	0.13	3.50
14	6.17	4.72	1.31	0.61	3.46
15	5.44	2.94	1.85	0.27	3.45
16	10.11	6.25	1.62	1.77	3.40
17	6.84	3.45	1.98	0.33	3.39
18	8.90	5.96	1.49	1.61	3.21
19	18.55	6.63	2.80	4.34	3.14
20	10.86	7.15	1.52	3.92	2.98
21	19.39	8.14	2.38	5.61	2.88
22	17.11	7.15	2.39	3.89	2.73
23	18.81	7.92	2.37	3.89	2.64
24	11.21	5.58	2.01	2.19	2.59
25	15.52	7.66	2.03	4.49	2.49
26	4.10	2.17	1.89	0.04	2.37
27	21.99	7.33	3.00	5.73	2.30
28	12.05	6.57	1.84	2.53	2.30
29	19.81	7.48	2.65	4.56	2.28
30	43.89	9.49	4.62	18.53	2.14
31	4.42	4.24	1.04	0.45	2.07
32	4.84	1.60	3.03	0.08	2.03
33	18.13	7.01	2.59	5.28	0.
34	8.61	6.09	1.41	1.06	0.
35	8.98	7.59	1.18	2.67	0.

Cumulative Quantities for Round 4128

Particle	Cumulative Length (mm)	Cumulative Mass (gm)	Cumulative Momentum (kg m/s)	Cumulative Energy (kJ)	Breakup Time (us)
1	4.4	0.2	0.7	1.5	0.
2	11.3	0.8	3.5	7.8	92.5
3	14.3	0.8	3.7	8.2	42.8
4	19.0	1.0	4.3	9.5	54.1
5	24.8	1.9	8.0	17.2	49.5
6	30.0	2.3	9.8	20.8	45.6
7	37.4	3.5	14.5	30.1	57.1
8	42.4	4.0	16.6	34.3	60.8
9	46.0	4.1	16.8	34.7	56.4
10	49.5	4.1	17.0	35.0	58.0
11	60.9	6.6	25.8	50.9	59.7
12	69.3	7.0	27.2	53.4	61.8
13	74.5	7.1	27.6	54.2	68.1
14	80.7	7.7	29.7	57.8	70.5
15	86.1	8.0	30.7	59.5	75.0
16	96.2	9.7	36.7	69.7	78.8
17	103.1	10.1	37.8	71.6	85.8
18	112.0	11.7	43.0	79.9	79.7
19	130.5	16.0	56.6	101.2	85.7
20	141.4	19.9	68.3	118.7	86.7
21	160.8	25.6	84.5	142.0	90.6
22	177.9	29.4	95.1	156.6	93.1
23	196.7	33.3	105.4	170.1	98.0
24	207.9	35.5	111.1	177.5	103.5
25	223.4	40.0	122.3	191.4	104.7
26	227.5	40.1	122.4	191.5	103.6
27	249.5	45.8	135.5	206.6	105.9
28	261.5	48.3	141.4	213.3	113.9
29	281.4	52.9	151.7	225.1	119.6
30	325.2	71.4	191.4	267.6	126.2
31	329.7	71.9	192.3	268.6	132.6
32	334.5	71.9	192.5	268.8	132.2
33	352.6	77.2	192.5	268.8	0.
34	361.2	78.3	192.5	268.8	0.
35	370.2	80.9	192.5	268.8	0.

Virtual Origin = -32.1140

	With Tip	Without Tip
Average Length	10.58	10.76
Average Diameter	5.13	5.20
Average L/D	1.978	1.988
Average Velocity Change	0.080	0.081

Summary Table For Round 4129

Particle	Length (mm)	Diameter (mm)	L/D	Mass (gm)	Velocity (km/s)
1	4.75	3.60	1.32	0.17	5.01
2	6.76	3.49	1.94	0.35	4.94
3	2.60	1.68	1.54	0.03	4.73
4	5.45	2.64	2.06	0.16	4.70
5	7.24	3.74	1.94	0.48	4.69
6	9.10	3.91	2.33	0.77	4.54
7	3.29	2.15	1.53	0.04	4.54
8	4.08	2.89	1.42	0.18	4.35
9	11.09	4.63	2.40	1.05	4.36
10	7.94	4.34	1.83	0.66	4.30
11	10.10	5.07	1.99	1.27	4.18
12	10.36	5.91	1.75	1.58	4.04
13	13.67	5.94	2.30	1.91	3.84
14	7.73	5.05	1.53	0.93	3.79
15	17.48	5.48	3.19	1.94	3.67
16	5.83	6.04	0.97	0.64	3.62
17	23.35	5.77	4.04	3.67	3.57
18	24.16	5.32	4.54	3.03	3.38
19	18.57	6.05	3.07	3.19	3.33
20	27.37	6.14	4.45	5.02	3.16
21	12.54	7.19	1.74	2.52	3.05
22	5.08	3.39	1.50	0.16	3.05
23	25.21	7.02	3.59	4.55	2.97
24	23.65	7.30	3.24	5.21	2.82
25	17.65	8.08	2.18	3.97	2.72
26	33.14	7.86	4.21	7.67	2.58
27	12.31	7.62	1.61	2.87	2.49
28	16.10	6.69	2.41	4.52	2.37
29	12.26	6.96	1.76	3.48	2.33
30	33.54	7.37	4.55	10.52	2.15
31	24.25	8.18	2.97	10.03	2.08
32	18.96	7.04	2.69	6.97	1.92
33	13.72	8.47	1.62	3.85	0.
34	11.89	4.02	2.96	0.82	0.
35	14.65	11.42	1.28	4.18	0.
36	3.93	2.67	1.47	0.16	0.

Cumulative Quantities for Round 4129

Particle	Cumulative Length (mm)	Cumulative Mass (gm)	Cumulative Momentum (kg m/s)	Cumulative Energy (kJ)	Breakup Time (us)
1	4.7	0.2	0.9	2.2	0.
2	11.5	0.5	2.6	6.4	88.7
3	14.1	0.6	2.7	6.8	36.7
4	19.6	0.7	3.5	8.6	46.1
5	26.8	1.2	5.8	13.8	65.4
6	35.9	2.0	9.3	21.8	62.0
7	39.2	2.0	9.5	22.3	74.7
8	43.3	2.2	10.2	23.9	59.2
9	54.4	3.2	14.8	33.9	71.8
10	62.3	3.9	17.6	40.0	79.3
11	72.4	5.2	23.0	51.1	78.1
12	82.8	6.7	29.3	64.0	77.8
13	96.4	8.7	36.7	78.1	74.3
14	104.2	9.6	40.2	84.8	80.3
15	121.6	11.5	47.3	97.8	82.7
16	127.5	12.2	49.6	102.0	88.2
17	150.8	15.8	62.7	125.5	95.2
18	175.0	18.9	73.0	142.8	98.4
19	193.5	22.0	83.6	160.4	108.2
20	220.9	27.1	99.4	185.4	110.6
21	233.5	29.6	107.1	197.1	114.5
22	238.5	29.8	107.6	197.9	119.4
23	263.7	34.3	121.1	217.9	121.7
24	287.4	39.5	135.8	238.6	124.7
25	305.0	43.5	146.6	253.3	128.5
26	338.2	51.2	166.4	278.8	131.4
27	350.5	54.0	173.5	287.7	135.5
28	366.6	58.5	184.2	300.4	135.0
29	378.8	62.0	192.3	309.8	138.3
30	412.4	72.5	215.0	334.2	137.7
31	436.6	82.6	235.8	355.8	143.9
32	455.6	89.5	249.2	368.7	143.5
33	469.3	93.4	249.2	368.7	0.
34	481.2	94.2	249.2	368.7	0.
35	495.8	98.4	249.2	368.7	0.
36	499.8	98.6	249.2	368.7	0.

Virtual Origin = -31.4408

	With Tip	Without Tip
Average Length	13.88	14.14
Average Diameter	5.59	5.64
Average L/D	2.387	2.418
Average Velocity Change	0.100	0.101

Summary Table For Round 4130

Particle	Length (mm)	Diameter (mm)	L/D	Mass (gm)	Velocity (km/s)
1	6.00	1.93	3.11	0.12	5.16
2	2.55	2.04	1.25	0.04	4.99
3	3.25	1.18	2.76	0.02	4.98
4	4.77	3.16	1.51	0.29	4.83
5	3.87	1.70	2.28	0.07	4.82
6	7.56	3.71	2.04	0.62	4.69
7	6.75	3.41	1.98	0.43	4.65
8	10.13	4.23	2.40	1.16	4.31
9	2.38	1.94	1.23	0.03	4.23
10	5.44	4.54	1.20	0.60	4.19
11	7.39	3.09	2.39	0.50	4.10
12	13.66	6.35	2.15	2.20	4.05
13	13.30	5.89	2.26	2.27	3.95
14	24.81	6.15	4.03	4.94	3.69
15	10.63	6.37	1.67	1.71	3.65
16	8.71	6.50	1.34	1.26	3.52
17	13.33	5.99	2.23	2.52	3.44
18	16.15	6.80	2.37	3.71	3.41
19	17.73	7.10	2.50	3.75	3.19
20	8.57	5.99	1.43	1.71	3.18
21	21.11	7.50	2.81	5.71	3.08
22	21.73	7.57	2.87	5.14	2.90
23	24.77	8.58	2.89	7.93	2.75
24	11.77	8.59	1.37	3.72	2.65
25	21.53	7.91	2.72	6.83	0.
26	24.85	7.59	3.27	7.01	0.
27	5.57	3.58	1.56	0.54	0.
28	28.19	7.48	3.77	9.44	0.
29	20.41	8.78	2.32	9.19	0.
30	5.27	3.68	1.43	0.42	0.
31	37.78	9.17	4.12	13.41	0.
32	10.45	7.85	1.33	4.36	0.
33	17.14	11.48	1.49	6.97	0.
34	7.69	3.62	2.12	0.33	0.
35	6.00	2.71	2.21	0.27	0.
36	9.27	3.60	2.57	0.53	0.
37	5.69	4.64	1.23	0.52	1.57
38	13.06	10.88	1.20	3.75	0.03

Cumulative Quantities for Round 4130

Particle	Cumulative Length (mm)	Cumulative Mass (gm)	Cumulative Momentum (kg m/s)	Cumulative Energy (kJ)	Breakup Time (us)
1	6.0	0.1	0.6	1.6	0.
2	8.5	0.2	0.8	2.1	25.2
3	11.8	0.2	0.9	2.3	39.5
4	16.6	0.5	2.3	5.7	33.7
5	20.4	0.5	2.6	6.4	45.9
6	28.0	1.1	5.5	13.2	45.3
7	34.7	1.6	7.5	17.9	56.0
8	44.9	2.7	12.5	28.7	43.2
9	47.3	2.8	12.7	29.0	46.4
10	52.7	3.4	15.2	34.3	48.5
11	60.1	3.9	17.3	38.5	50.5
12	73.8	6.1	26.2	56.5	57.7
13	87.1	8.3	35.1	74.1	63.9
14	111.9	13.3	53.3	107.8	65.7
15	122.5	15.0	59.6	119.2	75.9
16	131.2	16.3	64.0	127.0	75.5
17	144.5	18.8	72.7	141.9	78.3
18	160.7	22.5	85.3	163.4	85.5
19	178.4	26.2	97.3	182.6	84.8
20	187.0	28.0	102.7	191.2	91.1
21	208.1	33.7	120.3	218.3	93.4
22	229.8	38.8	135.2	239.8	95.5
23	254.6	46.7	157.0	269.8	99.4
24	266.4	50.4	166.8	282.8	102.6
25	287.9	57.3	166.8	282.8	0.
26	312.7	64.3	166.8	282.8	0.
27	318.3	64.8	166.8	282.8	0.
28	346.5	74.3	166.8	282.8	0.
29	366.9	83.5	166.8	282.8	0.
30	372.2	83.9	166.8	282.8	0.
31	410.0	97.3	166.8	282.8	0.
32	420.4	101.6	166.8	282.8	0.
33	437.5	108.6	166.8	282.8	0.
34	445.2	108.9	166.8	282.8	0.
35	451.2	109.2	166.8	282.8	0.
36	460.5	109.7	166.8	282.8	0.
37	466.2	110.3	167.7	283.5	128.3
38	479.2	114.0	167.8	283.5	91.6

Virtual Origin = -3.94860

	With Tip	Without Tip
Average Length	12.61	12.79
Average Diameter	5.61	5.71
Average L/D	2.195	2.170
Average Velocity Change	0.169	0.169

Summary Table For Round 4131

Particle	Length (mm)	Diameter (mm)	L/D	Mass (gm)	Velocity (km/s)
1	4.10	2.51	1.63	0.10	5.29
2	2.30	1.39	1.66	0.01	5.19
3	2.59	1.57	1.65	0.04	5.09
4	2.71	1.62	1.67	0.04	5.08
5	2.91	1.71	1.70	0.03	5.08
6	3.89	2.66	1.46	0.09	5.07
7	2.57	1.81	1.42	0.02	5.05
8	3.53	3.04	1.16	0.13	4.90
9	2.97	1.38	2.15	0.02	4.87
10	9.47	5.64	1.68	0.86	4.78
11	3.23	1.57	2.07	0.02	4.65
12	9.83	4.10	2.39	0.91	4.53
13	3.70	2.61	1.42	0.08	4.40
14	6.05	4.72	1.28	0.79	4.33
15	8.01	5.09	1.57	1.47	4.20
16	3.95	2.04	1.94	0.08	4.05
17	9.85	6.07	1.62	1.81	4.02
18	10.90	6.14	1.77	2.40	3.81
19	7.51	5.21	1.44	1.57	3.77
20	14.77	6.04	2.45	2.16	3.69
21	2.27	1.34	1.69	0.02	3.59
22	16.93	6.75	2.51	2.77	3.52
23	22.17	6.87	3.23	4.05	3.38
24	24.90	7.18	3.47	6.04	3.26
25	15.94	7.51	2.12	3.14	3.13
26	23.72	7.57	3.13	6.40	2.98
27	12.72	8.53	1.49	3.88	2.80
28	34.32	7.51	4.57	9.53	2.78
29	23.91	9.04	2.64	9.88	2.51
30	15.89	7.75	2.05	4.37	0.
31	56.25	7.69	7.32	13.76	0.
32	31.81	8.86	3.59	14.65	0.
33	35.13	7.46	4.71	11.34	0.
34	11.45	17.51	0.65	12.85	1.72
35	12.82	10.99	1.17	4.00	0.03
36	9.35	2.64	3.55	0.36	0.08

Cumulative Quantities for Round 4131

Particle	Cumulative Length (mm)	Cumulative Mass (gm)	Cumulative Momentum (kg m/s)	Cumulative Energy (kJ)	Breakup Time (us)
1	4.1	0.1	0.5	1.4	0.
2	6.4	0.1	0.8	1.6	34.1
3	9.0	0.2	0.8	2.2	27.9
4	11.7	0.2	1.0	2.7	40.9
5	14.6	0.2	1.2	3.1	52.4
6	18.5	0.3	1.6	4.2	66.7
7	21.1	0.3	1.8	4.5	74.1
8	24.6	0.5	2.4	6.1	53.6
9	27.6	0.5	2.5	6.3	57.0
10	37.0	1.3	6.6	16.1	59.9
11	40.3	1.4	6.7	16.3	57.4
12	50.1	2.3	10.8	25.7	57.0
13	53.8	2.4	11.2	26.5	56.0
14	59.8	3.1	14.6	33.9	57.1
15	67.9	4.6	20.8	46.9	56.8
16	71.8	4.7	21.1	47.5	54.9
17	81.7	6.5	28.4	62.2	58.9
18	92.6	8.9	37.5	79.5	57.4
19	100.1	10.5	43.4	90.7	62.2
20	114.8	12.6	51.4	105.4	66.0
21	117.1	12.7	51.5	105.6	67.2
22	134.0	15.4	61.2	122.8	70.0
23	156.2	19.5	74.9	145.9	75.1
24	181.1	25.5	94.6	178.0	82.1
25	197.0	28.7	104.5	193.4	86.8
26	220.8	35.1	123.6	221.9	89.8
27	233.5	38.9	134.4	237.2	90.6
28	267.8	48.5	160.9	274.0	99.2
29	291.7	58.4	185.7	305.1	100.0
30	307.6	62.7	185.7	305.1	0.
31	363.8	76.5	185.7	305.1	0.
32	395.7	91.1	185.7	305.1	0.
33	430.8	102.5	185.7	305.1	0.
34	442.2	115.3	207.8	324.1	121.8
35	455.1	119.3	207.9	324.1	85.0
36	464.4	119.7	208.0	324.1	87.9

Virtual Origin = -13.4885

	With Tip	Without Tip
Average Length	12.90	13.15
Average Diameter	5.34	5.42
Average L/D	2.279	2.297
Average Velocity Change	0.147	0.149

Summary Table For Round 4134

Particle	Length (mm)	Diameter (mm)	L/D	Mass (gm)	Velocity (km/s)
1	6.52	7.07	0.92	1.53	4.18
2	8.83	6.08	1.45	1.65	4.10
3	9.14	6.17	1.48	1.68	4.08
4	10.18	5.87	1.73	1.80	3.90
5	11.37	6.37	1.78	2.08	3.86
6	3.42	2.52	1.36	0.13	3.79
7	17.22	7.18	2.40	2.96	3.71
8	5.47	2.64	2.07	0.17	3.56
9	17.92	6.39	2.81	3.06	3.54
10	13.43	6.54	2.05	2.19	3.45
11	17.93	7.24	2.48	3.33	3.30
12	17.84	6.76	2.64	3.57	3.24
13	18.11	7.64	2.37	4.46	3.10
14	6.69	4.61	1.45	0.69	2.98
15	19.79	7.48	2.64	5.09	2.94
16	20.18	8.51	2.37	6.20	2.80
17	23.73	7.95	2.99	8.78	2.58
18	15.80	8.26	1.91	5.59	2.49
19	19.50	8.22	2.37	5.94	2.31
20	5.21	3.86	1.35	0.32	2.27
21	10.46	8.01	1.31	3.26	2.21
22	4.31	6.37	0.68	0.83	2.23
23	11.01	6.78	1.62	2.66	2.13
24	4.14	3.93	1.05	0.26	2.05
25	20.96	8.38	2.50	9.72	2.05
26	6.28	3.23	1.95	0.41	0.
27	5.67	5.72	0.99	0.71	0.
28	30.44	8.61	3.53	14.33	0.
29	7.59	4.23	1.80	0.37	0.

Cumulative Quantities for Round 4134

Particle	Cumulative Length (mm)	Cumulative Mass (gm)	Cumulative Momentum (kg m/s)	Cumulative Energy (kJ)	Breakup Time (us)
1	6.5	1.5	6.4	13.4	0.
2	15.4	3.2	13.2	27.3	95.1
3	24.5	4.9	20.0	41.3	171.7
4	34.7	6.7	27.1	55.0	92.4
5	46.0	8.7	35.1	70.4	113.8
6	49.5	8.9	35.6	71.4	112.6
7	66.7	11.8	46.6	91.7	116.8
8	72.2	12.0	47.2	92.8	106.6
9	90.1	15.1	58.0	112.0	121.1
10	103.5	17.3	65.6	125.1	127.9
11	121.4	20.6	76.6	143.2	124.4
12	139.3	24.2	88.1	161.9	134.3
13	157.4	28.6	102.0	183.4	134.6
14	164.1	29.3	104.0	186.5	131.0
15	183.9	34.4	119.0	208.5	137.5
16	204.0	40.6	136.3	232.7	137.8
17	227.8	49.4	159.0	262.0	133.0
18	243.6	55.0	172.9	279.4	137.5
19	263.1	60.9	186.6	295.2	133.4
20	268.3	61.2	187.3	296.0	137.2
21	278.8	64.5	194.5	303.9	136.8
22	283.1	65.3	196.4	306.0	142.5
23	294.1	68.0	202.0	312.0	138.7
24	298.2	68.2	202.6	312.5	137.6
25	319.2	78.0	222.5	332.9	143.2
26	325.5	78.4	222.5	332.9	0.
27	331.1	79.1	222.5	332.9	0.
28	361.6	93.4	222.5	332.9	0.
29	369.2	93.8	222.5	332.9	0.

Virtual Origin = -32.9038

	With Tip	Without Tip
Average Length	12.73	12.95
Average Diameter	6.30	6.27
Average L/D	1.933	1.970
Velocity Change	0.089	0.089

Summary Table For Round 4135

Particle	Length (mm)	Diameter (mm)	L/D	Mass (gm)	Velocity (km/s)
1	15.37	7.81	1.97	4.34	4.21
2	16.73	5.04	3.32	1.80	4.14
3	13.55	5.73	2.36	1.89	4.00
4	6.95	4.24	1.64	0.50	3.96
5	10.79	5.87	1.84	1.80	3.89
6	17.95	5.65	3.18	3.76	3.75
7	23.48	5.62	4.18	4.15	3.54
8	25.08	6.37	3.94	4.46	3.40
9	21.50	6.41	3.35	3.98	3.27
10	32.05	6.60	4.86	5.98	3.13
11	32.01	7.97	4.02	6.71	2.98
12	16.66	6.93	2.40	4.04	2.90
13	17.92	7.18	2.50	4.86	2.74
14	18.37	6.76	2.72	5.03	2.68
15	20.23	6.84	2.96	5.63	2.61
16	6.87	4.42	1.55	0.57	2.45
17	23.33	7.31	3.19	7.05	2.43
18	9.43	6.57	1.43	1.48	2.34
19	13.37	6.36	2.10	3.48	2.33
20	23.06	6.98	3.30	7.69	2.19
21	4.04	3.31	1.22	0.15	2.19
22	19.57	9.58	2.04	9.23	2.06
23	31.24	8.89	3.52	14.34	2.01
24	8.15	5.79	1.41	0.80	0.
25	9.44	7.02	1.34	3.99	0.
26	11.64	5.96	1.95	2.79	0.

Cumulative Quantities for Round 4135

Particle	Cumulative Length (mm)	Cumulative Mass (gm)	Cumulative Momentum (kg m/s)	Cumulative Energy (kJ)	Breakup Time (us)
1	15.4	4.3	18.3	38.5	0.
2	32.1	6.1	25.7	53.9	210.0
3	45.6	8.0	33.3	69.0	145.4
4	52.6	8.5	35.3	73.0	163.7
5	63.4	10.3	42.3	86.6	155.3
6	81.3	14.1	56.3	113.0	137.8
7	104.8	18.2	71.0	139.0	127.3
8	129.9	22.7	86.2	164.7	134.3
9	151.4	26.7	99.2	186.0	141.0
10	183.5	32.6	117.9	215.4	147.6
11	215.5	39.4	137.9	245.2	155.4
12	232.1	43.4	149.7	262.2	164.1
13	250.0	48.3	163.0	280.4	158.0
14	268.4	53.3	176.5	298.5	164.1
15	288.7	58.9	191.2	317.6	168.5
16	295.5	59.5	192.6	319.3	160.8
17	318.9	66.6	209.7	340.1	167.6
18	328.3	68.0	213.2	344.2	168.3
19	341.7	71.5	221.3	353.7	173.8
20	364.7	79.2	238.1	372.1	170.4
21	368.8	79.4	238.4	372.4	176.9
22	388.3	88.6	257.4	392.0	171.9
23	419.6	102.9	286.2	420.9	179.7
24	427.7	103.7	286.2	420.9	0.
25	437.2	107.7	286.2	420.9	0.
26	448.8	110.5	286.2	420.9	0.

Virtual Origin = -30.8423

	With Tip	Without Tip
Average Length	17.26	17.34
Average Diameter	6.43	6.38
Average L/D	2.627	2.653
Average Velocity Change	0.100	0.101

Summary Table For Round 4140

Particle	Length (mm)	Diameter (mm)	L/D	Mass (gm)	Velocity (km/s)
1	2.64	1.81	1.46	0.03	4.75
2	8.10	3.44	2.36	0.45	4.74
3	3.38	2.08	1.63	0.10	4.69
4	5.82	4.46	1.31	0.52	4.54
5	4.27	3.33	1.28	0.21	4.53
6	6.30	4.00	1.57	0.48	4.51
7	9.92	4.15	2.39	0.87	4.32
8	7.38	4.34	1.70	0.73	4.32
9	10.04	6.01	1.67	1.15	4.16
10	6.00	4.59	1.31	0.44	4.13
11	8.91	5.23	1.70	1.00	4.05
12	5.06	4.07	1.24	0.39	3.93
13	8.09	5.26	1.54	1.09	3.91
14	13.50	5.74	2.35	2.02	3.84
15	9.34	5.54	1.69	1.21	3.68
16	14.68	6.80	2.16	2.73	3.66
17	23.25	6.50	3.58	3.79	3.45
18	14.22	5.89	2.42	2.10	3.37
19	18.47	6.84	2.70	4.22	3.23
20	5.21	5.28	0.99	0.73	3.25
21	21.90	7.54	2.90	4.73	3.11
22	20.28	7.37	2.75	4.96	2.95
23	20.73	7.70	2.69	5.89	2.83
24	14.70	8.08	1.82	4.77	2.71
25	9.09	8.03	1.13	2.89	2.62
26	12.11	10.41	1.16	5.44	2.58
27	14.61	9.11	1.60	6.18	2.40
28	20.64	7.84	2.63	6.69	2.30
29	11.88	8.51	1.40	3.24	2.20
30	25.67	7.96	3.23	9.20	2.08
31	20.27	7.88	2.57	5.29	2.01
32	21.22	8.91	2.38	6.89	0.

Cumulative Quantities for Round 4140

Particle	Cumulative Length (mm)	Cumulative Mass (gm)	Cumulative Momentum (kg m/s)	Cumulative Energy (kJ)	Breakup Time (us)
1	2.6	0.0	0.2	0.4	0.
2	10.7	0.5	2.3	5.4	2609.3
3	14.1	0.6	2.7	6.4	196.7
4	19.9	1.1	5.1	11.8	77.7
5	24.2	1.3	6.0	14.0	95.9
6	30.5	1.8	8.2	18.9	111.0
7	40.4	2.7	11.9	26.9	79.9
8	47.8	3.4	15.1	33.7	99.9
9	57.8	4.5	19.9	43.7	88.4
10	63.8	5.0	21.7	47.5	97.6
11	72.8	6.0	25.8	55.7	96.9
12	77.8	6.4	27.3	58.7	90.6
13	85.9	7.5	31.6	67.1	96.2
14	99.4	9.5	39.3	82.0	101.1
15	108.7	10.7	43.8	90.2	96.7
16	123.4	13.4	53.8	108.4	105.6
17	146.7	17.2	66.9	131.1	103.6
18	160.9	19.3	74.0	143.0	110.5
19	179.4	23.5	87.6	165.0	111.5
20	184.6	24.3	90.0	168.9	120.8
21	206.5	29.0	104.7	191.7	118.5
22	226.8	34.0	119.3	213.3	120.0
23	247.5	39.8	136.0	236.9	123.3
24	262.2	44.6	148.9	254.4	124.4
25	271.3	47.5	156.5	264.3	124.9
26	283.4	52.9	170.5	282.3	127.2
27	298.0	59.1	185.3	300.1	123.3
28	318.6	65.8	200.7	317.8	125.6
29	330.5	69.1	207.8	325.7	127.2
30	356.2	78.3	226.9	345.5	128.1
31	376.5	83.5	237.6	356.2	133.5
32	397.7	90.4	237.6	356.2	0.

Virtual Origin = -43.0984

	With Tip	Without Tip
Average Length	12.43	12.74
Average Diameter	6.08	6.22
Average L/D	1.978	1.995
Average Velocity Change	0.091	0.094

Summary Table For Round 4141

Particle	Length (mm)	Diameter (mm)	L/D	Mass (gm)	Velocity (km/s)
1	11.17	8.13	1.37	2.77	4.22
2	6.15	4.07	1.51	0.43	4.23
3	7.70	5.83	1.32	1.01	4.18
4	20.57	6.59	3.12	3.93	4.03
5	6.67	5.18	1.29	0.80	3.88
6	1.95	1.52	1.28	0.01	3.86
7	23.73	6.85	3.46	4.70	3.70
8	6.51	4.05	1.61	0.59	3.62
9	10.32	5.85	1.76	1.58	3.57
10	13.50	7.75	1.74	2.82	3.51
11	5.82	3.80	1.53	0.29	3.46
12	19.10	6.84	2.79	4.20	3.36
13	12.41	5.94	2.09	1.18	3.23
14	14.39	6.87	2.09	3.40	3.14
15	21.62	7.77	2.78	4.20	3.04
16	18.15	7.93	2.29	3.60	2.99
17	25.59	8.21	3.12	7.25	2.85
18	21.39	8.24	2.59	7.84	2.67
19	10.81	6.43	1.68	2.46	2.65
20	17.97	8.57	2.10	6.27	2.51
21	10.19	7.55	1.35	2.86	2.45
22	22.19	7.67	2.89	6.48	2.28
23	12.09	7.85	1.54	3.81	2.24
24	26.95	8.69	3.10	10.89	2.06
25	19.85	9.10	2.18	6.74	2.00
26	8.80	6.78	1.30	2.16	1.84
27	24.79	21.43	1.16	27.21	0.

Cumulative Quantities for Round 4141

Particle	Cumulative Length (mm)	Cumulative Mass (gm)	Cumulative Momentum (kg m/s)	Cumulative Energy (kJ)	Breakup Time (us)
1	11.2	2.8	11.7	24.7	0.
2	17.3	3.2	13.5	28.5	******
3	25.0	4.2	17.7	37.3	315.2
4	45.6	8.1	33.6	69.3	152.4
5	52.3	8.9	36.6	75.2	126.5
6	54.2	8.9	36.7	75.3	132.0
7	77.9	13.6	54.1	107.6	116.3
8	84.5	14.2	56.2	111.4	125.5
9	94.8	15.8	61.9	121.5	128.3
10	108.3	18.6	71.8	138.9	134.8
11	114.1	18.9	72.8	140.6	137.8
12	133.2	23.1	86.9	164.4	137.2
13	145.6	24.3	90.7	170.6	134.4
14	160.0	27.7	101.4	187.3	135.3
15	181.6	31.9	114.2	206.7	139.6
16	199.8	35.5	124.9	222.8	149.8
17	225.4	42.8	145.6	252.2	150.0
18	246.7	50.6	166.5	280.1	148.2
19	257.5	53.1	173.0	288.8	156.6
20	275.5	59.3	188.7	308.4	151.8
21	285.7	62.2	195.7	317.0	154.6
22	307.9	68.7	210.5	333.8	149.4
23	320.0	72.5	219.0	343.3	155.2
24	346.9	83.4	241.4	366.4	151.2
25	366.8	90.1	254.9	379.9	158.1
26	375.6	92.3	258.9	383.5	153.3
27	400.4	119.5	258.9	383.5	0.

Virtual Origin = -39.4162

	With Tip	Without Tip
Average Length	14.83	14.97
Average Diameter	7.24	7.21
Average L/D	2.039	2.065
Average Velocity Change	0.095	0.100

Summary Table For Round 4145

Particle	Length (mm)	Diameter (mm)	L/D	Mass (gm)	Velocity (km/s)
1	6.74	5.03	1.34	0.62	4.31
2	10.38	5.18	2.00	1.72	4.23
3	10.97	5.28	2.08	1.18	4.21
4	15.32	5.41	2.83	1.97	4.04
5	9.85	4.98	1.98	0.80	4.02
6	7.56	5.08	1.49	1.09	3.95
7	14.79	5.66	2.61	1.91	3.79
8	15.84	5.93	2.67	2.53	3.66
9	7.19	4.59	1.57	0.83	3.64
10	23.35	6.21	3.76	3.64	3.48
11	23.41	6.20	3.77	4.17	3.32
12	17.21	5.93	2.90	2.93	3.18
13	29.87	5.99	4.99	7.09	3.10
14	29.32	7.41	3.96	7.24	2.92
15	23.87	7.26	3.29	6.79	2.73
16	13.74	6.15	2.24	2.30	2.65
17	11.15	6.60	1.69	2.68	2.65
18	26.14	6.83	3.83	8.65	2.49
19	27.82	7.54	3.69	11.13	2.28
20	23.07	7.71	2.99	8.34	0.
21	19.41	8.20	2.37	7.80	0.
22	46.41	8.53	5.44	15.90	0.
23	26.34	20.19	1.30	20.87	0.

Cumulative Quantities for Round 4145

Particle	Cumulative Length (mm)	Cumulative Mass (gm)	Cumulative Momentum (kg m/s)	Cumulative Energy (kJ)	Breakup Time (us)
1	6.7	0.6	2.7	5.8	0.
2	17.1	2.3	9.9	21.1	97.3
3	28.1	3.5	14.9	31.6	179.0
4	43.4	5.5	22.9	47.6	117.6
5	53.2	6.3	26.1	54.1	151.4
6	60.8	7.4	30.4	62.6	146.7
7	75.6	9.3	37.6	76.2	122.8
8	91.4	11.8	46.8	93.1	122.5
9	98.6	12.6	49.9	98.6	135.9
10	122.0	16.3	62.5	120.7	128.3
11	145.4	20.4	76.4	143.6	131.2
12	162.6	23.4	85.7	158.4	132.6
13	192.5	30.5	107.6	192.4	143.0
14	221.8	37.7	128.7	223.3	146.2
15	245.7	44.5	147.3	248.6	145.6
16	259.4	46.8	153.4	256.7	150.0
17	270.6	49.5	160.5	266.1	157.3
18	296.7	58.1	182.0	292.8	153.3
19	324.5	69.3	207.4	321.8	151.1
20	347.6	77.6	207.4	321.8	0.
21	367.0	85.4	207.4	321.8	0.
22	413.4	101.3	207.4	321.8	0.
23	439.7	122.2	207.4	321.8	0.

Virtual Origin = -50.0214

	With Tip	Without Tip
Average Length	19.12	19.68
Average Diameter	6.86	6.95
Average L/D	2.817	2.884
Average Velocity Change	0.113	0.114

Summary Table For Round 4146

Particle	Length (mm)	Diameter (mm)	L/D	Mass (gm)	Velocity (km/s)
1	13.10	6.89	1.90	2.48	4.19
2	10.91	5.77	1.89	1.66	4.11
3	9.68	6.25	1.55	1.44	3.97
4	4.59	2.72	1.69	0.13	3.93
5	12.08	5.59	2.16	1.42	3.89
6	4.75	3.01	1.58	0.24	3.85
7	17.21	6.29	2.74	3.49	3.77
8	11.86	6.37	1.86	2.49	3.53
9	15.70	5.55	2.83	2.08	3.52
10	14.95	6.92	2.16	2.66	3.43
11	16.99	7.81	2.18	3.59	3.31
12	20.92	7.84	2.67	4.97	3.13
13	5.73	5.15	1.11	0.69	3.02
14	23.16	8.21	2.82	5.61	3.00
15	18.74	7.85	2.39	5.81	2.87
16	22.29	8.73	2.55	7.40	2.73
17	7.68	5.11	1.50	0.97	2.71
18	24.30	8.00	3.04	6.37	2.57
19	19.56	8.82	2.22	6.88	2.40
20	22.52	8.76	2.57	11.27	2.27
21	9.44	7.86	1.20	2.67	2.13
22	9.36	7.78	1.20	2.78	2.13
23	19.22	9.01	2.13	9.43	2.01
24	13.82	9.72	1.42	10.93	0.
25	17.25	8.29	2.08	7.63	0.
26	4.97	6.37	0.78	1.41	0.
27	3.55	4.51	0.79	0.45	0.
28	20.21	16.53	1.22	15.46	0.

Cumulative Quantities for Round 4146

Particle	Cumulative Length (mm)	Cumulative Mass (gm)	Cumulative Momentum (kg m/s)	Cumulative Energy (kJ)	Breakup Time (us)
1	13.1	2.5	10.4	21.7	0.
2	24.0	4.1	17.2	35.8	148.3
3	33.7	5.6	22.9	47.1	101.2
4	38.3	5.7	23.4	48.1	116.3
5	50.4	7.1	28.9	58.8	126.5
6	55.1	7.4	29.8	60.5	135.1
7	72.3	10.8	43.0	85.3	136.5
8	84.2	13.3	51.8	100.8	109.4
9	99.9	15.4	59.1	113.7	128.3
10	114.8	18.1	68.2	129.3	133.4
11	131.8	21.7	80.1	148.9	132.5
12	152.7	26.6	95.6	173.3	128.8
13	158.5	27.3	97.7	176.5	127.5
14	181.6	32.9	114.6	201.8	138.1
15	200.4	38.7	131.2	225.7	140.1
16	222.7	46.1	151.4	253.2	140.2
17	230.3	47.1	154.1	256.8	149.3
18	254.6	53.5	170.4	277.8	145.8
19	274.2	60.4	187.0	297.7	144.4
20	296.7	71.6	212.5	326.6	145.1
21	306.2	74.3	218.2	332.7	143.5
22	315.5	77.1	224.1	339.0	148.1
23	334.7	86.5	243.1	358.1	146.5
24	348.6	97.4	243.1	358.1	0.
25	365.8	105.1	243.1	358.1	0.
26	370.8	106.5	243.1	358.1	0.
27	374.3	106.9	243.1	358.1	0.
28	394.5	122.4	243.1	358.1	0.

Virtual Origin = -46.1647

	With Tip	Without Tip
Average Length	14.09	14.13
Average Diameter	7.20	7.22
Average L/D	1.937	1.938
Average Velocity Change	0.099	0.100

No of Copies	Organization
2	Administrator Defense Technical Info Center ATTN: DTIC-DDA Cameron Station Alexandria, VA 22304-6145
1	HQDA (SARD-TR) WASH DC 20310-0001
1	Commander US Army Materiel Command ATTN: AMCDRA-ST 5001 Eisenhower Avenue Alexandria, VA 22333-0001
1	Commander US Army Laboratory Command ATTN: AMSLC-DL Adelphi, MD 20783-1145
2	Commander US Army, ARDEC ATTN: SMCAR-IMI-I Picatinny Arsenal, NJ 07806-5000
2	Commander US Army, ARDEC ATTN: SMCAR-TDC Picatinny Arsenal, NJ 07806-5000
1	Director Benet Weapons Laboratory US Army, ARDEC ATTN: SMCAR-CCB-TL Watervliet, NY 12189-4050
1	Commander US Army Armament, Munitions and Chemical Command ATTN: SMCAR-ESP-L Rock Island, IL 61299-5000
1	Commander US Army Aviation Systems Command ATTN: AMSAV-DACL 4300 Goodfellow Blvd. St. Louis, MO 63120-1798

No of Copies	Organization
1	Director US Army Aviation Research and Technology Activity ATTN: SAVRT-R (Library) M/S 219-3 Ames Research Center Moffett Field, CA 94035-1000
1	Commander US Army Missile Command ATTN: AMSMI-RD-CS-R (DOC) Redstone Arsenal, AL 35898-5010
1	Commander US Army Tank-Automotive Command ATTN: AMSTA-TSL (Technical Library) Warren, MI 48397-5000
1	Director US Army TRADOC Analysis Command ATTN: ATRC-WSR White Sands Missile Range, NM 88002-5502
1	(Class. only)] Commandant US Army Infantry School ATTN: ATSH-CD (Security Mgr.) Fort Benning, GA 31905-5660
1	(Unclass. only)] Commandant US Army Infantry School ATTN: ATSH-CD-CSO-OR Fort Benning, GA 31905-5660
1	Air Force Armament Laboratory ATTN: AFATL/DLODL Eglin AFB, FL 32542-5000

Aberdeen Proving Ground

2	Dir, USAMSAA ATTN: AMXSY-D AMXSY-MP, H. Cohen
1	Cdr, USATECOM ATTN: AMSTE-TD
3	Cdr, CRDEC, AMCCOM ATTN: SMCCR-RSP-A SMCCR-MU SMCCR-MSI
1	Dir, VLAMO ATTN: AMSLC-VL-D

No. of Copies | Organization

4 Commander
Naval Surface Warfare Center
ATTN: Code DG-50,
W. Reed, R10A
E. Johnson
W. Bullock
Code DX-21, Lib Br
White Oak, MD 20910

2 Commander
US Army, ARDEC
ATTN: SMCAR-AWE,
J. Pearson
J. Grant
Picatinny Arsenal, NJ 07806-5000

3 Director
DARPA
ATTN: J. Richardson
LTC Quinn
T. Hafer
1400 Wilson Blvd.
Arlington, VA 22209-2308

3 Commander
US Army Missile Command
ATTN: AMSMI-RD-ST-WF,
M. Schexnayder
S. Cornelius
D. Lovelace
Redstone Arsenal, AL 35898-5247

1 AFATL/DLJR (J. Foster)
Eglin AFB, FL 32542

1 WRDC/MTX
ATTN: Mr. Lee Kennard
Wright Patterson AFB, OH 45443-6533

1 US Army Harry Diamond Laboratories
ATTN: SLCHD-TA-SS,
Bob Christopherson
2800 Powder Mill Road
Adelphi, MD 20783-1197

No. of Copies | Organization

4 Director
Lawrence Livermore Laboratory
ATTN: Technical Library
Dr. J. Kury
Dr. M. Van Thiel
Dr. C. Cline
P.O. Box 808
Livermore, CA 94550

2 Battelle-Columbus Laboratories
ATTN: Technical Library
Dr. L. Vescilius
505 King Avenue
Columbus, OH 43201

3 Sandia Laboratories
ATTN: Dr. M. Forrestal
Dr. M. Vigil
Dr. A. Robinson
P.O. Box 5800
Albuquerque, NM 87185

7 University of California
Los Alamos Scientific Lab
ATTN: Dr. J. Walsh
Dr. R. Karpp
Dr. C. Mautz
L. Hull, M-8
J. Repa
D. Fradkin
Technical Library
P.O. Box 1663
Los Alamos, NM 87545

1 University of Dayton
Research Institute
ATTN: Dr. S. J. Bless
P.O. Box 283
Dayton, OH 45409

1 Southwest Research Institute
ATTN: A. Wenzel
P.O. Drawer 28255
San Antonio, TX 78284

No. of Copies	Organization
	Battelle Edgewood Operations ATTN: R. Jameson 2113 Emmorton Park Road Suite 200 Edgewood, MD 21040
1	E.I. DuPont De Nemours & Company ATTN: B. Scott Chestnut Run - CR 702 Wilmington, DE 19898
1	Dyna East Corporation ATTN: P.C. Chou 3201 Arch Street Philadelphia, PA 19104-2588
1	Aerojet Electro Systems Company ATTN: Warhead Systems, Dr. J. Carleone 1100 W. Hollyvale St. P.O. Box 296 Azusa, CA 91702
1	Physics International Company Tactical Systems Group Eastern Division P.O. Box 1004 Wadsworth, OH 44281-0904
2	Honeywell, Inc. Government and Aeronautical Products Division ATTN: G. Johnson J. Houlton 600 Second Street, NE Hopkins, NM 55343
1	Nuclear Metals, Inc. ATTN: M. Waltz 2229 Main Street Concord, MA 01742
1	Shock Transients, Inc. ATTN: David Davison, President P.O. Box 5357 Hopkins, MN 55343

No. of Copies	Organization
1	S-Cubed ATTN: Dr. R. Sedgwick P.O. Box 1620 La Jolla, CA 92038-1620
1	SRI International ATTN: Dr. L. Seaman 333 Ravenswood Avenue Menlo Park, CA 94025
1	College of Engineering ATTN: Dr. R.D. Dick University of Maryland College Park, MD 2074.

INTENTIONALLY LEFT BLANK.

USER EVALUATION SHEET/CHANGE OF ADDRESS

This Laboratory undertakes a continuing effort to improve the quality of the reports it publishes. Your comments/answers to the items/questions below will aid us in our efforts.

1. BRL Report Number BRL-TR-3169 Date of Report NOVEMBER 1990

2. Date Report Received _____

3. Does this report satisfy a need? (Comment on purpose, related project, or other area of interest for which the report will be used.) _____

4. Specifically, how is the report being used? (Information source, design data, procedure, source of ideas, etc.) _____

5. Has the information in this report led to any quantitative savings as far as man-hours or dollars saved, operating costs avoided, or efficiencies achieved, etc? If so, please elaborate. _____

6. General Comments. What do you think should be changed to improve future reports? (Indicate changes to organization, technical content, format, etc.) _____

CURRENT ADDRESS

Name

Organization

Address

City, State, Zip Code

7. If indicating a Change of Address or Address Correction, please provide the New or Correct Address in Block 6 above and the Old or Incorrect address below.

OLD ADDRESS

Name

Organization

Address

City, State, Zip Code

(Remove this sheet, fold as indicated, staple or tape closed, and mail.)

----------FOLD HERE----------

DEPARTMENT OF THE ARMY
Director
U.S. Army Ballistic Research Laboratory
ATTN: SLCBR-DD-T
Aberdeen Proving Ground, MD 210(-5066
OFFICIAL BUSINESS

NO POSTAGE
NECESSARY
IF MAILED
IN THE
UNITED STATES

BUSINESS REPLY MAIL
FIRST CLASS PERMIT No 0001, APG, MD

POSTAGE WILL BE PAID BY ADDRESSEE

Director
U.S. Army Ballistic Research Laboratory
ATTN: SLCBR-DD-T
Aberdeen Proving Ground, MD 21005-9989

----------FOLD HERE----------